

INSTITUTO TECNOLÓGICO DE COSTA RICA

ESCUELA DE INGENIERÍA ELECTRÓNICA



Optimization of an analogue circuit design
for a portable nanoparticle detection device
(POND) using printed sensors

Informe de Proyecto de Graduación para optar por
el título de Ingeniero en Electrónica con el grado
académico de Licenciatura

Oscar Osvaldo Soto Rivera

Cartago, Costa Rica

I Semestre

6 de septiembre, 2018

INSTITUTO TECNOLÓGICO DE COSTA RICA

ESCUELA DE INGENIERÍA ELECTRÓNICA

PROYECTO DE GRADUACIÓN

ACTA DE APROBACIÓN


**Defensa de Proyecto de Graduación
Requisito para optar por el título de Ingeniero en Electrónica
Grado Académico de Licenciatura
Instituto Tecnológico de Costa Rica**

El Tribunal Evaluador aprueba la defensa del proyecto de graduación denominado *Optimization of an analogue circuit design for a portable nanoparticle detection device (POND) using printed sensors*, realizado por el señor Oscar Osvaldo Soto Rivera y, hace constar que cumple con las normas establecidas por la Escuela de Ingeniería Electrónica del Instituto Tecnológico de Costa Rica.

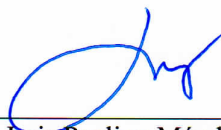
Miembros del Tribunal Evaluador


M.Sc. Jorge Castro-Godínez

Profesor lector


Ing. Marvin Hernández Cisneros

Profesor lector


M.Sc. Luis Paulino Méndez Badilla

Profesor asesor

Cartago, 6 de septiembre, 2018

Declaratoria de autenticidad

Declaro que el presente Proyecto de Graduación ha sido realizado enteramente por mi persona, utilizando y aplicando literatura referente al tema e introduciendo conocimientos propios.

En los casos en que he utilizado bibliografía he procedido a indicar las fuentes mediante las respectivas citas bibliográficas. En consecuencia, asumo la responsabilidad total por el trabajo realizado y por el contenido del correspondiente informe final.



Oscar Osvaldo Soto Rivera

Cartago, 6 de septiembre, 2018

Cédula: 1-1458-0083

Abstract

The growing use of nanoparticles in different sectors of the industry has generated interest in their study to understand the effect they have on the human body and the environment. The Neuroelectronics group at the Technical University of Munich is conducting a research to develop a portable device for the detection of silver nanoparticles *in situ*. Taking advantage of the widespread use of cell phones it is possible to use the computational capacity of these to establish communication with the sensor and carry out relevant analyzes for the study of silver nanoparticles. Due to the importance that the analog circuit has in the record of small signals generated by the silver nanoparticles, this project focuses on the study of this to characterize and reduce the thermal and electromagnetic noise as well as to determine its frequency response. In addition, using Altium designer software, the power management PCB was developed to provide the system with portability. In this work, the design process is detailed from the selection of components, through the schematics and layout to the assembly and verification of the PCB.

Keywords: Silver nanoparticles detection, electrochemistry, printed sensors, noise, power management.

Resumen

El creciente uso de nanopartículas en diferentes sectores de la industria ha generado interés en su estudio para comprender el efecto que tienen en el cuerpo humano y el medio ambiente. El grupo de Neuroelectrónica en la Universidad Técnica de Múnich conduce una investigación para desarrollar un dispositivo portable para la detección de nanopartículas de plata *in situ*. Aprovechando el extendido uso de teléfonos celulares es posible utilizar la capacidad computacional de estos para establecer la comunicación con el sensor y llevar a cabo análisis relevantes para el estudio de nanopartículas de plata. Por la importancia que el circuito analógico tiene en el registro de pequeñas señales generadas por las nanopartículas de plata, este proyecto se centra en el estudio de este para caracterizar y reducir el ruido térmico y electromagnético así como determinar su respuesta en frecuencia. Además, utilizando el programa Altium Designer, se desarrolló el PCB de manejo de potencia para dotar al sistema de portabilidad. Se detalla el proceso de diseño desde la selección de componentes, pasando por los esquemáticos y *layout*, hasta el ensamblado y verificación del PCB.

Palabras clave: Detección de nano partículas de plata, electroquímica, sensores impresos, ruido, administración de energía.

To God, to my family and friends

Acknowledgments

First of all, I want to thank God for accompanying from beginning of this journey, for guiding and giving me the will, intelligence and above all people to cope with this path, but more, to enjoy it.

I want to give a special acknowledgement to group of Neuroelectronics from the Technical University of Munich and to my supervisor M.Eng. Leroy Grob, for all the support during the development of this project, without them this would not have been possible. Thank you for allowing be a part of the group, I will always remember as one of the greatest experiences of my life. I would also like to thank the Costa Rica Institute of Technology for giving me the chance of study, and each professor that has contributed to my formation as an engineer. They all have my eternal gratitude.

To my parents and sister, for all the sacrifices they have made for me all these years, for their unconditional love and for always believing in me. To Yesenia for pushing me to grow and be better. Throughout this path they never let me alone and I always felt their support, that helped me to continue and finish my studies. Someday I hope to give back everything they have done for me. The best part of this time has been you.

Finally I want to thank all the persons that were by my side this years, friends, colleagues and professors. Thanks for the teachings and for the good times.

*"If I have seen further, it is by standing upon the shoulders of giants."
Isaac Newton*

Contents

1	Introduction	2
1.1	Motivation	2
1.2	Project approach	3
1.2.1	PicoAmp circuit	4
1.2.2	System power distribution	6
1.2.3	Objectives	7
1.2.4	Report organization	7
2	Fundamentals	9
2.1	Silver nanoparticles	9
2.1.1	Nano-impacts	10
2.2	Noise	12
2.2.1	Internal sources	13
2.2.2	External sources	16
2.3	Noise measurements	18

2.3.1	Peak to peak and RMS	18
2.3.2	PSD	18
2.4	Power management	20
2.4.1	Buck converters or step-down	21
2.4.2	Boost converter or step-up	25
2.4.3	LDO	28
2.4.4	Battery charge	31
3	Materials and Methods	33
3.1	Feedback resistors	33
3.2	Noise characterization	35
3.2.1	Analogue circuit's thermal noise	35
3.2.2	Evaluation and reduction of electromagnetic noise	35
3.2.3	Noise experiments	35
3.2.4	Measurement procedure	38
3.2.5	RMS and Peak to peak values: Algorithm	39
3.2.6	PSD plot: Algorithm	41
3.2.7	Aluminium enclosure	44
3.3	Frequency response analysis	46
3.3.1	Measurement procedure	48
3.3.2	Frequency response: Algorithm	49
3.4	Power board: Choosing the design	52

3.4.1	Solution 1	53
3.4.2	Solution 2	54
3.4.3	Solution 3	55
3.4.4	Choosing a solution	56
3.5	Power board: Development of the design	58
3.5.1	Battery	58
3.5.2	Battery charger	59
3.5.3	Boost: Positive voltage to feed LDOs TPS7A47	61
3.5.4	LDO: Digital positive output voltage (+5V)	65
3.5.5	LDO: Analog positive output voltage (+3.3V)	69
3.5.6	Inverter: Negative voltage to feed the LDO TPS7A33	72
3.5.7	LDO: Analog negative output voltage (-5V)	75
3.5.8	Layout considerations	77
4	Results and Discussion	79
4.1	Noise experiments: Without aluminium enclosure	80
4.1.1	Printed sensor is not coupled to the circuit input	80
4.1.2	Printed sensor is not coupled to the circuit input. The circuit input is covered by a Faraday cage	86
4.1.3	Printed sensor is coupled to the circuit input and it is not covered by a Faraday cage	92
4.1.4	Printed sensor is coupled to the circuit input. The printed sensor/circuit input is covered by a Faraday cage	98

4.2	Noise experiments: With aluminium enclosure	105
4.2.1	Printed sensor is not coupled to the circuit input	105
4.3	Frequency response	109
4.4	Power board	110
4.4.1	PCB	110
4.4.2	Noise analysis: TENMA 72-10495 power supply vs power board	111
4.4.3	Battery charge/discharge curve	111
4.4.4	Efficiency	114
4.5	Noise experiment: Offset analysis	116
4.5.1	Without printed sensor	116
4.5.2	With printed sensor	117
4.6	Noise experiment: Noise added by the electrolyte	119
5	Conclusions	122
6	Recommendations	124
	Bibliography	126
A	Appendix	130
A.1	Abbreviations	130
A.2	DCDC converter parameters	131
A.3	Phase response	134

A.4	Schematics	135
A.5	Layout	142

List of Figures

1.1	Schematic of the PicoAmp circuit designed and implemented by Jonathan N. Rapp [1].	4
1.2	Block diagram of the system power distribution. Lucidchart.	6
2.1	Potentiostat setup with 3 electrodes: WE, RE and CE [2].	11
2.2	Current spike generated by electron transfer due to a nano-impact [3].	12
2.3	Gaussian distribution of thermal and shot noise [4].	14
2.4	Spectrum of noise colors [5].	15
2.5	Spectral density for white noise and noise $1 / f$ [4].	16
2.6	External sources of noise. Word 2016.	17
2.7	Superposition of three fixed frequency sine waves. MatLab.	19
2.8	Illustration of the time domain and the frequency domain [6].	19
2.9	Buck converter basic schematic [7].	21
2.10	Buck converter: On state simplification [7].	22
2.11	Buck converter: Off state simplification [7].	23
2.12	Boost converter basic schematic [8].	25

2.13	Boost converter: On state simplification [8].	26
2.14	Boost converter: Off state simplification [8].	27
2.15	LDO basic schematic [9].	28
2.16	LDO dropout characteristic [10].	30
2.17	LI-ION charge description [11].	31
3.1	Feedback resistors placement. Power point 2016.	34
3.2	Analog circuit without input.	36
3.3	Faraday cage of 30x30 mm placed on analog circuit input.	36
3.4	Printed sensor coupled to the analog circuit input.	37
3.5	Faraday cage of 30x30 mm on printed sensor.	37
3.6	Algorithm for the calculation of the RMS and Peak to Peak values. Lucidchart.	40
3.7	Algorithm for the calculation of the PSD plot. Lucidchart.	43
3.8	Faraday cage principle. Lucidchart.	44
3.9	Illustration of the attenuation of an electric wave due to the skin effect in a good conductor. MatLab.	45
3.10	Illustration of current spike produced by nano-impacts [12].	46
3.11	Measurement setup for the frequency response of the analog circuit. Lucidchart.	49
3.12	Algorithm for the calculation of cutoff frequency. Lucidchart.	51
3.13	Battery configuration to obtain 6V. Power point 2016.	53
3.14	Block diagram for solution 1. Power point 2016.	54

3.15	Block diagram for solution 2. Power point 2016.	55
3.16	Block diagram for solution 3. Power point 2016.	56
3.17	Battery charger schematic. Source: WEBENCH [®] Power Designer tool by Texas Instruments.	60
3.18	Boost converter schematic [13].	61
3.19	LDO schematic to get +5 V [14].	65
3.20	LDO schematic to get -5 V [15].	75
4.1	Root mean square and peak to peak noise channel 1 when printed sensor is not coupled to the circuit input. MatLab.	80
4.2	Root mean square and peak to peak noise channel 2 when printed sensor is not coupled to the circuit input. MatLab.	81
4.3	Root mean square and peak to peak noise channel 4 when printed sensor is not coupled to the circuit input. MatLab.	82
4.4	Power spectral density channel 1 when printed sensor is not coupled to the circuit input. MatLab.	83
4.5	Power spectral density channel 2 when printed sensor is not coupled to the circuit input. MatLab.	84
4.6	Power spectral density channel 4 when printed sensor is not coupled to the circuit input. MatLab.	85
4.7	Root mean square and peak to peak noise channel 1 when printed sensor is not coupled to the circuit input but a Faraday cage of 30x30 mm is placed on the circuit input. MatLab.	86
4.8	Root mean square and peak to peak noise channel 2 when printed sensor is not coupled to the circuit input but a Faraday cage of 30x30 mm is placed on the circuit input. MatLab.	87

4.9	Root mean square and peak to peak noise channel 4 when printed sensor is not coupled to the circuit input but a Faraday cage of 30x30 mm is placed on the circuit input. MatLab.	88
4.10	Power spectral density channel 1 when printed sensor is not coupled to the circuit input but a Faraday cage of 30x30 mm is placed on the circuit input. MatLab.	89
4.11	Power spectral density channel 2 when printed sensor is not coupled to the circuit input but a Faraday cage of 30x30 mm is placed on the circuit input. MatLab.	90
4.12	Power spectral density channel 4 when printed sensor is not coupled to the circuit input but a Faraday cage of 30x30 mm is placed on the circuit input. MatLab.	91
4.13	Root mean square and peak to peak noise channel 1 when printed sensor is coupled to the circuit input without a Faraday cage. MatLab.	92
4.14	Root mean square and peak to peak noise channel 2 when printed sensor is coupled to the circuit input without a Faraday cage. MatLab.	93
4.15	Root mean square and peak to peak noise channel 4 when printed sensor is coupled to the circuit input without a Faraday cage. MatLab.	94
4.16	Power spectral density channel 1 when printed sensor is coupled to the circuit input without a Faraday cage. MatLab.	95
4.17	Power spectral density channel 2 when printed sensor is coupled to the circuit input without a Faraday cage. MatLab.	96
4.18	Power spectral density channel 4 when printed sensor is coupled to the circuit input without a Faraday cage. MatLab.	97
4.19	Root mean square and peak to peak noise channel 1 when printed sensor is coupled to the circuit input with a Faraday cage of 30x30 mm. MatLab.	98

4.20	Root mean square and peak to peak noise channel 2 when printed sensor is coupled to the circuit input with a Faraday cage of 30x30 mm. MatLab.	99
4.21	Root mean square and peak to peak noise channel 4 when printed sensor is coupled to the circuit input with a Faraday cage of 30x30 mm. MatLab.	100
4.22	Power spectral density channel 1 when printed sensor is coupled to the circuit input with a Faraday cage of 30x30 mm. MatLab.	101
4.23	Power spectral density channel 2 when printed sensor is coupled to the circuit input with a Faraday cage of 30x30 mm. MatLab.	102
4.24	Power spectral density channel 4 when printed sensor is coupled to the circuit input with a Faraday cage of 30x30 mm. MatLab.	103
4.25	Modified aluminium enclosure.	105
4.26	Root mean square and peak to peak noise channel 1 when printed sensor is not coupled to the circuit input. MatLab.	106
4.27	Power spectral density channel 1 when printed sensor is not coupled to the circuit input. MatLab.	107
4.28	Frequency response of channel 1. MatLab.	109
4.29	PCB Power board: Implementation vs 3D Model.	110
4.30	Battery charge curve. MatLab.	112
4.31	Battery discharge curve. MatLab.	113
4.32	Efficiency for 3.3V output voltage. MatLab.	114
4.33	Efficiency for 5V output voltage. MatLab.	114
4.34	Efficiency for -5V output voltage. MatLab.	115
4.35	Noise added by the electrolyte: Channel 1. MatLab.	119

4.36	Noise added by the electrolyte: Channel 2. MatLab.	120
4.37	Noise added by the electrolyte: Channel 4. MatLab.	120
A.1	Phase response channel 1. MatLab.	134
A.2	Phase response channel 2. MatLab.	134
A.3	Phase response channel 4. MatLab.	134
A.4	Schematic top sheet. Altium designer 18.	135
A.5	Schematic battery charger BQ25606. Altium designer 18.	136
A.6	Schematic boost/inverter TPS65131. Altium designer 18.	137
A.7	Schematic LDO TPS7A47 to obtain 5V. Altium designer 18.	138
A.8	Schematic LDO TPS7A47 to obtain 3.3V. Altium designer 18.	139
A.9	Schematic LDO TPS7A33 to obtain -5V. Altium designer 18.	140
A.10	Schematic output connector. Altium designer 18.	141
A.11	Layout power board. Altium designer 18.	142

List of Tables

3.1	Noise experiments performed. LaTeX.	38
3.2	Voltage and current supplied to digital components. LaTeX.	52
3.3	Voltage and current supplied to digital components. LaTeX.	52
3.4	Maximum voltage and current requirements for the power board. LaTeX.	53
3.5	Battery specifications taken from [16]	58
3.6	Battery charger requirements. LaTeX.	59
3.7	ANY-OUT Programmable Output Voltage. LaTeX.	66
3.8	Corresponding pin settings to get +5 V. LaTeX.	67
3.9	Corresponding pin settings to get +5 V. LaTeX.	70
4.1	Noise experiment results for channel 1. LaTeX.	103
4.2	Noise experiment results for channel 2. LaTeX.	104
4.3	Noise experiment results for channel 4. LaTeX.	104
4.4	Noise experiment results for channel 1. LaTeX.	107
4.5	Noise experiment results for channel 2. LaTeX.	108

4.6	Noise experiment results for channel 4. LaTeX.	108
4.7	Frequency response. LaTeX.	109
4.8	RMS and peak-to-peak noise for TENMA 72-10495. LaTeX.	111
4.9	RMS and peak-to-peak noise for power board. LaTeX.	111
4.10	Results of the analysis when applying the offset potential of channel 1 without printed sensor. LaTeX.	116
4.11	Results of the analysis when applying the offset potential of channel 2 without printed sensor. LaTeX.	116
4.12	Results of the analysis when applying the offset potential of channel 4 without printed sensor. LaTeX.	117
4.13	Results of the analysis when applying the offset potential of channel 1 with printed sensor. LaTeX.	117
4.14	Results of the analysis when applying the offset potential of channel 2 with printed sensor. LaTeX.	118
4.15	Results of the analysis when applying the offset potential of channel 4 with printed sensor. LaTeX.	118
4.16	Evaluation of noise when the electrolyte is placed on the printed sensor and the power board is used. LaTeX.	121

Chapter 1

Introduction

1.1 Motivation

A growing interest in silver nanoparticles (particles that comprise sizes between 1 and 100 nm [17]) has arisen due to its physical and chemical properties, since at the nano scale some characteristics change, such as optical, electronic, magnetic, mechanical, and antimicrobial properties [17], [18], [19]. This has extended its use in different industries such as automotive, health products, textiles, water and air treatment, electronics and, many other fields of application [18]. Therefore, the human being is exposed to a large amount of this nano material. The long-term effect of exposing silver nanoparticles is not completely understood due to the limited studies on this matter. Less knowledge exists about the effects of silver nanoparticles in the environment [19], [20].

Among the different approaches to study nanoparticles, the nano-impacts technique based on the pioneering experiments by Micka stands out [3]. The basic configuration of the system consists of an electrode in a solution that contains the nanoparticles under study. To carry out the experiment, the potential in an electrode is controlled; when the nanoparticles interact with it, a charge is transferred which produces a current spike of pico amperes order. Using this signal it is possible to determine some characteristics in the nanoparticles [3], a detailed explanation is given in the next section. Particularly important is to develop a device based on the

nano-impacts technique that is portable in order to carry out *in situ* experiments and obtain comparable results with other techniques such as electron microscopy imaging [12].

In order to create a portable device based on nano-impacts it is necessary to improve different aspects involved in obtaining the signals of interest, these problems are related to the physical-chemical phenomena that occur in the nanoparticle-electrode interaction and with the measurement system because the influence of recording and manipulating the input signal.

1.2 Project approach

This project focuses on the characterization and reduction of thermal and electromagnetic noise and the determination of the frequency response of an analog system known as PicoAmp circuit designed and implemented by Jonathan N. Rapp. This circuit is based on one built by Norbert Wolters in FZ Juelich that allows a conversion from 1pA to 1mV [1].

On the other hand, the system has a digital circuit designed by Handenur Çalışkan and implemented by Julian Feuerbach [21]. The digital circuit is responsible for digitizing the signal from the output of the analog circuit and send it to a cell phone for later analysis. Due to the electrical characteristics of the electronic components (analog and digital) that are involved and in order to have a portable system, it is necessary to design a power management board. This power board must be able to supply the required voltage and current by the system without neglecting the role played by the power supply in the addition of noise.

configured as a voltage follower. The purpose of this amplifier is applied the offset potential in the electrode; However,, this offset must be removed later. Then, a comparison of the input Iin with V_{offset} is performed in U1; the difference between these inputs is amplified thus generating the output of U1. The offset voltage generated by U3 is inverted by U4 (AD822A) which has been configured as a unity gain inverter amplifier. Finally, the inverted offset voltage of U4 is added to the output of U1, this sum is made using U2 (AD820A) that has been configured as a summing amplifier with all resistors of equal value, making the gain 1 for each input [1].

The above description is shown in 1.2 and 1.3 [1].

$$Vout = ((-Iin \times R_{FB1} + V_{offset}) - V_{offset}) \times -1 \quad (1.2)$$

$$Vout = Iin \times R_{FB1} \quad (1.3)$$

1.2.2 System power distribution

figure 1.2 shows a general block diagram of the silver nanoparticle sensor that involves the different components; it also specifies the necessary voltage for each block [21]. This project will be responsible for designing and implementing the battery charge, battery and power management blocks.

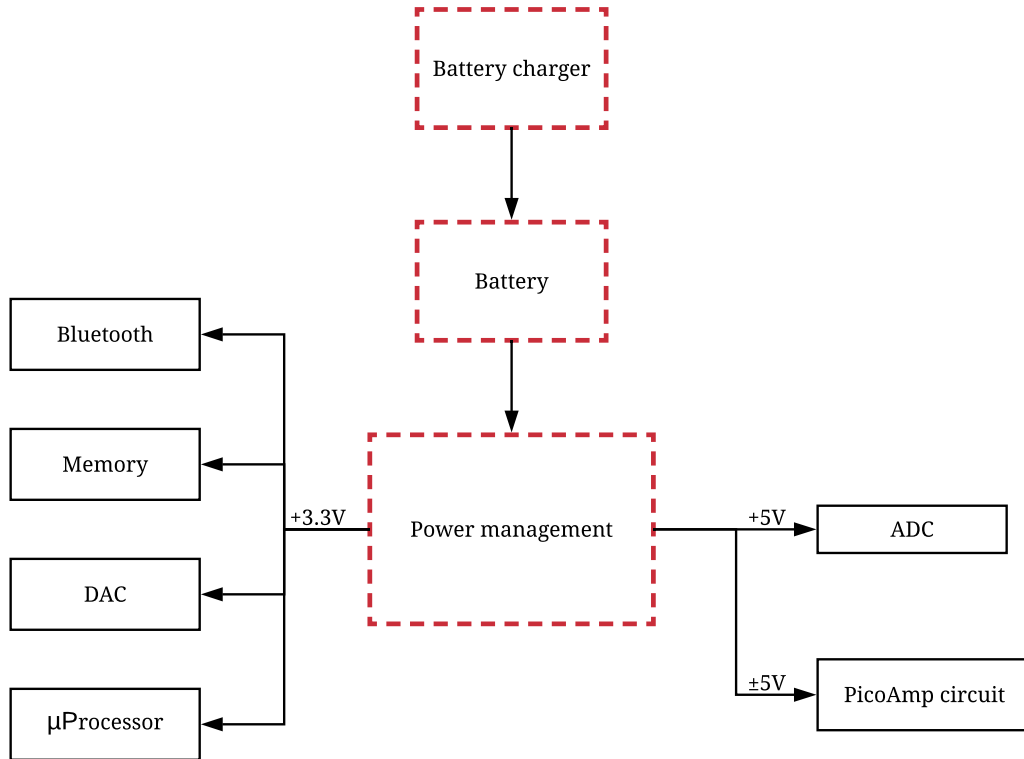


Figure 1.2: Block diagram of the system power distribution. Lucidchart.

1.2.3 Objectives

General objective

- Perform the solutions for noise problems, frequency response, and implementation of the power system, thus optimizing the analogue circuit for the detection of silver nanoparticles.

Specific objectives

- To determine the analogue circuit's thermal noise when coupled to varying input signals emulating nanoparticle impacts at a microelectrode.
- To reduce and evaluate any electromagnetic noise by the use of a Faraday cage (PSD plot evaluation).
- Evaluate the transfer response and phase response of the analogue circuit with varying frequencies.
- Design of a power circuit board, including battery management, for a portable sensor.

1.2.4 Report organization

The report is organized as follows:

1. **Chapter 2:** The theoretical concepts that were used during the development of the project are described. A brief description of the silver nanoparticles is given, as well as the current methods to detect them and the nano-impact technique and its dependence on the measurement system. Subsequently, relevant aspects of noise definition and noise measurements are described. Finally, the design of the power board, the most common topologies, and a brief description about the charging of LI-ION batteries is given.

2. **Chapter 3:** The experiments carried out for the measurement and characterization of thermal noise and frequency response are described, the conditions and the materials that were used are also detailed. The considerations made to reduce the noise of the system are explained. In addition, the design of the power circuit is detailed, describing the different proposed solutions that were generated, the considerations that mediated to discard some of them, and choose the final solution.
3. **Chapter 4:** The results are shown sequentially obtained through the different experiments performed on the analog circuit for the measurement of thermal and electromagnetic noise and frequency response, as well as the power board. The results are discussed and analyzed.

Chapter 2

Fundamentals

This section provides some theoretical foundations that make it possible to understand the project carried out. In this section, the fundamentals behind the detection of silver nanoparticles will be explained. In addition, since this project is part of the development of a new device to detect silver nanoparticles *in situ*, the noise of the system must be characterized; therefore, a review on the concepts of noise, noise measurements, and power management systems design is described.

2.1 Silver nanoparticles

Currently, many studies focus on the characterization of nanoparticles to determine their toxicity that is related to the physical properties of the nanoparticle such as size, chemical nature, surface area and reactivity [20]. To study the nanoparticles and their properties there are different methods among the most common are the electron microscope (TEM and SEM) that are *ex situ* methods. Besides, because the preparation of the sample the characterization of aggregation is difficult and agglomeration does not provide kinetic information on these characteristics [3]. There are also optical methods, for example light scattering techniques (DLS and NTA) that are based on nanoparticle's absorption and scattering [12]. Some problems with light scattering techniques are the case where there are large and small particles concurrently that can skew the results to larger particles. The monitoring of small nanoparticles of weak dispersion and the determination of geometry are other chal-

lenges to be solved in this technique [3]. Both methods electron microscope and light scattering techniques are also expensive and difficult to use.

2.1.1 Nano-impacts

As an alternative in the last 20 years, a technique capable of sizing nanoparticles *in situ* has been developed, this method is known as nano-impact electrochemistry. This method is based on recording the events that are produced by the impacts of a single nanoparticle on an electrode [22]. The basic configuration of this system is shown in figure 2.1 consists of a working electrode (WE) that measures the electric current, a reference electrode (RE) that establishes the reference to measure the necessary potential so that the required reaction between the nanoparticle and the electrode is carried out and a counter electrode (CE) or auxiliary electrode (AE) that injects current to control the potential difference [3], [23]. In contrast to the three-electrode system where the current is measured through CE, in this project two electrodes (WE and RE) are used. CE is not required because current is not measured but individual charges that are absorbed by the electronics. However,, it was shown in [12] that depending on the composition of the electrolyte, silver nanoparticles can be detected without a reference electrode making it possible to have configurations of only one electrode (WE).

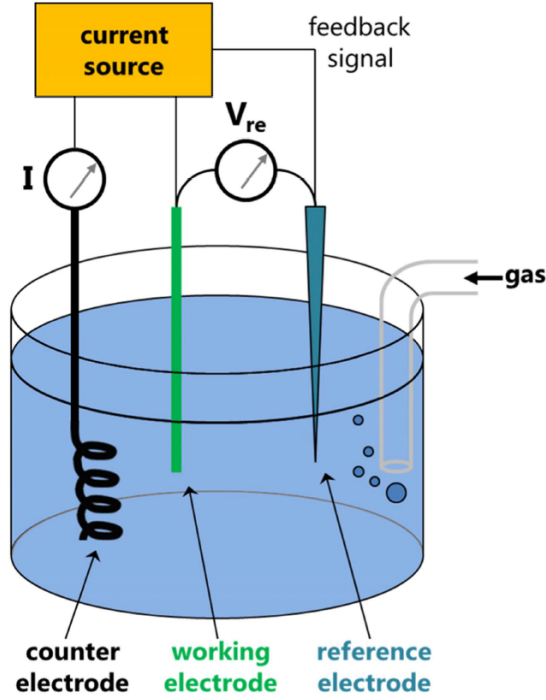
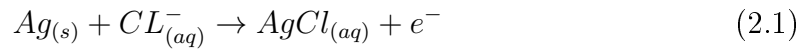


Figure 2.1: Potentiostat setup with 3 electrodes: WE, RE and CE [2].

In the configuration of two electrodes the silver nanoparticle approaches by Brownian motion to the WE and releases a charge. The release of this charge is due to oxidation of the particle, which is influenced by the potential difference between WE and RE. The following chemical reaction describes this process:



The charge is adsorbed by the electrode and generates a current spike that can be measured using an electronic circuit. Once this information is obtained it is possible to perform various mathematical operations on the signal such as integrating the spikes that reveals information about the size of an ideal spherical particle. It is also possible to know the concentration of silver nanoparticles in the solution counting the number of spikes [19], [3], [22].

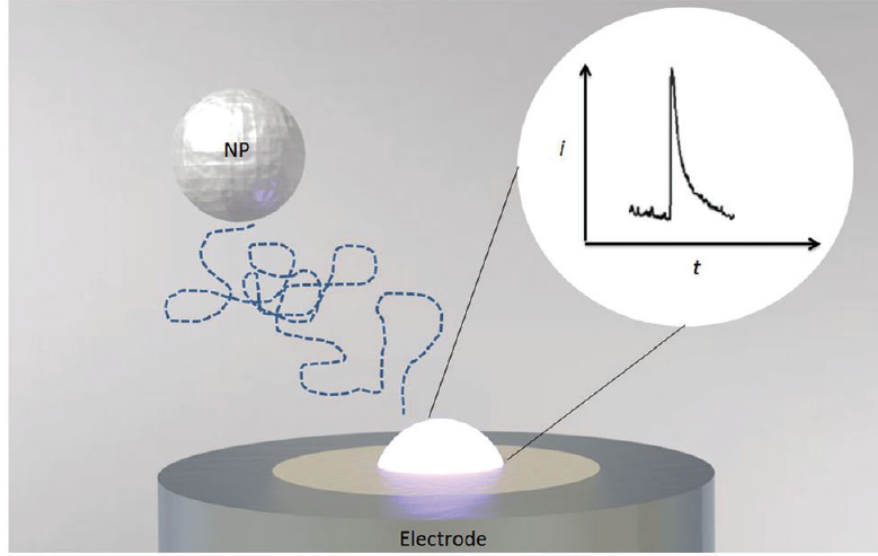


Figure 2.2: Current spike generated by electron transfer due to a nano-impact [3].

The precision of the measurements made with the nano-impact technique depends mainly on particle's mass transport, the charge transfer characteristic of the nanoparticle and the electronics to carry out the measurements. Special attention must be paid to noise sources in the electronic circuit because the current signal generated by the nanoparticles is generally of the order of pico amperes which is comparable to the noise of an electronic system [3].

2.2 Noise

Noise, in most cases, is an unwanted and unpredictable signal that is present in any circuit, the instantaneous value and phase of the waveform are unknown. There are several sources of noise, some of them could be internal such as the op-amps, passive components or PCB layout; However,, there also are external sources that come from other electronic systems or the environment. The level of noise can affect the general performance of the circuit. For example, the noise floor is the noise present at the output of the circuit when any input signal is applied, and it helps to determine the minimum signal with which the circuit can work, the lower the noise floor, the more sensitive the circuit will be. A well understanding of these concepts is important to

identity and reduce the noise in the circuit [5].

2.2.1 Internal sources

Shot noise: It is the random fluctuation of the current whenever charges pass through a potential barrier, the PN junctions are examples of potential barrier where this noise occurs [4], [24]. The shot noise is independent of temperature [4].

Thermal noise: It is the random movement of charge carriers (electrons/holes) in a resistive material or open-ended resistor due to thermal energy. It is also known as the Johnson noise [25], [26]. Thermal noise is independent of current flow [4].

Flicker noise: It is also known as $1/f$ noise, it is observed in the low frequency range and despite its origin is not very clear it is associated with failure contact between two conductors, also it is proportional to the dc current [4], [25], [27]. This noise appears with the thermal noise, so if the DC current is low the predominant noise will be the thermal noise [4].

Burst Noise: It is also known as popcorn noise because if it is amplified and reproduced through a speaker it produces a corn popping sound and it is also in the low frequency range [4]. This noise presents a constant amplitude but the switching time change. On an oscilloscope it presents a square waveform with fixed amplitude and variable pulse widths [24].

Avalanche noise: This noise occurs in reverse biased junctions, each time a load carrier has enough reverse junction voltage it collides with the crystal lattice and an additional electron-hole pair can be generated, these shocks can produce a current pulse, since this event is random also the current pulse is random [4], [24]. The intensity of this noise is often much more intense than any other source of noise [24].

In op-amps analysis noise the burst and avalanche noise are often negligible also if they are present in the circuit they can be eliminated [5].

As mentioned above, noise is an unpredictable signal, this means that the amplitude is random with time; However,, one way of characterizing noise is with probability density functions, specifically the thermal noise and shot noise have a Gaussian distribution [4].

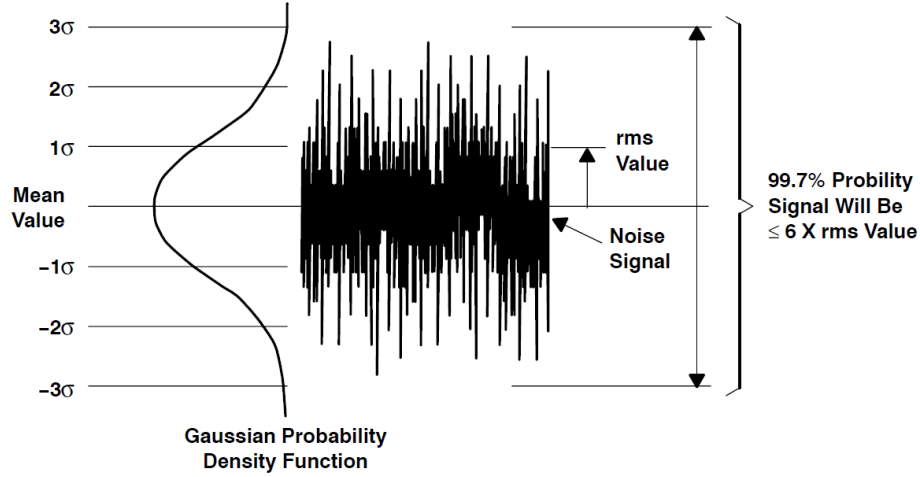


Figure 2.3: Gaussian distribution of thermal and shot noise [4].

Although noise is a random signal, it is possible to establish an amplitude that is given by the probability that the mean value in the Gaussian distribution will occur. To determine the probability that the noise presents other values higher or lower than the mean, it is only necessary to observe the Gaussian distribution, since the bell shape is centered at zero, the greater the amplitude, the lower the probability that the noise reaches that amplitude [5], [4].

Here are some important annotations:

1. σ is the standard deviation of the Gaussian distribution [4].
2. The RMS value of noise and standard deviation (σ) are the same [4].
3. The instantaneous amplitude of the noise will be from the average value to $\pm 1\sigma$ 68% of the time, from the average value to $\pm 3\sigma$ 99.7% of the time and from the average value to $\pm 3.4\sigma$ 99.94% of the time [5].
4. σ^2 is the average mean square variation about the average value [5].

5. The average mean square variation about the average value is the variance σ^2 [5].

Noise colors

Although different sources of noise have been described, they often appear in a circuit simultaneously and it is not practical to separate them. It is possible to classify noise sources to analyze their effect. One way to do this is to make an analogy between noise and the spectrum of light that is related to the frequencies, that is the reason why this analogy is known as noise colors. The portion of the spectrum where the noise sources described above fit is from white noise to brown noise [5].

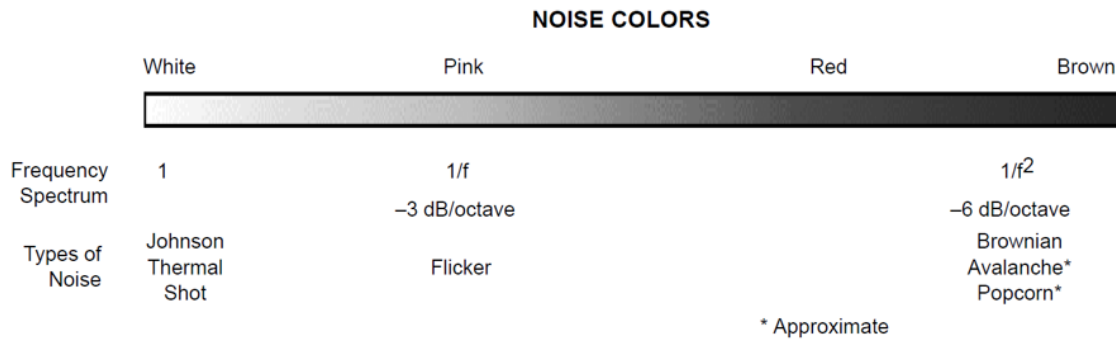


Figure 2.4: Spectrum of noise colors [5].

White noise: thermal noise and shot noise are approximately white noise because they are constant throughout the spectrum and they are frequency independent. The analogy comes from white light that is made up of the same amount of all colors [5].

Pink noise: Flicker noise present $1/f$ characteristic that means that the amplitude decreases logarithmically with frequency (3 dB/octave) [5].

Red/Brown noise: Popcorn and avalanche noise are comparable with red/brown colors, this type of noise shows a frequency response of -6 dB/octave and a frequency spectrum of $1/f^2$ excluding DC. However,, popcorn and avalanche noise are more often related to pink noise due to the behavior of the frequency [5].

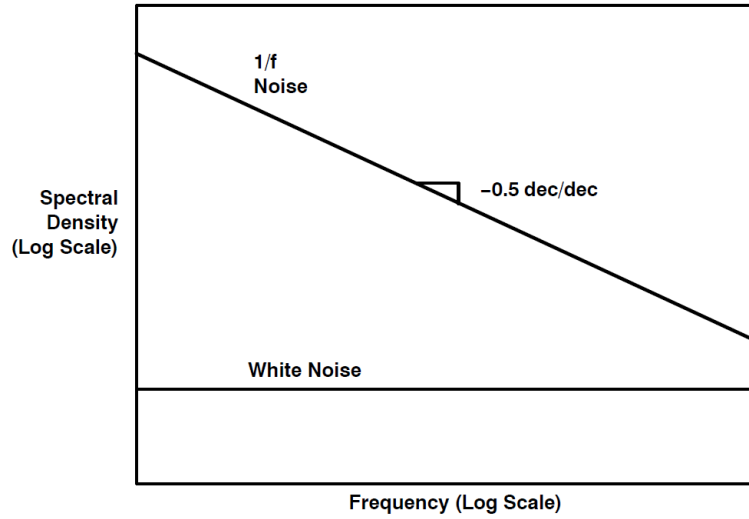


Figure 2.5: Spectral density for white noise and noise $1 / f$ [4].

2.2.2 External sources

Conducted emissions: Electromagnetic noise generated by the connections between two circuits [5]. These connections could be signals, power rails or data cables [28].

Radiated emissions: Some components in the circuit can act as antennas and emit electromagnetic noise through the air [29].

Conducted susceptibility: It is the ability of a circuit to operate properly when noise from another circuits or systems is coupled through connections [30]. This feature is important because the circuit under test must be connected to other systems either by ground, inputs or outputs, that is why this noise is always present and evaluating the performance of the circuit under these conditions is required [5].

Radiated susceptibility: When a current is induced in a conductor by a variable electromagnetic field it is possible to determine the strength of this field by measuring the amplitude of the current and the voltage induced not only in the conductor but also in the circuits connected to it. The radiated susceptibility limit is the field

strength that induced enough current so that the circuit does not work properly [30]. In a PCB some sources that can generate an electromagnetic field that induces currents are high speed digital logic, high speed clocks, switching digital signals and switching power supplies. External systems can also generate this electromagnetic fields such as cellphones, broadcast radio and TV and fluorescent lights [5].

For the external sources of noise explained above the conducted and radiated emissions are negligible except for high power and high frequency respectively [5].

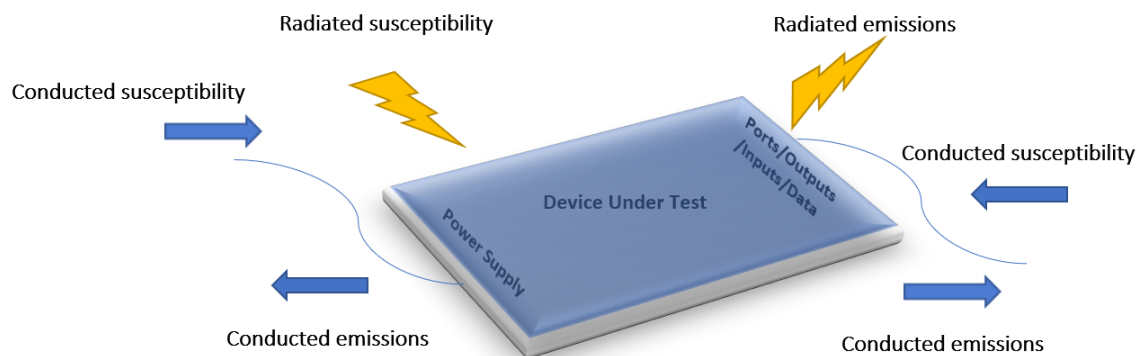


Figure 2.6: External sources of noise. Word 2016.

In general, the noise sources in a circuit are present together by superposition, this means that is very difficult to separate and evaluate each of the noise sources above individually, nor it is a common practice to separate noise by colors [5]. When analyzing the noise in a circuit, the peak to peak value, the root mean square (RMS) and power spectral density (PSD) are suitable tools to carry out this task because they show information about this random process, in the following section they will be explained [31].

2.3 Noise measurements

2.3.1 Peak to peak and RMS

Peak to peak is an instantaneous measure that provides the maximum and minimum data points that the signal has. This could be an important measure in applications where noise peaks could affect circuit performance [31].

The standard deviation describes how scattered each data point is with respect to the average of the signal, so it gives an idea about the effective amplitude of the signal [32]. By definition, the standard deviation takes into account the AC component and the RMS uses the AC and DC components. However, when a signal has a DC component of zero, the RMS and the standard deviation are the same, this is the case of white noise [32], [33]. The RMS can also be understood as the equivalent DC voltage that generate the same power as the RMS value for an AC signal [34]. The next formula shows how to compute the RMS value [35].

$$RMS = \sqrt{\frac{\sum (x_n - \bar{x}_n)^2}{N}} \quad (2.2)$$

Where x_n is a data point, \bar{x}_n is the mean of the set of data and N is the number of data.

2.3.2 PSD

While the peak-to-peak value and the RMS are measurements that provide information in the time domain, the PSD is a measure in the frequency domain (power versus frequency) and is often expressed in units of $\mu V/\sqrt{Hz}$ [36]. The PSD is a very useful tool in the analysis of noise because they reveal information about noise sources and their power [31].

When an electrical signal is analyzed in the time domain, Fourier theory states

that this signal is composed of one or more sinusoidal waves with their own frequency and phase. Each sinusoidal wave has its own energy, the name of each of these sine waves in the frequency domain are known as spectral components. However,, in the time domain it is not possible to distinguish these spectral components nor the energy contribution of each one to the resulting signal. As an example, this can be seen in figure 2.7 as the sum of three sine waves with discrete frequencies are superimposed and produce the signal on the right, in which it is not possible to distinguish at first sight each of the sinusoidal waves that make it up [6].

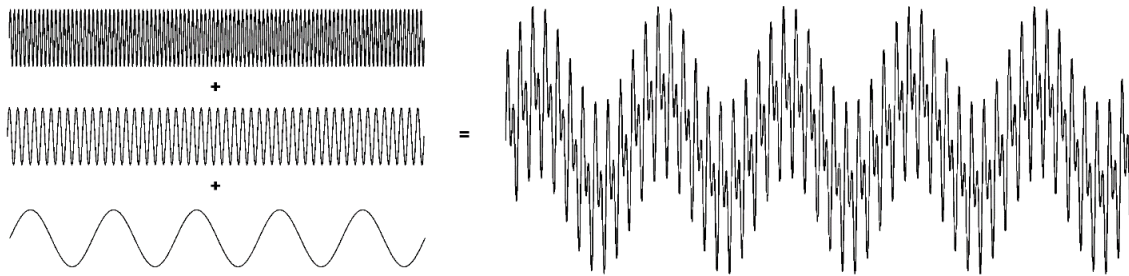


Figure 2.7: Superposition of three fixed frequency sine waves. MatLab.

It is therefore useful to apply the Fourier theory to move from the time domain to the frequency domain, once there it is possible to obtain the frequency spectrum of the signal which is a graph that shows the energy of each component on the vertical axis and the frequency of each component on the horizontal axis [6].

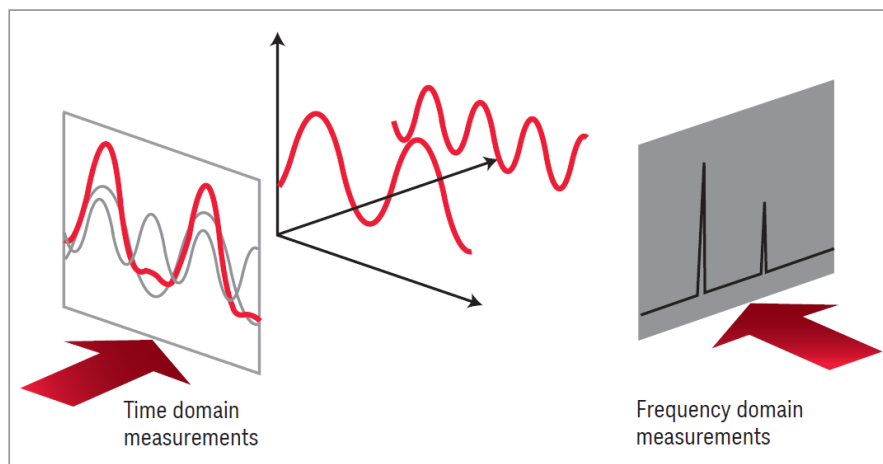


Figure 2.8: Illustration of the time domain and the frequency domain [6].

In the specific case of noise analysis, it is useful to know the spectral components that made it up because with this information it is possible to identify the sources of noise in order to reduce it. It could be determined if the noise is external or internal, for example, the signal of 50-60 Hz that comes from the power line can be coupled to the circuit, which is an external noise, this information could be obtained in the frequency domain [37].

2.4 Power management

Power management is the concept that is responsible for supplying and regulating the necessary energy with the goal to reach the best possible efficiently and decrease the power losses, so that the systems that depend on that energy can work properly [38], [39]. This concept has a more relevant importance in portable devices because most of them depend on a battery that is discharged with use. For this reason the system must be designed with low consumption. In addition aspects such as battery life, charging time, rails power, system power requirements and cost should be considered when designing a portable system [38]. To make a power management system, it is important to know the basic topologies and how to select the appropriate ones, these topologies are known as voltage regulators and they are divided in three categories:

1. Linear regulators.
2. Switching regulators.
3. Charge pumps.

In appendix A.2 are some basic concepts that can help in the selection of the best voltage regulator for the specific application. Among those concepts some of them will be crucial in the selection of the topology to meet the minimum requirements of the system and to adjust the general performance of the power management system, meanwhile others can be considered like extra features, these depends of the specific application [39].

The first step to design the power management system once the input voltage will be established is to determine the topology to allow reach the desire output voltage.

In the following section three of the most common topologies will be explain, the buck converter, the boost converter and the LDO [40].

2.4.1 Buck converters or step-down

This switching power supply topology provides an output voltage that is less than the input voltage with the same polarity and the input and the voltage share the same ground, it means, it is a not isolated topology [40], [7].

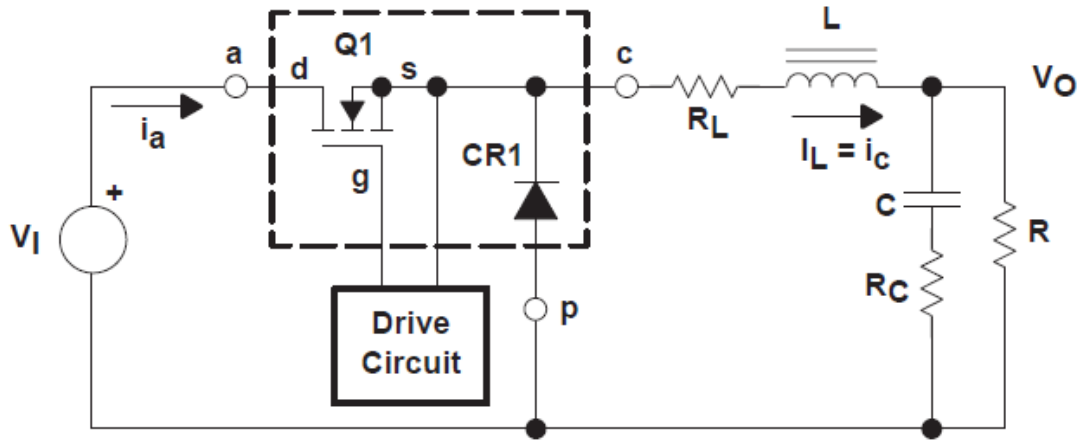


Figure 2.9: Buck converter basic schematic [7].

Analysis considerations

This topology can operate in two modes, continuous inductor current mode or discontinuous current mode. This analysis will focus on the first mode where the inductor current is continuous in the switching cycle under the following conditions: input voltage, output voltage, output load current and duty-cycle are constant, this is defined as steady-state. In addition, for the Q1 component shown in figure 2.9, an N-channel power MOSFET will be used. Two states are defined:

1. ON state if Q1 is on and the diode CR1 is off.
2. OFF state if Q1 is off and the diode CR1 is on.

On state

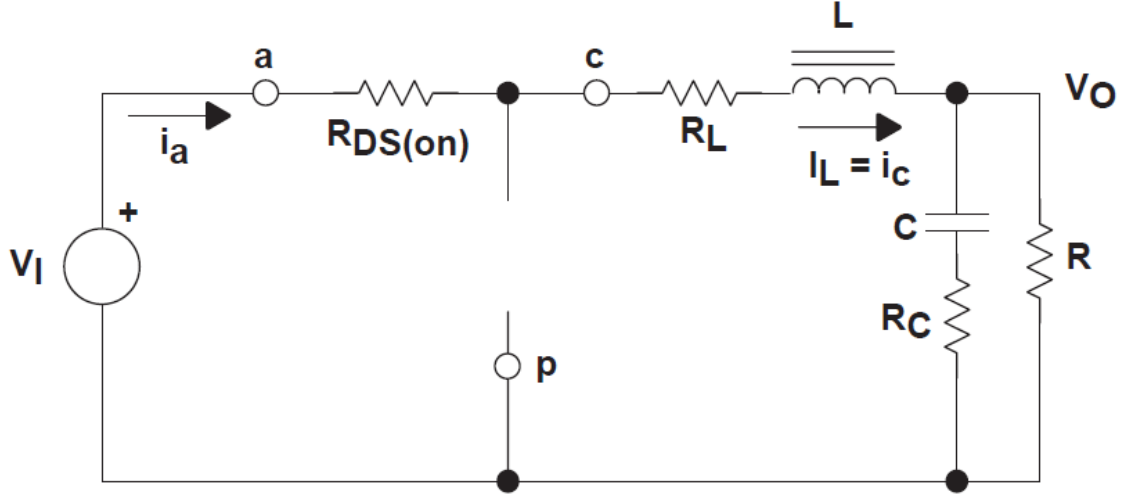


Figure 2.10: Buck converter: On state simplification [7].

In this state the current in the load is provided by the source and the capacitor at the output of the circuit is charged. If the transistor Q1 is replaced by a low resistance R_{ds} as illustrated in figure 2.10, it can be seen that the current goes from the source to the inductor because the diode is in reverse biased, this current increases linearly due to the constant voltage applied across the inductor, which is defined as:

$$V_L = V_I - V_{DS} - I_L \times R_L - V_O \quad (2.3)$$

The increase in the inductor current can be calculated as follows:

$$V_L = L \times \frac{di_L}{dt} \quad (2.4)$$

Where:

$$\frac{di_L}{dt} \Rightarrow \Delta I_L \quad (2.5)$$

$$\Delta I_L = \frac{V_L}{L} \times \Delta T \quad (2.6)$$

$$\Delta I_L (+) = \frac{(V_I - V_{DS} - I_L \times R_L) - V_O}{L} \times T_{ON} \quad (2.7)$$

Where T_{ON} is the duration of the on state given by:

$$T_{ON} = D \times T_s \quad (2.8)$$

Where D is the duty cycle and T_s is the total switching cycle. $I_L(+)$ is the inductor current ripple in the on state.

Off state

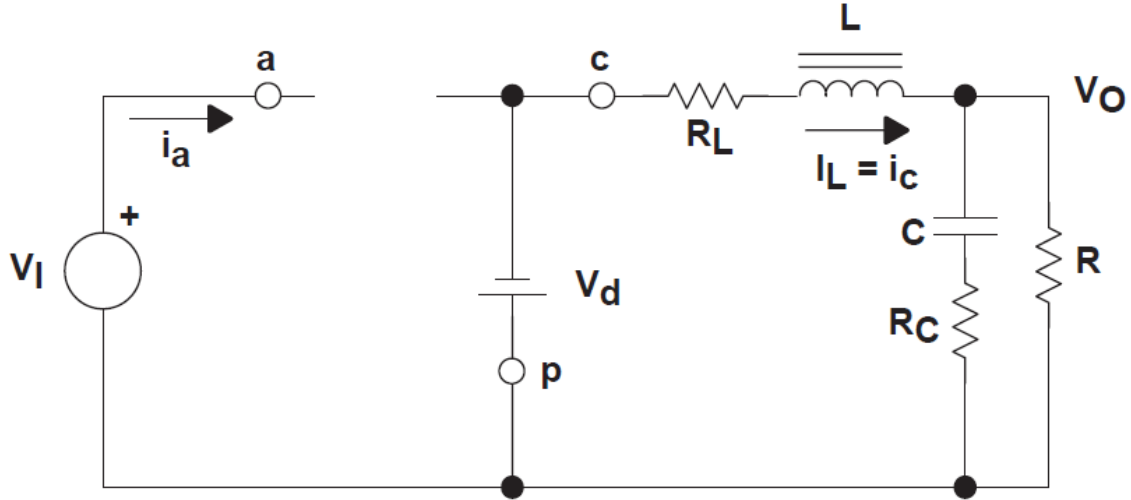


Figure 2.11: Buck converter: Off state simplification [7].

In this state the transistor Q1 is replaced by an open circuit as illustrated in figure 2.11 where the current of the inductor follows a path that passes through ground, then through the diode CR1 and finally through the output capacitor and load resistance, this current decreases linearly due to the constant voltage applied

to the inductor, this voltage has the opposite sign in comparison with the inductor voltage in the on state which is defined as:

$$V_L = V_O + V_d + I_L \times R_L \quad (2.9)$$

Using the formula 2.6, the decrease in the current of the inductor can be calculated as follows:

$$\Delta I_L(-) = \frac{V_O + (V_d + I_L \times R_L)}{L} \times T_{OFF} \quad (2.10)$$

Where T_{OFF} is the duration of the off state given by:

$$T_{OFF} = (1 - D) \times T_s \quad (2.11)$$

$I_L(-)$ is the inductor current ripple in the off state.

Circuit operation

In steady state $I_L(+)$ and $I_L(-)$ must be equal, due to this condition it is possible to equate the above formulas and solve to find the value of V_{out} :

$$V_O = (V_I - V_{DS}) \times \frac{T_{ON}}{T_{ON} + T_{OFF}} - V_d \times \frac{T_{OFF}}{T_{ON} + T_{OFF}} - I_L \times R_L \quad (2.12)$$

Where $T_s = T_{ON} + T_{OFF}$, $D = T_{ON}/T_s$ and $(1 - D) = T_{OFF}/T_s$.

$$V_O = (V_I - V_{DS}) \times D - V_d \times (1 - D) - I_L \times R_L \quad (2.13)$$

V_{out} is always less than V_{in} and its value can be determined by the duty cycle (since D is always between 0 and 1), which is established by the control circuit [7].

2.4.2 Boost converter or step-up

This switching power supply topology provides an output voltage that is greater than the input voltage with the same polarity and the input and the voltage share the same ground, it means, it is a not isolated topology [40], [8].

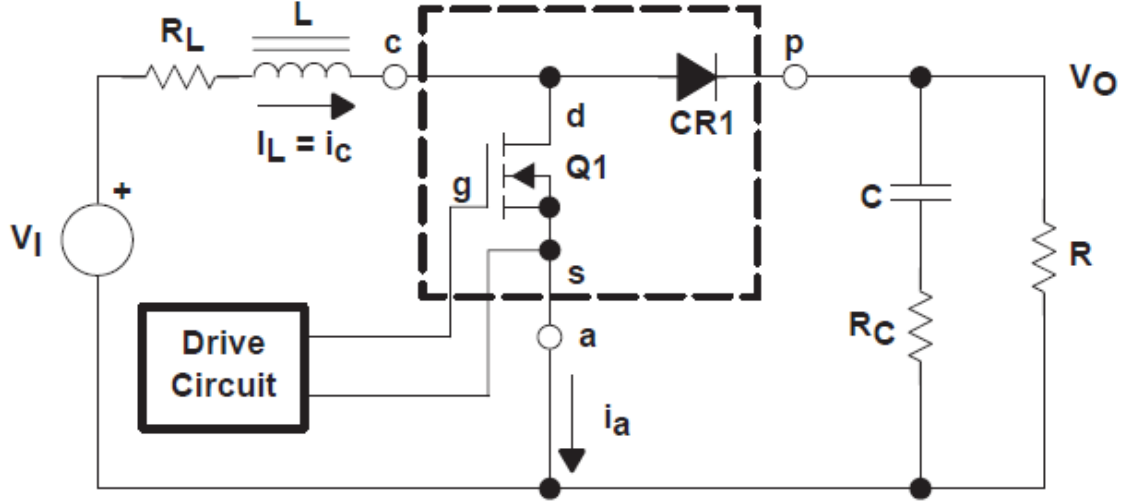


Figure 2.12: Boost converter basic schematic [8].

Analysis considerations

This topology can operate in two modes, continuous inductor current mode or discontinuous current mode, this analysis will focus on the first mode where the inductor current is continuous in the switching cycle under the following conditions: input voltage, output voltage, output load current and duty-cycle are constant, this is defined as steady-state. In addition, for the Q1 component shown in figure 2.12, an N-channel power MOSFET will be used. Two states are defined:

1. ON state if Q1 is on and the diode CR1 is off.
2. OFF state if Q1 is off and the diode CR1 is on.

On state

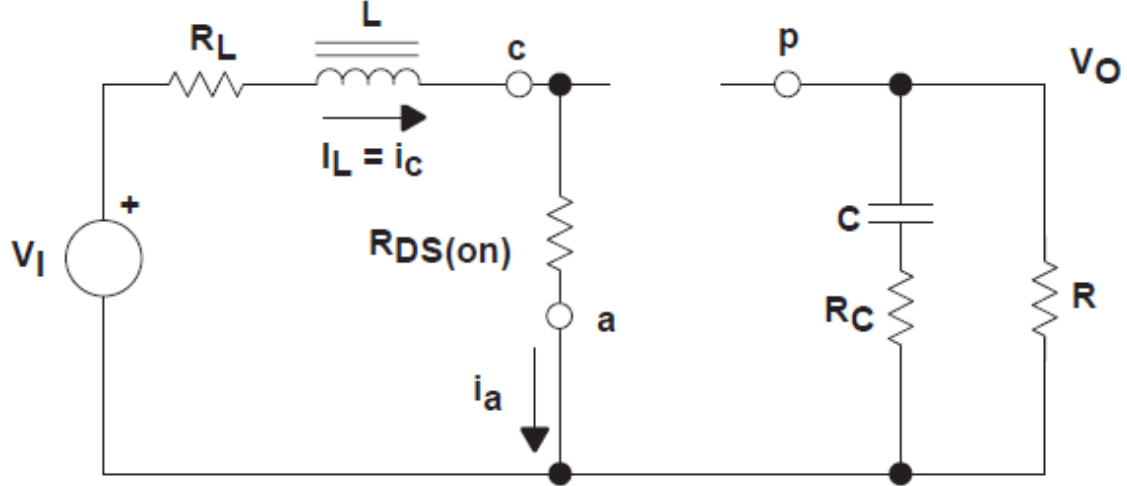


Figure 2.13: Boost converter: On state simplification [8].

In this state the current in the load is supplied by the output capacitor. If the transistor Q1 is replaced by a low resistance R_{ds} as illustrated in figure 2.13, it can be seen that the current goes from the source through the inductor and R_{ds} to ground because the diode is in reverse biased, this current increases linearly due to the constant voltage applied to the inductor, which is defined as:

$$V_L = V_I - (V_{DS} + I_L \times R_L) \quad (2.14)$$

Using the formula 2.6, the increase in the current of the inductor can be calculated as follows:

$$\Delta I_L (+) = \frac{V_I - (V_{DS} + I_L \times R_L)}{L} \times T_{ON} \quad (2.15)$$

Where T_{on} is the duration of the on state given by the formula 2.8. $I_L (+)$ is the inductor current ripple in the on state.

Off state

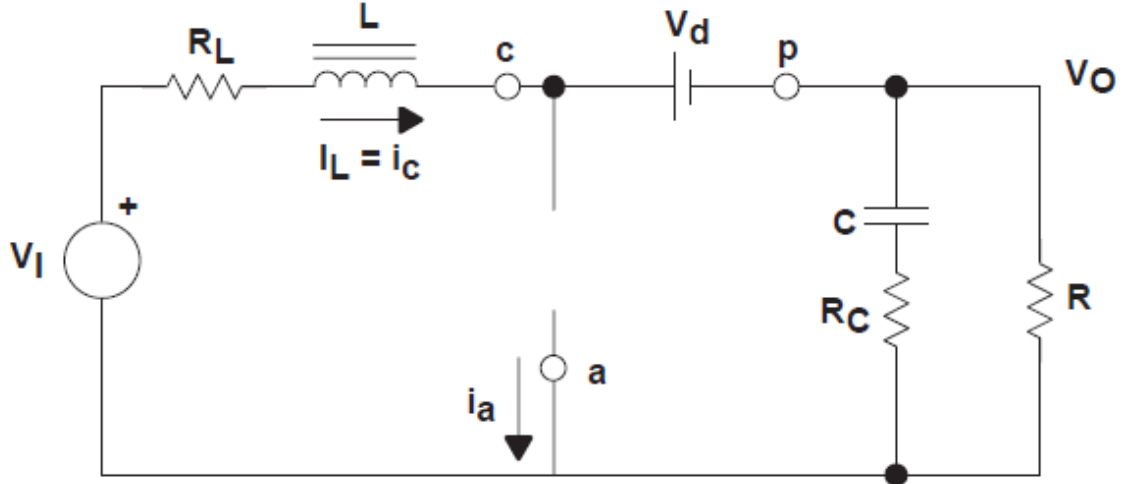


Figure 2.14: Boost converter: Off state simplification [8].

In this state the transistor Q1 is replaced by an open circuit as illustrated in figure 2.14 where the inductor current goes from the power supply to the output capacitor and load resistance, this current decreases linearly due to the constant voltage applied on the inductor, this voltage has the opposite sign in comparison with the inductor voltage in the on state which is defined as:

$$V_L = (V_O + V_d + I_L \times R_L) - V_I \quad (2.16)$$

Using the formula 2.6, the decrease in the current of the inductor can be calculated as follows:

$$\Delta I_L(-) = \frac{(V_O + V_d + I_L \times R_L) - V_I}{L} \times T_{OFF} \quad (2.17)$$

Where T_{OFF} is the duration of the Off state given by the formula 2.11.

Circuit operation

In steady state $I_L(+)$ and $I_L(-)$ must be equal, due to this condition it is possible to equate the above formulas and solve to find the value of V_{out} :

$$V_O = (V_I - I_L \times R_L) \times \left(1 + \frac{T_{ON}}{T_{OFF}}\right) - V_d - V_{DS} \times \left(\frac{T_{ON}}{T_{OFF}}\right) \quad (2.18)$$

Where $T_s = T_{ON} + T_{OFF}$, $D = T_{ON}/T_s$ and $(1 - D) = T_{OFF}/T_s$.

V_o is always greater than V_i and its value can be determined by the duty cycle (since D is always between 0 and 1), which is established by the control circuit [8].

2.4.3 LDO

This topology provides an output voltage that is lower than the input voltage with the same polarity [40], [8].

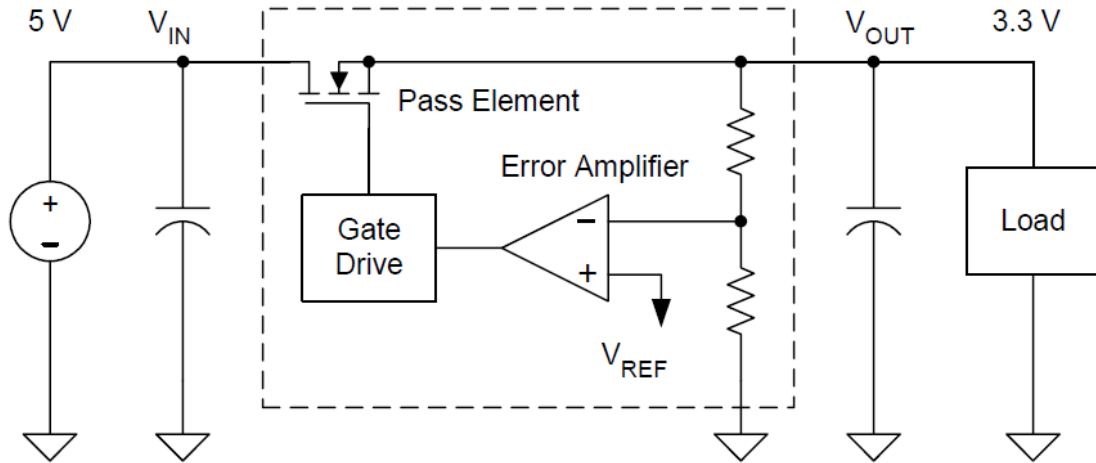


Figure 2.15: LDO basic schematic [9].

The LDOs are common in the power management systems of microcontrollers

and portable systems as blocks to provide stable regulated voltage and minimum ripple, this feature is very attractive for low noise systems [41].

One way that the system adds noise to the signals of interest is through the power supply due to switching converters or due to the power line that can have a frequency of 50-60 Hz. To deal with this noise there are two common options, one is using a passive low-pass pi filter that may require a lot of area on the PCB because the inductor a capacitor or a low noise LDO with a good PSRR, the advantage of this solution compared to the low-pass pi filter is a smaller size and lower implementation cost [30]. Linear dropout regulators need a minimum dropout voltage which is the minimum difference that must exist between the input voltage and the output voltage at a given output current and temperature.

$$V_{dropout} = V_{in_{min}} - V_{out} \quad (2.19)$$

To maintain regulated output voltage at the configured value, the LDO relies on an error amplifier and a transistor (the pass element). The amplifier error senses the output through the feedback pin and compares the value with a given reference, in this way the LDO tries to make the output equal to the reference by controlling the pass-element [9], [42]. This information is normally found in the manufacturer's data sheet and it is important to check that the operating conditions given for the specific application are within the ranges given by the manufacturer [9].

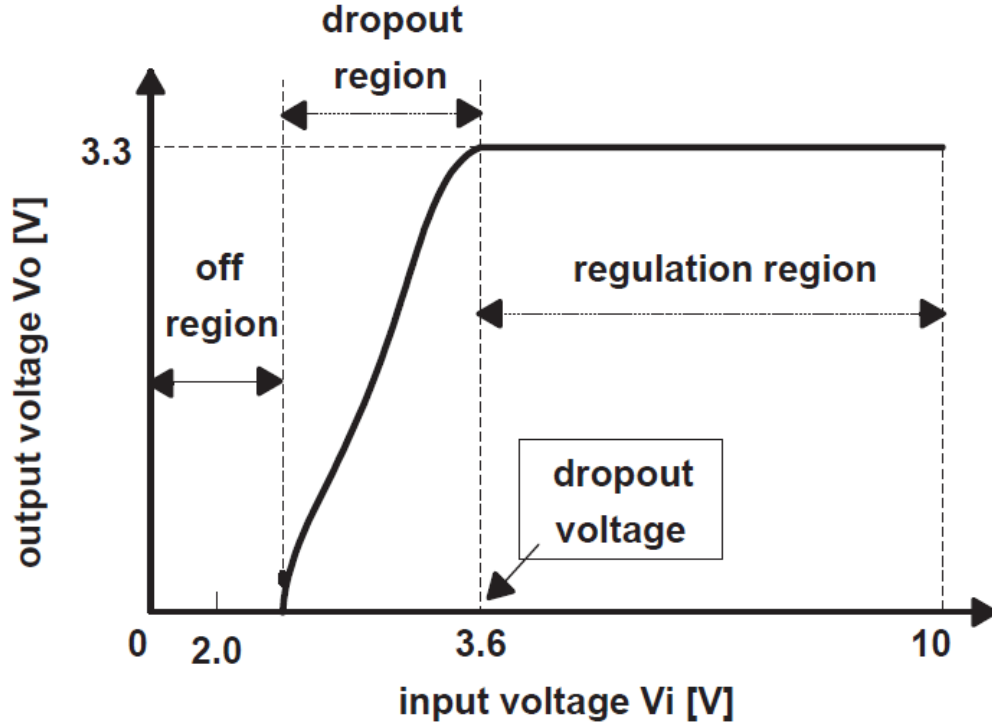


Figure 2.16: LDO dropout characteristic [10].

As an example, figure 2.16 shows the relationship between the input and output voltage of the TPS76733 3.3-V LDO regulator. The data sheet specifies that the dropout voltage is 350 mV to 1A.

$$0.35V = V_{in_{min}} - 3.3V \quad (2.20)$$

$$V_{in_{min}} = 3.3V + 0.35V \quad (2.21)$$

$$V_{in_{min}} = 3.65V \quad (2.22)$$

The minimum input voltage allowed by this LDO is 3.65V, less than that the LDO would no longer be in the regulation region and the pass element will not be able to set the output voltage to the desired value [9], [10].

2.4.4 Battery charge

In this section the charge of the LI-ION batteries will be explained. The battery charge is divided into two phases known as current limit phase and constant voltage phase illustrated in figure 2.17.

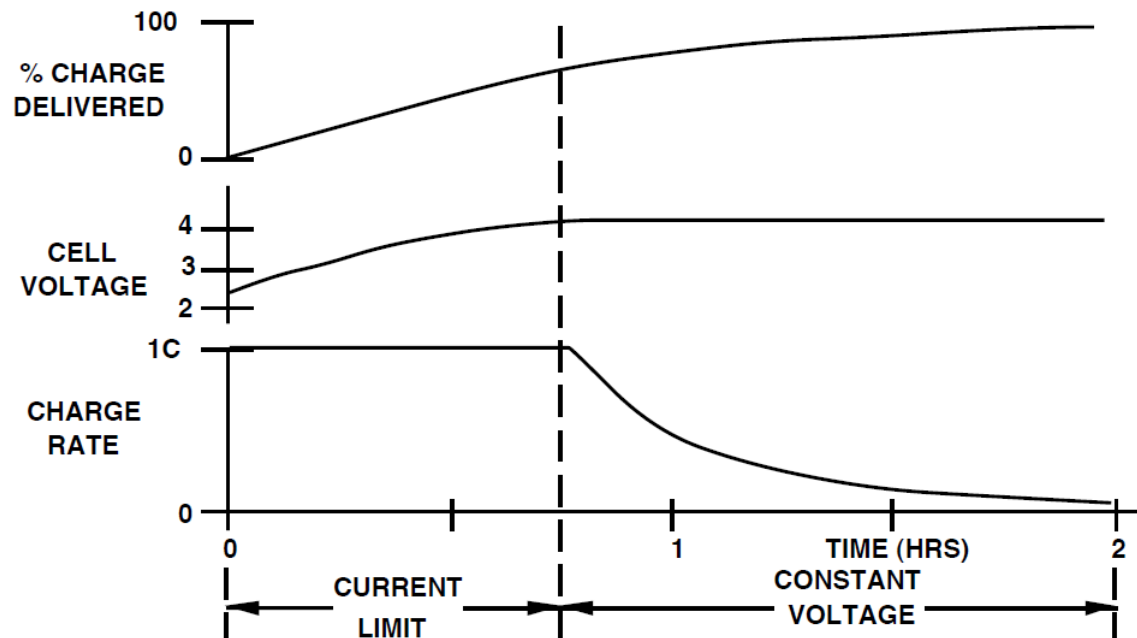


Figure 2.17: LI-ION charge description [11].

Current limit: In this phase the battery voltage will be below from the set point that most manufacturers recommend that it be at $4.2 \pm 0.05V$. To bring the level of the battery to the set point, the current limit is the maximum load current that flows into the battery to reach the set point, the voltage at the terminals of the battery is sensed and once it reaches the set point the constant voltage phase will continue. The current limit phase charges the battery at 65% in approximately 40 minutes [11].

Constant voltage: In this phase the current flowing to the battery is reduced to maintain the sensed voltage in 4.2V causing the current to fall exponentially, this is the reason why even though it just have to complete 35% of the remaining charge,

this phase lasts approximately 2 hours. The battery will be fully charged when the voltage drop in the equivalent series resistor (ESR) is negligible, which implies that the battery will have a voltage at its terminals of 4.2V and a very small current flows to the battery [11].

Chapter 3

Materials and Methods

This section presents the actions that were carried in order to characterize and reduce the noise in the analog circuit, determine the frequency response and design the power board. For the measurement and noise characterization, the measurement procedures, the tools used and the programs developed to analyze the measurements are detailed. For the design of the power board, three design options are shown and each is evaluated to choose the most appropriate one. Finally, the PCB design process for the power board is detailed. In some cases a brief theoretical description appears that is directly related to the actions carried out, this helps to understand the reasons behind each of them.

3.1 Feedback resistors

In order to evaluate the performance of the circuit as a function of the feedback resistance, they were soldered in three different positions (the feedback resistor in channel 1 and 3 has the same position). Each position corresponding to each of the four available channels. The following figure illustrates the three different positions where each feedback resistor was placed.

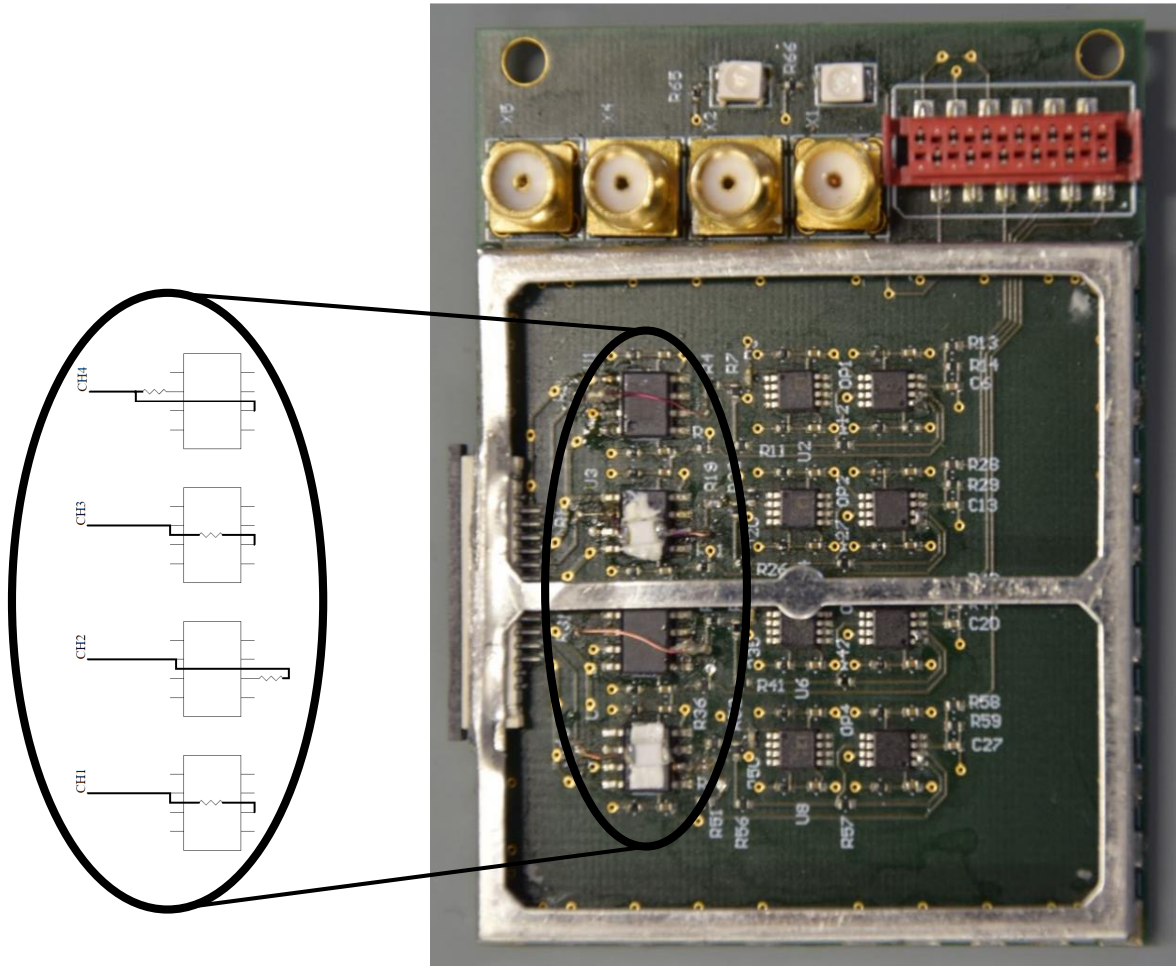


Figure 3.1: Feedback resistors placement. Power point 2016.

With the placement of the feedback resistors, it is now possible to evaluate three different aspects: the noise of the analog circuit when the electrolyte is placed in the printed sensor, the internal and external noise in the circuit and the impact on the noise level due to the different positions of the feedback resistor.

3.2 Noise characterization

3.2.1 Analogue circuit's thermal noise

For the detection of silver nanoparticles, it is required to place the electrolyte in the microelectrodes array (printed sensor) that adds noise to the system due to the electrode-electrolyte interface, but how much noise? That question will be answered with the experiments described in this section.

On the other hand, for the characterization of noise in the analog circuit it was necessary the evaluation of the internal noise produced by internal sources such as the components, the PCB or the power rails. This information is useful to evaluate if the magnitude of the signal recorded by the electrodes is distinguishable from the noise in such a way that it is not affected by it. This allows a correct obtaining and digitalization of the signal for its later analysis.

3.2.2 Evaluation and reduction of electromagnetic noise

Before the internal noise characterization of the system, it was necessary to analyze the existing noise sources in the analog circuit. In the case of external sources of noise, their effects should be attenuated, in such a way that the noise from internal sources of the system was predominant.

3.2.3 Noise experiments

Four experiments were established to be performed on the analog circuit, where the output measurements were obtained without having any input signal. The first experiment was the most simple setup. The output of the analog circuit was read directly and it was completely exposed to the environment (apart from the Faraday cage that is observed above the Pico Amp circuits) as shown in the figure 3.2.

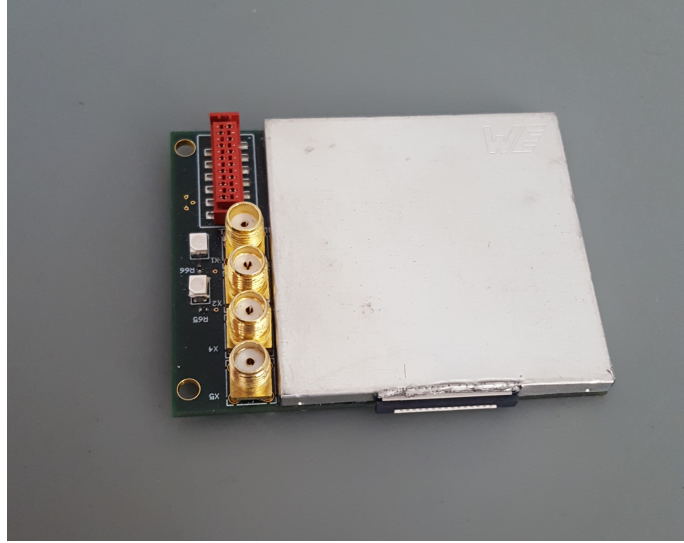


Figure 3.2: Analog circuit without input.

The second experiment consists of a 30x30 mm Faraday cage placed rudimentarily on the input of the analog circuit as shown in figure 3.2. This was done with the aim of analyzing if the circuit input had an antenna behavior to which coupled unwanted signals and if the use of some sort of shielding could improve the performance of the circuit.

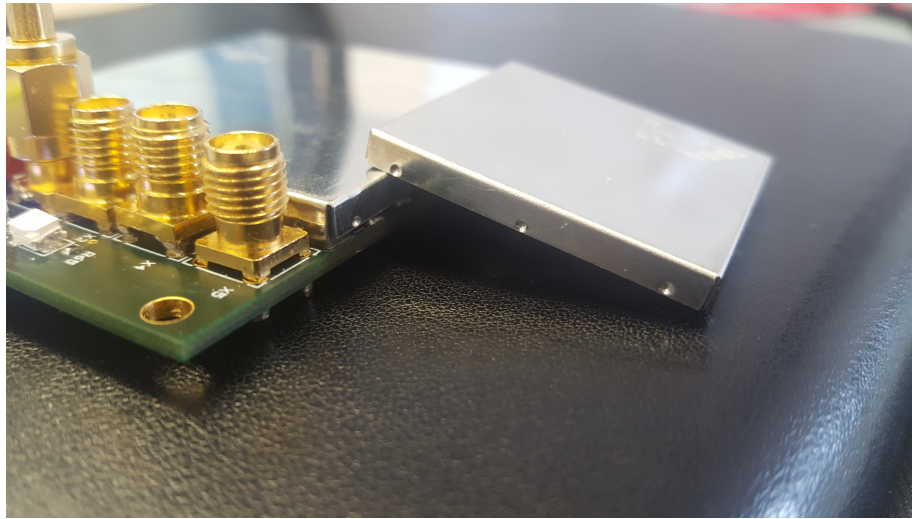


Figure 3.3: Faraday cage of 30x30 mm placed on analog circuit input.

The third configuration was based on a printed sensor (microelectrode array) at

the input of the circuit, without any input signal applied on it. Since the analog circuit requires this sensor to work, it was of interest to know the addition of noise caused by it. As mentioned in Fundamentals, the result of the analysis of the silver nanoparticles depends on the entire measurement system and the effects that each element adds [3].



Figure 3.4: Printed sensor coupled to the analog circuit input.

The fourth and last experiment carried out repeats the idea of placing a 30x30 mm Faraday cage on the input of the circuit, but with the printed sensor coupled to the circuit input. In the same way the effect of shielding the input of the analog circuit was analyzed.



Figure 3.5: Faraday cage of 30x30 mm on printed sensor.

The table 3.1 summarizes the experiments and the order in where they were carried out.

Tabla 3.1: Noise experiments performed. LaTeX.

Order	Experiment
1	Printed sensor is not coupled to the circuit input.
2	Printed sensor is not coupled to the circuit input. The circuit input is covered by a Faraday cage.
3	Printed sensor is coupled to the circuit input and it is not covered by a Faraday cage.
4	Printed sensor is coupled to the circuit input. The printed sensor/circuit input is covered by a Faraday cage.

3.2.4 Measurement procedure

The materials used for the noise analysis are listed below:

Materials

- Keysight DSOX2024A oscilloscope.
- TENMA 72-10495 power supply.
- VSP-300, Bio-Logic Science Instruments.
- SMA connector.
- Analog circuit.
- Faraday cage of 30x30 mm.
- Printed sensor.

To carry out the measurements of noise in the different conditions, the first step was to feed the integrated circuits with $+5V$ and $-5V$, this was done with the help of the TENMA 72-10495 power source or VSP - 300 power supply. The ground connection was done from the power supply ground to the analog circuit ground. Using the Keysight DSOX2024A oscilloscope and the SMA connector it was possible to read the output of each channel in the time domain. Using the oscilloscope menu,

the data was saved in a .csv file for further analysis.

With the measurements taken from the previous experiments, a written algorithm in MatLab was used to analyze the data and obtain the RMS and peak-to-peak values of the signal, likewise to obtain the PSD graph.

3.2.5 RMS and Peak to peak values: Algorithm

First of all, the file named as scope_n.csv is read, where n represents the measurement that is made, the oscilloscope assigns this number automatically or it can be edited in the options menu. Once the file is read, the information of the second column (voltage) is stored in a matrix of Nx1 where N is the number of samples taken by the oscilloscope.

Due to the power line the circuit had a signal with a frequency of 50 Hz. To eliminate this signal and only analyze the internal noise of the circuit, the signal of 50 Hz was separated, and it was subtracted from the original signal. The resultant signal is the internal noise of the circuit. To obtain the 50 signal, a running average filter with a windows size of 5 is applied to the voltage matrix. Once the signal was obtained without external noise, the RMS and peak to peak values of the signal were calculated. Figure 3.6 shows the flow diagram of this script.

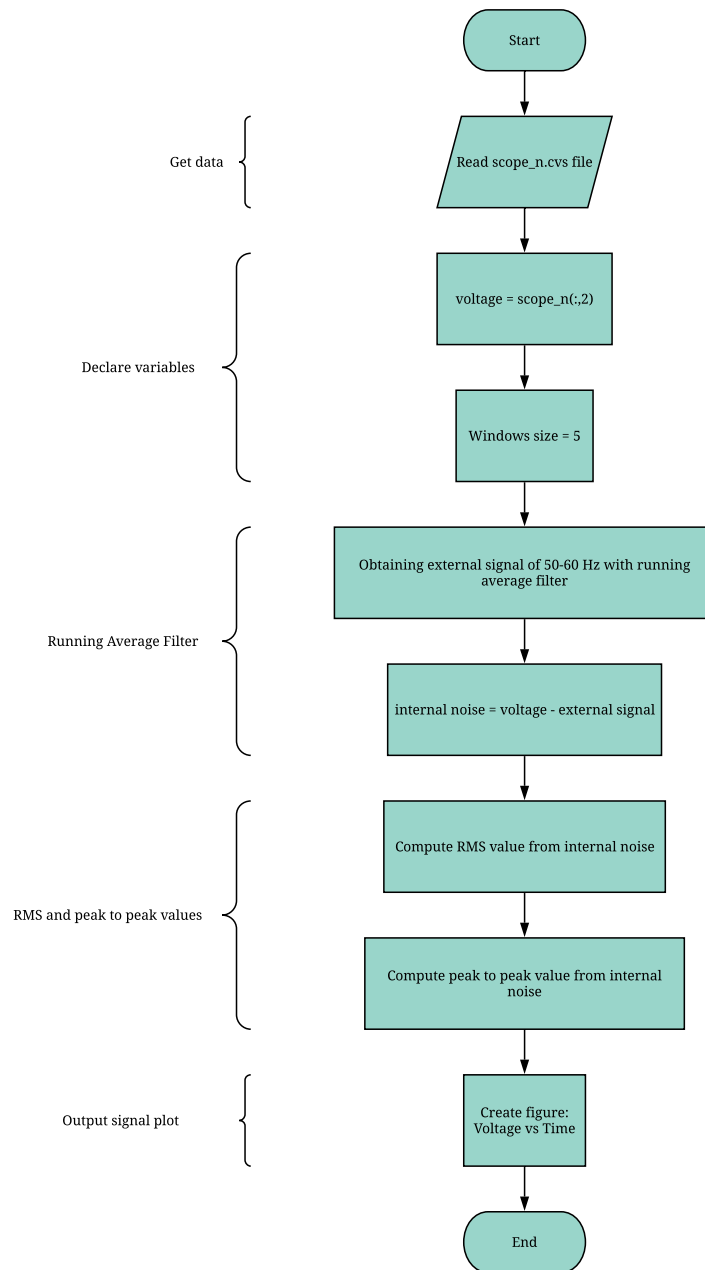


Figure 3.6: Algorithm for the calculation of the RMS and Peak to Peak values. Lucidchart.

3.2.6 PSD plot: Algorithm

The file named as scope_n.csv is read, where n represents the measurement that is made, the oscilloscope assigns this number automatically or it can be edited in the options menu. Once the file is read, two consecutive data are taken from the first column that represents time, these two values are subtracted, and the absolute value is calculated. The result corresponds to the time between each sample (dt), and the inverse of this value, represents the sampling frequency f_s . The information of the second column (voltage) is also stored in a matrix of Nx1 where N is the number of samples taken by the oscilloscope.

To generate the range of visible frequencies it is required to know both the minimum possible visible frequency and the maximum possible visible frequency. The minimum possible visible frequency is determined by the time in which all samples were taken. This can be calculated by multiplying the time between each sample (dt) by the total samples (N) and then calculate the inverse of that result, in other words, the sampling frequency must be divided by the number of samples taken.

$$f_{v_{min}} = \frac{1}{dt \times N} \quad (3.1)$$

$$f_{v_{min}} = \frac{f_s}{N} \quad (3.2)$$

The maximum possible visible frequency must meet Nyquist's theorem, that establishes that to digitize a signal correctly it must be sampled by a frequency of at least 2 times its maximum frequency. Because the signal is sampled by the oscilloscope and this frequency is known, the maximum possible visible frequency is:

$$f_{v_{max}} = \frac{f_s}{2} \quad (3.3)$$

To generate the set of visible frequencies that are used to create the plot including the minimum and maximum frequencies, the following formula is applied.

$$f = f_{v_{min}} \times \left[1, 2, 3, \dots, \frac{N}{2}\right] \quad (3.4)$$

Note that $f_{v_{min}} = \frac{f_s}{N}$ and when is multiplied by $\frac{N}{2}$ the result is the maximum possible visible frequency:

$$f = \frac{f_s}{N} \times \frac{N}{2} \quad (3.5)$$

$$f = \frac{f_s}{2} \quad (3.6)$$

The next step is to eliminate any offset in the signal. For that the mean of the data points is calculated and subtracted from the original signal. Then the fast Fourier transform (FFT) is calculated and the equation of the periodogram is applied to calculate the PSD through the FFT:

$$PSD = \frac{dt}{N} \times |FFT|^2 \quad (3.7)$$

However, since FFT is symmetric, a column matrix similar to the following would be obtained:

$$FFT = \begin{bmatrix} x \\ y \\ z \\ z \\ y \\ x \end{bmatrix} \quad (3.8)$$

Where only half of the matrix A multiplied by 2 is taken. Finally, the PSD graph is made. Figure 3.7 shows the flow diagram of this script.

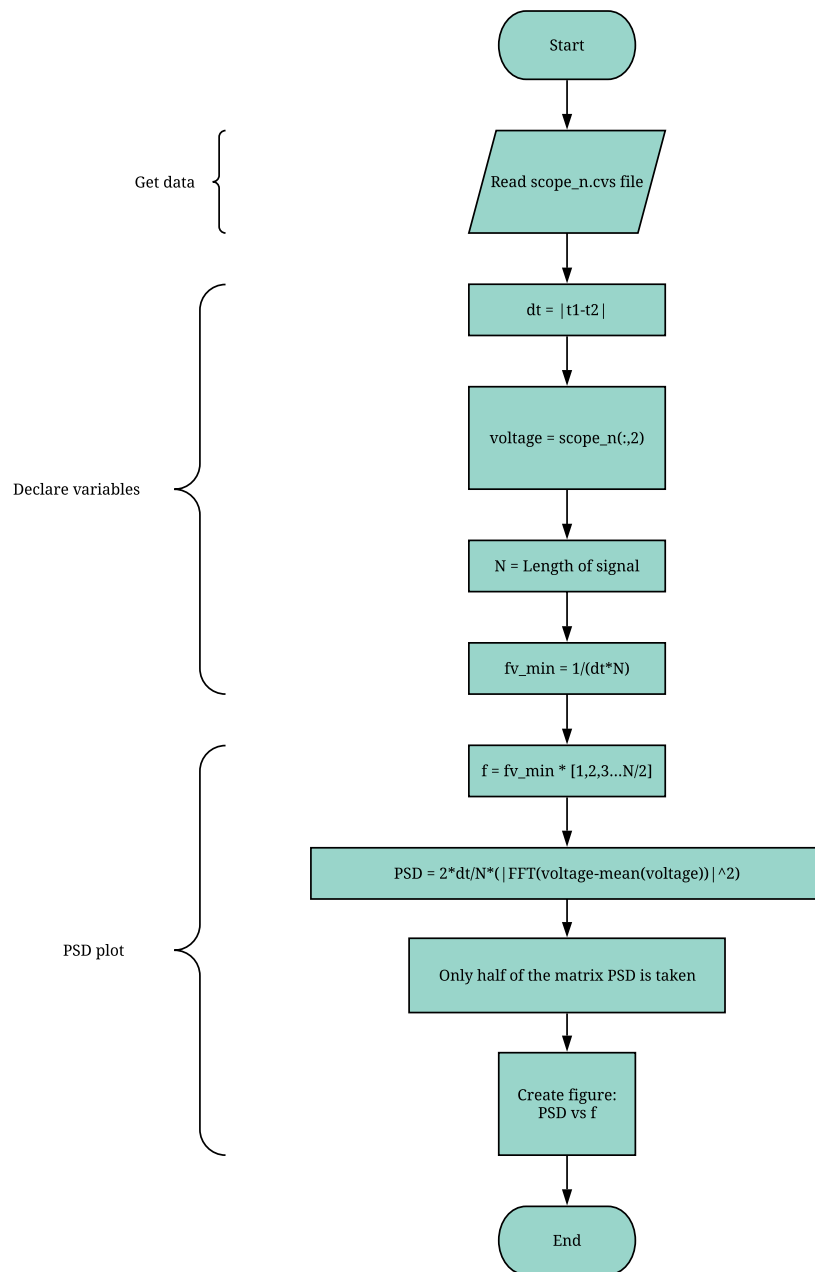


Figure 3.7: Algorithm for the calculation of the PSD plot. Lucidchart.

3.2.7 Aluminium enclosure

To reduce noise from external sources an aluminium enclosure was used as a Faraday cage. When there is a static electric field present in a closed cage made of conductive material, the free charges on the surface are redistributed. The negative charges (electrons) are accumulated on the positive side of the external electric field, this leaves the other side of the cage with positive charge (for the lack of electrons). This results in an electric field of opposite polarity respect the external electric field, thus canceling the effect of the latter. In this way no static electric field can go inside the conductor or leave it (due to the same effect) and the electrostatic balance is maintained (there is no movement of charges). This cage is known as Faraday cage [43].

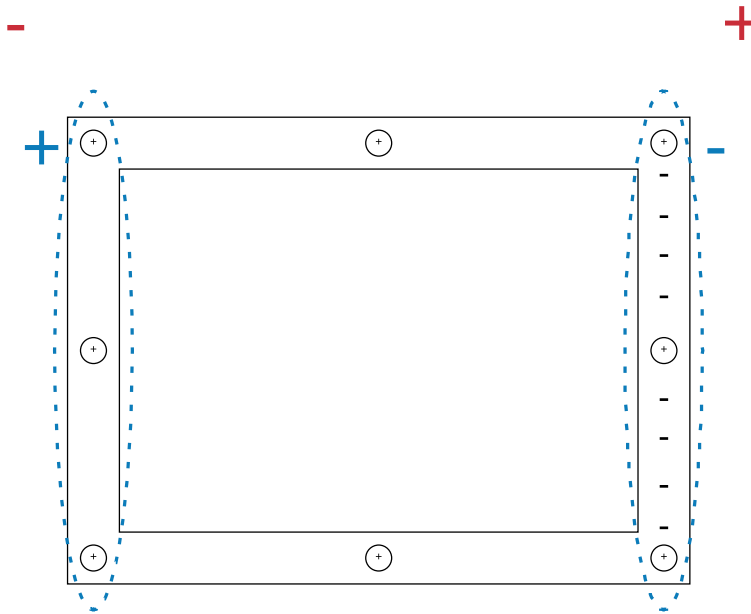


Figure 3.8: Faraday cage principle. Lucidchart.

However, for non-static fields, that is they vary with time, another effect occurs in the same enclosure aluminium called skin effect. Electromagnetic waves remain in a very thin layer on the surface of the conductor due to the film depth. This depth is a measure of penetration (δ) that a wave has in a good conductor and is given by

the following equation [44]:

$$\delta = \frac{1}{\sqrt{\pi f \mu \sigma}} \quad (3.9)$$

Where f is the frequency of the electromagnetic wave, μ is the permeability constant and σ is the conductivity of the medium. The above gives rise to the skin effect that describes the attenuation suffered by an electromagnetic wave when it travels deeper in a good conductor. The attenuation is produced by the factor $e^{-\alpha\delta}$ that multiplies the amplitude of the electromagnetic wave [44].

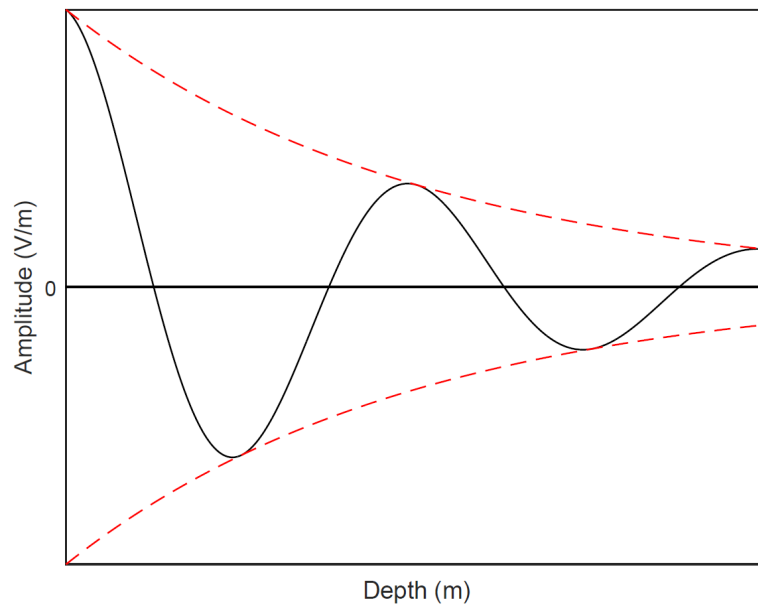


Figure 3.9: Illustration of the attenuation of an electric wave due to the skin effect in a good conductor. MatLab.

For experiments related to electrochemistry where the signals to be measured are less than $1\mu\text{A}$, the use of Faraday cages is recommended, especially if they are affected by the power line. The potential in the aluminium enclosure may be different from the ground potential of the measuring instrument. This produces AC voltages that can be coupled to the electrodes by adding noise to the measurement. To avoid that effect and ensure proper operation it is necessary that the aluminium enclosure

is connected to the same ground as the measuring instrument [43], [45].

Therefore, an aluminium enclosure was modified to contain the analog circuit inside, where the only connections with the outside are the power inputs, the potential offset and the circuit output. It is important to mention that the Faraday cage loses effectiveness the more perforations it has, for that reason, the holes made were barely the necessary measure to introduce the required connectors. Once the aluminium enclosure was modified, the same experiments detailed in table 3.1 were carried out.

3.3 Frequency response analysis

If an individual impact of a silver nanoparticle is assumed, it produces a current spike similar to that observed in figure 3.10 where the red trace is the impact of a 10 nm particle on a 3 μm electrode. The blue trace is the impact of a 20 nm particle on a 24 μm electrode [12].

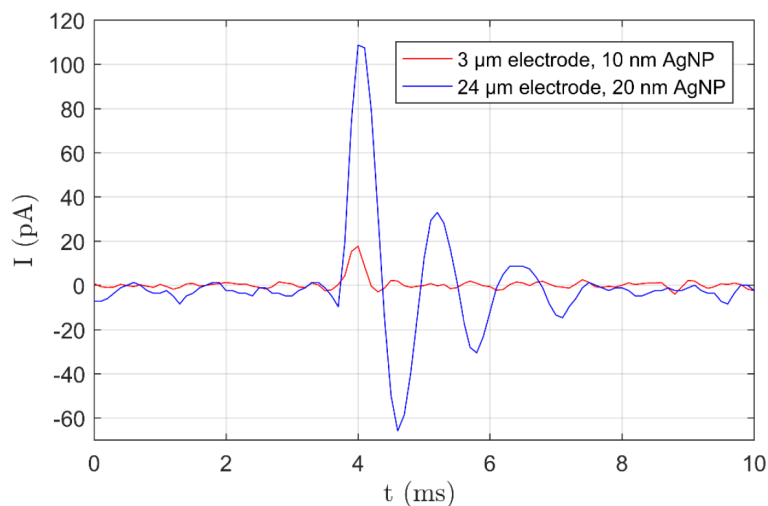


Figure 3.10: Illustration of current spike produced by nano-impacts [12].

The useful information occurs in the first instant since the other oscillations are made by instabilities in the electronics. These instabilities are generated by electrode-electrolyte capacitance. One way to reduce these oscillations is by using a low pass

filter, however this has another use. The first instant, that is, the time of the first oscillation of interest can be determined by this filter, more specifically by its cutoff frequency. In addition, this influences the shape of the measured peak. The higher the cutoff frequency, the greater the amplitude and the shorter the time of the first oscillation. The area under the curve is the same what changes is the distribution of that area. Because at lower cutoff frequency the peak time increases, it is difficult to identify several current peaks, this is related to the concentration of silver nanoparticles. It is advisable to analyze the effect of different cutoff frequencies in the study of nano impacts. As an example, for the case of a 50 nm silver nanoparticle, the current spike depends of the transferred charge. Assuming that the whole particle is oxidized, Q is given by [12]:

$$Q = \frac{VF\rho}{M} \quad (3.10)$$

Where V is the volume of the particle (assuming a spherical shape), F is the Faraday's constant, ρ is the density of silver and M is the molar mass of silver. If $V = 6.54498 \times 10^{-23} \text{ m}^3$, $\rho = 10490 \text{ kg/m}^3$ and $M = 0.10787 \frac{\text{Kg}}{\text{mol}}$:

$$Q = 615fC \quad (3.11)$$

To calculate the current spike of the silver nanoparticle by assuming that it is completely oxidized, the following formula is used:

$$I = \frac{Q}{t} \quad (3.12)$$

Where t is the duration of the spike of interest.

$$I = \frac{615fC}{0.303ms} \quad (3.13)$$

$$I = 2030pA \quad (3.14)$$

In the case of the analog circuit under study, this was designed to have the cutoff frequency of 3.3 KHz, that makes the first oscillation occur in the first 0.303 ms. The main task of this section was to characterize the frequency response of the analog circuit to verify that effectively the cutoff frequency is 3.3 KHz.

3.3.1 Measurement procedure

The materials used for the frequency response analysis are listed below:

Materials

- Keysight DSOX2024A oscilloscope.
- TENMA 72-10495 power supply.
- RIGOL DG4162 waveform generator.
- SMA connector.
- Analog circuit.
- Printed sensor
- 1 M Ω resistor.

To measure the frequency response in the analog circuit in terms of the ratio between the output current and the input current, a printed sensor coupled to the input of the analog circuit was used to apply an input current of 2 nA. With this current the analog circuit delivers an output voltage of 2 V (because 1 pA at the input is translated into 1 mV at the output according to the topology of the Pico-Amp circuit). The output current due to the feedback resistor of 1 G Ω must be 2 nA by Ohm's law. To obtain 2 nA at the circuit input, the function generator RIGOL DG4162 was configured with sinusoidal waveform with an amplitude of 20 mV with a series resistance of 10 M Ω and thus to obtain a current of 2 nA. The frequency of the wave was changed from 20 Hz to 50 Hz, then from 400 Hz to 10 KHz with steps of 400 Hz, additional data were taken at 11 KHz and 12 KHz. At the end 29 different frequency measurements on each channel were taken. Using the oscilloscope

menu, the data were saved in a .csv file and use it for further analysis. Figure 3.11 illustrates the measurement configuration for the frequency response.

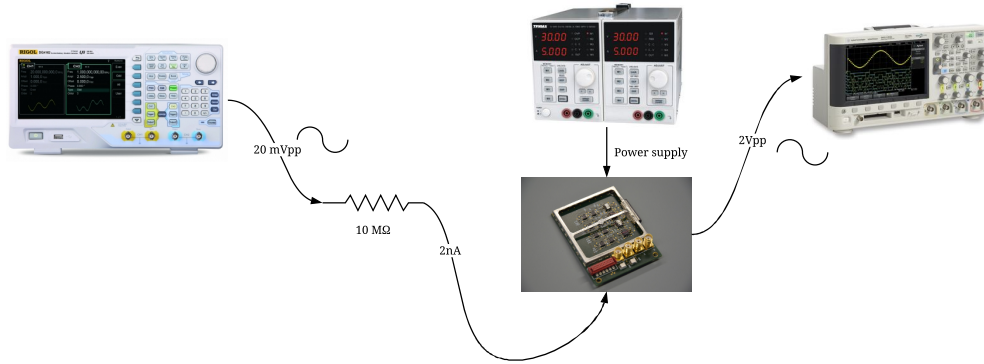


Figure 3.11: Measurement setup for the frequency response of the analog circuit. Lucidchart.

3.3.2 Frequency response: Algorithm

To calculate the cutoff frequency of the system, the 29 .csv files are analyzed. Each file contains 3 columns, the first is time, the second is the output voltage and the third is the input voltage. First, the current related to each voltage is calculated by Ohm's law. 10 MΩ for the input voltage and 1 GΩ for the output voltage. Then the running average filter is applied since the signals present noise, especially the input signal because it has the lower amplitude.

With the above results, the peak-to-peak value of each signal is calculated. With

this information it is possible to know the gain of the system that in terms of current should be 1. The gain is calculated as:

$$Gain = 20 \log \frac{I_{out}}{I_{in}} \quad (3.15)$$

In addition, a vector is generated that includes the 29 frequencies used. Then the amplitude response of the system is plotted. Finally, the cutoff frequency is calculated when the gain drops 3dB. Figure 3.12 shows the flow diagram of this script.

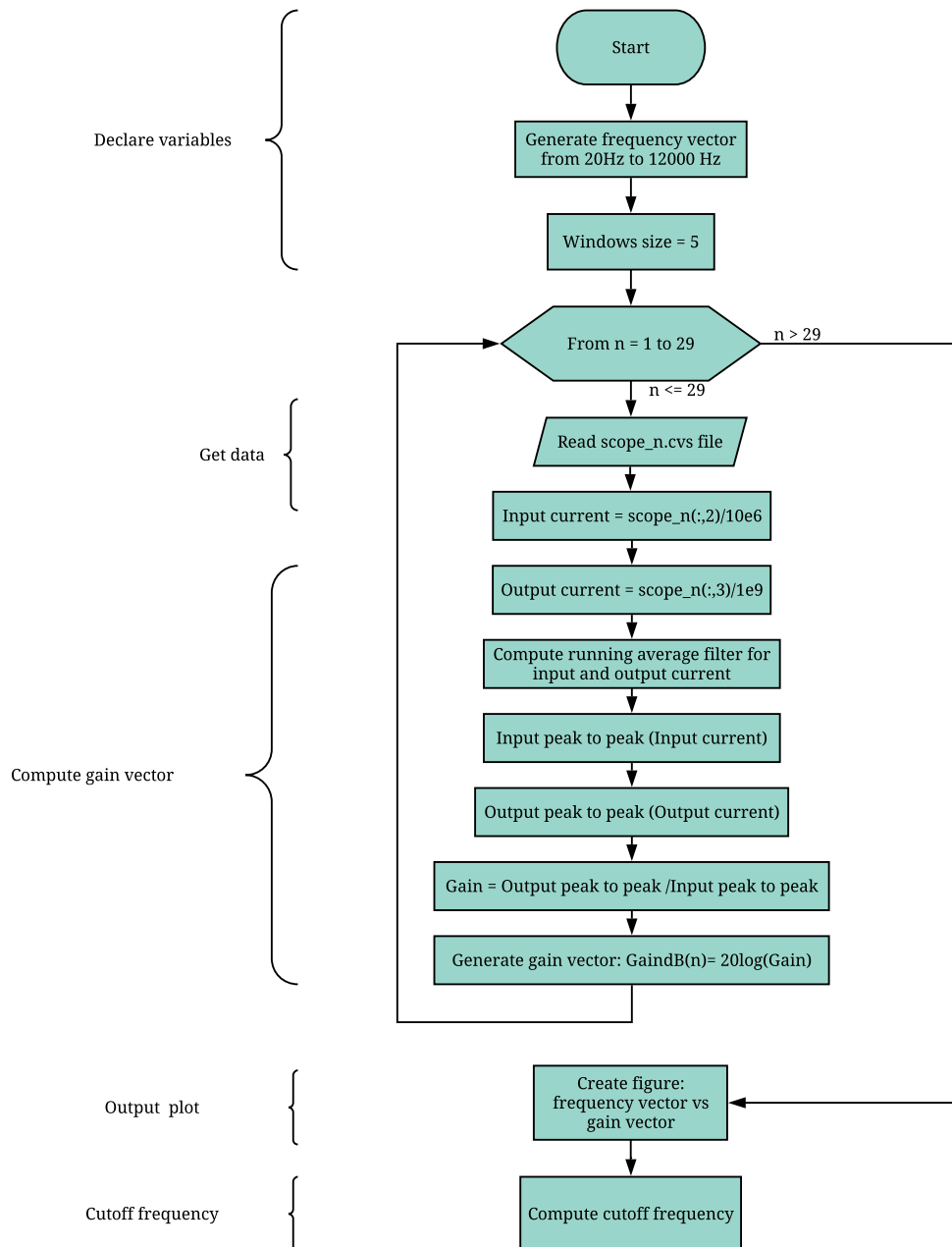


Figure 3.12: Algorithm for the calculation of cutoff frequency. Lucidchart.

3.4 Power board: Choosing the design

The first step in the design of the power board was to determine the current and voltage required for the analog circuit and the digital circuit. In the case of the analog circuit, the current value that was used was the quiescent current. Quiescent current is defined as the current that flows through the op-amp when it has not load connected to the output (high impedance). Because the operational amplifiers are connected one behind the other, being the output of the first the input of the second, and the input of an op-amp is high impedance, the current used by each op-amp corresponds to the value of the quiescent current. The theoretical quiescent current was obtained with the information in the data sheets and subsequently its value was compared by measuring the current given by the power supply. The voltage value was also extracted from the data sheets and the design of the Pico-Amp circuit.

Although the analog circuit has four channels which implies four Pico-amps circuits, it is desired to increase the capacity to 8 channels, this was considered when the power board was designed. To determine the voltage and current required by the digital components, the maximum current and voltage information given by the data sheets was used. The voltage and current consumption characteristics due to the different digital and analog components are summarized in the following tables.

Tabla 3.2: Voltage and current supplied to digital components. LaTeX.

Device	Model number	Number of components	Voltage supplied (V)	Maximum current supplied (mA)	Total maximum current supplied (mA)
ADC	ADS8688	1	+5	16	16
4.096V voltage reference - 30 mA output	REF5040	1	+5	1.2	1.2
DAC	DAC8563	1	+3.3	1.6	1.6
1.65V, 3.3V voltage reference -20 mA output	REF2033	1	+5	0.46	0.46
Dual op-amp	OPA2188	1	+5	0.6	0.6
Bluetooth module	RN-42	1	+3.3	50	50
Voltage inverter - 200 mA output	LM2776	1	+5	0.2	0.2
Microprocessor (260 μ A/ MHz) for 180 MHz	STM32F429I	1	+3.3	46.8	46.8

Tabla 3.3: Voltage and current supplied to digital components. LaTeX.

Device	Model number	Number of components	Voltage supplied (V)	Maximum quiescent current (mA)	Total maximum quiescent current (mA)
Ultra-Low input biased amplifier	OPA129UB	8	± 5	1.8	14.4
Voltage offset amplifier	AD822A	8	± 5	1.6	12.8
Summing amplifier	AD820A	8	± 5	0.8	6.4

The following table shows the required voltage of the power rails, as well as the current that each rail must supply.

Table 3.4: Maximum voltage and current requirements for the power board. LaTeX.

Voltage (V)	Current (mA)
+3.3	52.06
+5	33.6
-5	98.4

With the objective to keep the nanoparticle sensor working for one hour, a battery of at least 200 mAh is required. However, it is easy to find commercial batteries between 1800 mAh and 2000 mAh and this increases the time in which the device can work. Below are three different configurations of batteries and topologies to meet the requirements of table 3.4.

3.4.1 Solution 1

A possible option is to use AA batteries that have a voltage of 1.5V and a current from 1100 mAh to 2050 mAh depending on the manufacturer. Using a battery holder, it is possible to connect 4 batteries in series and generate 6V. All the voltages that are required are below 6V, so the appropriate topology would be the LDO to establish the power rails of 3.3V, 5V and -5V. This system would allow to use single-use batteries or to buy an external AA battery charger and use rechargeable batteries. Figures 3.13 and 3.14 illustrate the previous solution.

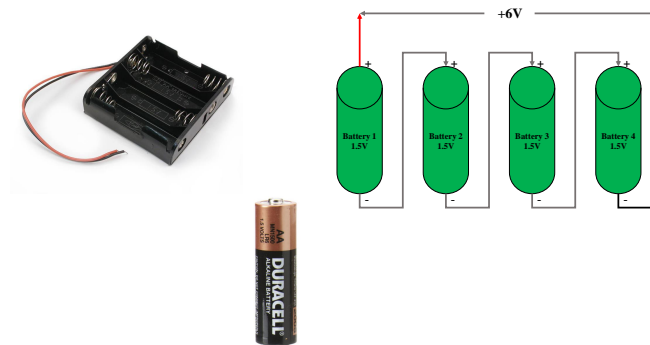


Figure 3.13: Battery configuration to obtain 6V. Power point 2016.

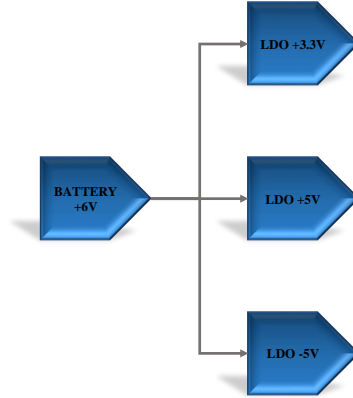


Figure 3.14: Block diagram for solution 1. Power point 2016.

The disadvantage of this solution is the stability of the output voltage. Due to the discharge curve of any battery, the voltage of this is not constant in time, but goes from a maximum value, passing through the nominal value, to the minimum value given by the manufacturer. Since the LDO have the restriction of the dropout voltage, once the batteries are discharged to such an extent that the difference between the input and output voltages of the LDO is less than the dropout voltage, the regulation cannot be maintained anymore.

3.4.2 Solution 2

In this solution, it was decided to use a LI-ION 3.7 V battery. With which three topologies are required. The first one LDO to get 3.3V, this because the input voltage (3.7V) is greater than the output voltage (3.3V). The second topology is the boost converter, since the input voltage is lower than the output voltage (5V). Finally, the inverting converter topology is used since the input voltage in that block is opposite polarity to the output (-5V). Additionally, this design has a battery charger. The block diagram is illustrated in figure 3.15.

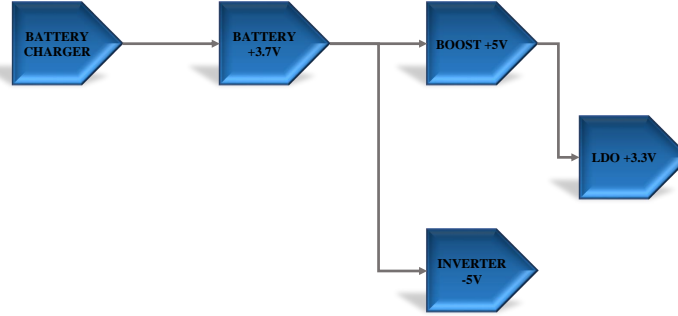


Figure 3.15: Block diagram for solution 2. Power point 2016.

The problem with this solution is that both the boost converter and the inverting converter are switching supplies that, due to the switching frequency, can add additional noise to the measurement of the analog circuit [37].

3.4.3 Solution 3

A third solution consists of combining the topologies of switching supplies with the LDO. In this solution, a 3.7V LI-ION battery is still used. The main idea of this proposal is to obtain stable voltages at the input of the LDO regardless of the variation in the voltage of the battery due to the discharge curve. To achieve this, the topology Boost converter and inverting converter are used to establish voltages of +6V and -6V respectively. The output voltages of the switching supplies will be the input voltages of the LDO, in this way the advantages of both topologies are combined to attenuate the negative effects of each one. While the switching supplies serve to maintain stable voltages to the benefit of the LDO, the LDO serve to attenuate noise due to the switching frequency. With this approach power rails will be as cleaner of noise as possible. This design also includes the battery charger.

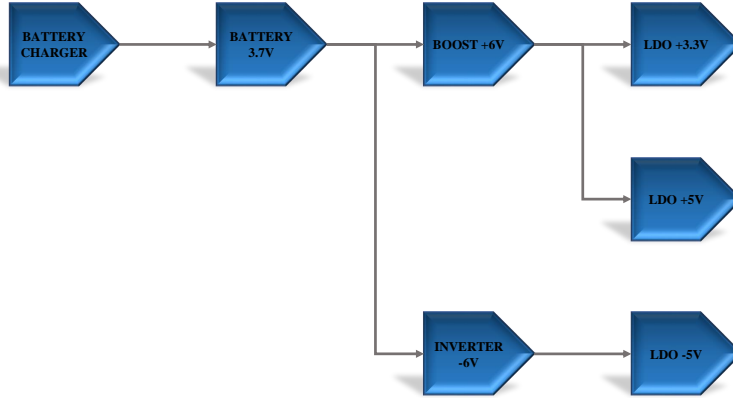


Figure 3.16: Block diagram for solution 3. Power point 2016.

The disadvantage of this solution implies a higher cost due to an increase in the number of components for the implementation, likewise its design is more complex than the previous ones and increases the development time.

3.4.4 Choosing a solution

Based on the description of the previous solutions, the aspects of functionality, cost and time of implementation are compared to determine the ideal solution to be implemented.

In the aspect of functionality, solution 1 is disadvantaged with respect to the other two, since it is not possible to guarantee that the system works within the requirements given by the analog circuit and the digital circuit. Because the functionality aspect is of critical importance this solution is discarded. However, the idea of the use of AA batteries is rescued because it is a quick way to generate a prototype to know its functionality. Solutions two and three comply with the functionality at a general level, since both are able to supply the current and voltage necessary for the

measurement system. However, because this is a project in development phase, it is not yet possible to determine how much the noise of the power source could affect the operation of the system. For that reason, it is decided to look for the alternatives that generate the least amount of noise possible and in that line solution 3 is the one that presents a clear advantage.

Regarding the cost of the system, solution 2 presents a lower cost. If compared with solution 1, solution 2 does not require the purchase of an external charger or multiple batteries during its useful life, which in the long term implies a lower cost. Compared to solution 3, solution 2 needs fewer components, which makes its implementation cheaper.

In terms of implementation time, solution 1 is the easiest to implement, since it only requires 3 integrated circuits and does not have the design of the battery charger. However, it has already been established that this solution is not useful due to its operation. This leaves the comparison in terms of the implementation time between the solution 2 and 3. Where both designs are similar with the only difference that the design 2 only use one LDO, which makes its implementation time lower. However, this saving over time is negligible between solution 2 and 3 since the topology of the LDO only requires a few external components.

Considering the previous analysis and despite the fact that the evaluation in the aspect of cost and time of implementation for solution 3 are worse compared to solution 2, none of the above is a critical disadvantage. Most LDOs cost around 2-3 euros. On the other hand, the difference in development time is given by the two extra LDOs and these only require a few external components for their operation. The above does not represent a substantial challenge to define the solution.

This is how the aspect of functionality is prioritized as the most critical to define the solution to be implemented. Of the three solutions presented, solution 3 presents the best performance in terms of functionality and is therefore the chosen design.

3.5 Power board: Development of the design

The design of the power board follows the block diagram shown in figure 3.16. Each block is a sub-circuit made by an integrated circuit with external components and connections. With the power requirements for the analog board and the digital board it was possible to determine the required topologies and analyze the different components offered in the market. All integrated circuits that were used have recommended values for most of the components that have to be tied to the pins to establish the required topology, only some of them should be calculated. The integrated circuits that were chosen, the calculations and considerations will be shown in this section.

3.5.1 Battery

Due to the discharge curve, capacity and stability, a rechargeable lithium ion battery was chosen, specifically 103456A-1S-3M because it was the option with more balance between price, features and delivery time. Some important features about this battery are listed below.

Tabla 3.5: Battery specifications taken from [16]

Parameter	Value
Nominal voltage	3.7V
Capacity	2050mAh (0.2C discharged from 4.2V to 2.75V)
Charge voltage	$4.20 \pm 0.05\text{V}$
Max charge current	0.5C(1025mA)
Max discharge current	2.2A

3.5.2 Battery charger

The component selected to perform this task is BQ2506 Standalone 3.0-A Single Cell Battery Charger from Texas Instruments [46], [47]. One advantages of this component is that it is completely analog, so other digital components are not necessary to configure it. If the battery voltage drops below 2.6 V the system will shut down completely to protect the battery from over discharge. The configuration of this component was done with the help of Webench, this is an online tool offered by Texas Instruments to design different projects depending on the requirements. The next table shows the requirements that must be met in order to configure the battery charger.

Tabla 3.6: Battery charger requirements. LaTeX.

Parameter	Value
Number of cells	1
Cells in parallel	0
Cells in series	0
Cell capacity	2050mAh
Total capacity	2050mAh
Charger source	USB
Minimum input voltage	4.75V
Maximum input voltage	5.25V
Maximum input current	500mA
Charge voltage	4.2V
Charge current	500mA
Ambient temperature	30°C

With the above information is easy to get an schematic from the Webench tool. In the following figure the schematic is shown.

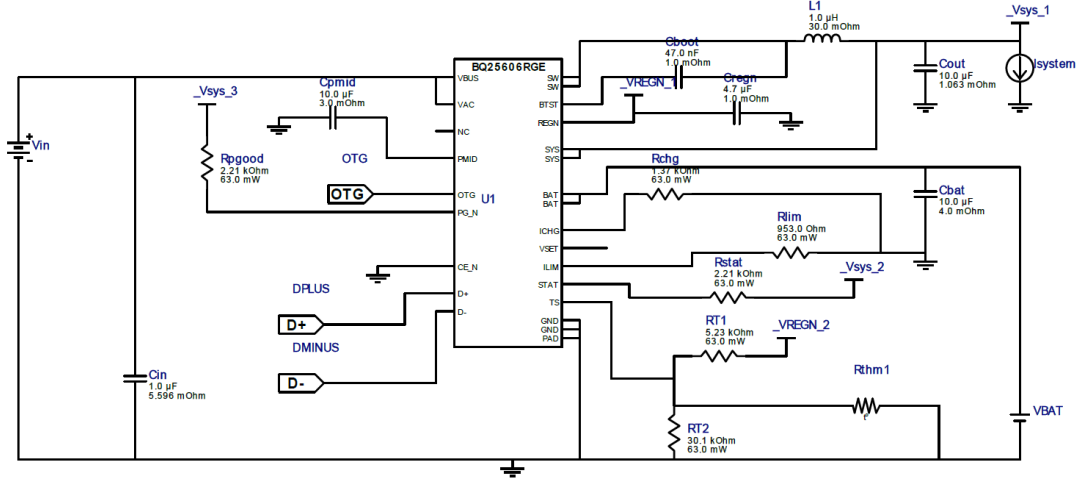


Figure 3.17: Battery charger schematic. Source: WEBENCH® Power Designer tool by Texas Instruments.

The values of the passive components above were compared with the recommended values in the data sheet, all of them are in the recommended ranges. One of the formulas provided in the data sheet is how to set the maximum input current using a resistor connected between ILIM pin and ground.

$$R_{ILIM} = \frac{K_{ILIM}}{I_{MAX}} \quad (3.16)$$

Using the typical value for $K_{ILIM} = 478A\Omega$ (according to the data sheet) and $I_{MAX} = 500mA$

$$R_{ILIM} = \frac{478A\Omega}{500mA} \quad (3.17)$$

$$R_{ILIM} = 956\Omega \quad (3.18)$$

The value given for this resistance in Webench was 953Ω .

Other advantage of using Webench tool is that it provided the part number of the components that could be used.

3.5.3 Boost: Positive voltage to feed LDOs TPS7A47

The boost converter was design to get +6V and use that output as the input of the positive LDOs to establish +3.3V and +5V. The selected boost converter was TPS65131 Positive and Negative Output DC-DC Converter from Texas Instruments [13], [48], [49]. This component can supply positive and negative voltage with a maximum output voltage of $\pm 15\text{V}$ and it has a switch current limit of 2 A (this parameter helps to define the maximum output current). The input voltage range is 2.7 V to 5.5 V. A typical schematic taken from the data sheet is shown below.

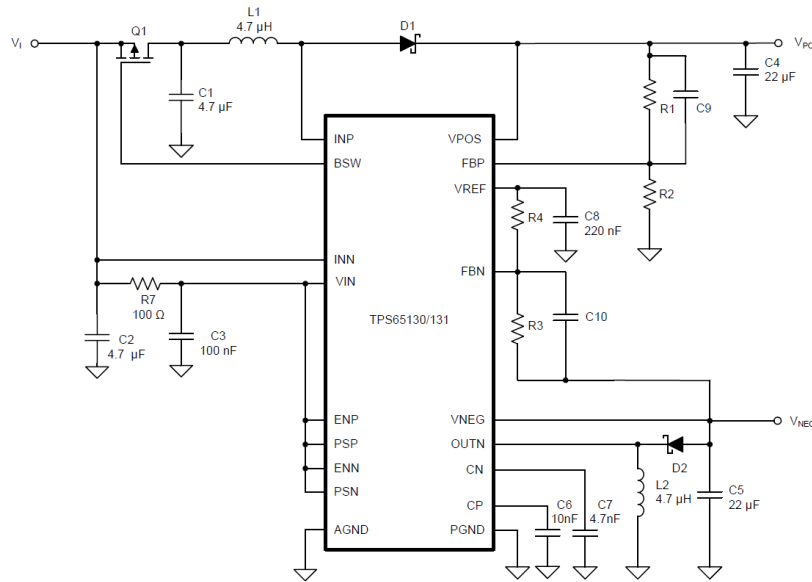


Figure 3.18: Boost converter schematic [13].

Most of the components or signals that must be connected to the pins have specific values given in the data sheet. However, the calculations written in the data sheet were followed in order to confirm the values and to finish the configuration of the values of the components that do not have a recommended value, but depend on the specific application. Although this boost converter can provide positive and negative outputs, in this section only the calculations of the positive output voltage are shown, later, when the analog negative power rail section is discussed the calculations for the negative output voltage will be shown.

Feedback resistor:

$$R_1 = R_2 \times \left(\frac{V_{POS}}{V_{REF}} - 1 \right) \quad (3.19)$$

Where V_{REF} is the reference voltage, R_2 is the resistor tied to ground in the voltage divider and V_{POS} is the positive output voltage. Using the typical value of $V_{REF} = 1.213V$, $R_2 = 130K\Omega$ (according to the data sheet) and $V_{POS} = +6V$, it is obtained:

$$R_1 = 130K\Omega \times \left(\frac{6V}{1.213V} - 1 \right) \quad (3.20)$$

$$R_1 = 513K\Omega \quad (3.21)$$

Inductor:

In order to know the value for the inductor it is necessary to compute the peak inductor current I_{L-P} , it must be lower than switch current limit (2A):

$$I_{L-P} = \frac{V_{POS}}{V_{I_MIN} \times 0.64} \times I_{POS} \quad (3.22)$$

Where V_{I_MIN} is the minimum input voltage, V_{POS} is the positive output voltage and I_{POS} is the positive output current. Using $V_{I_MIN} = 3.5V$, $V_{POS} = +6V$ and $I_{POS} = 400mA$, it is obtained:

$$I_{L-P} = \frac{6V}{3.5V \times 0.64} \times 400mA \quad (3.23)$$

$$I_{L-P} = 1.1A \quad (3.24)$$

It is now possible to compute the inductor value:

$$L_1 = \frac{V_{I_MIN} \times (V_{POS} - V_{I_MIN})}{\Delta I_{L-P} \times f \times V_{POS}} \quad (3.25)$$

Where ΔI_{L-P} is the 20% of I_{L-P} and f is the oscillator frequency given in the data sheet. Using $\Delta I_{L-P} = 0.22A$ and $f = 1380KHz$, it is obtained:

$$L_1 = \frac{3.5V \times (6V - 3.5V)}{0.22A \times 1380KHz \times 6V} \quad (3.26)$$

$$L_1 = 4.80\mu H \quad (3.27)$$

Output capacitor:

$$C_{4_MIN} = \frac{I_{POS} \times (V_{POS} - V_{I_MIN})}{f \times \Delta V_{POS} \times V_{POS}} \quad (3.28)$$

Where V_{I_MIN} is the minimum input voltage, V_{POS} is the positive output voltage, I_{POS} is the positive output current, f is the oscillator frequency and ΔV_{POS} is the maximum allowed ripple voltages. Using $V_{I_MIN} = 3.5V$, $V_{POS} = +6V$, $I_{POS} = 400mA$, $f = 1380KHz$ and $\Delta V_{POS} = 10\text{ mV}$, it is obtained:

$$C_{4_MIN} = \frac{400mA \times (6V - 3.5V)}{1380KHz \times 0.01V \times 6V} \quad (3.29)$$

$$C_{4_MIN} = 12\mu F \quad (3.30)$$

Texas Instruments recommends using a value greater than the calculated one.

Feed forward capacitor:

$$C_9 = \frac{6.8\mu s}{R_1} \quad (3.31)$$

Where R_1 is the resistor in the voltage divider that was calculated before ($513K\Omega$).

$$C_9 = 13.26pF \quad (3.32)$$

Power dissipation:

In order to know if the boost converter can dissipate a certain amount of power, it is necessary to calculate the maximum junction temperature rise and it must be lower than the maximum operating junction temperature which according to the data sheet is $T_J = 125^\circ C$. So,

$$T_{RT_MAX} = T_A + (R_{\theta JA} \times P_D) \quad (3.33)$$

Where T_{RT_MAX} is the maximum junction temperature rise, T_A is the maximum operating ambient temperature, $R_{\theta JA}$ is the junction to ambient thermal resistance and P_D is the power dissipation. Using $T_A = 85^\circ C$, $R_{\theta JA} = 34.1^\circ C/W$ (according with the data sheet) and P_D can be calculated as follows:

$$P_D = (V_{POS} - V_{I_MIN}) \times I_{POS} \quad (3.34)$$

Where V_{I_MIN} is the minimum input voltage, V_{POS} is the positive output voltage and I_{POS} is the positive output current. Using $V_{I_MIN} = 3.5V$, $V_{POS} = +6V$ and $I_{POS} = 400mA$, it is obtained:

$$P_D = (6V - 3.5V) \times 400mA \quad (3.35)$$

$$P_D = 1W \quad (3.36)$$

So,

$$T_{RT_MAX} = 85^{\circ}C + (34.1^{\circ}C/W \times 1W) \quad (3.37)$$

$$T_{RT_MAX} = 119.1^{\circ}C \quad (3.38)$$

The maximum operating junction temperature is $T_J = 125^{\circ}C$. Then $T_{RT_MAX} < T_J$, the requirement is met. Working with less ambient temperature allows greater power dissipation. Working with lower output current decreases the value of T_{RT_MAX} .

3.5.4 LDO: Digital positive output voltage (+5V)

The selected LDO was the TPS7A4701 36-V, 1-A, 4- μ VRMS, RF LDO Voltage Regulator from Texas Instruments [14], [50]. This component can supply positive output voltage between +1.4 V to +20.5 V with the help of the ANY-OUT programmable output voltage feature, so, no external feedback resistors or forward capacitors are required. However, this component also has an adjustable output voltage using feedback resistors, the output voltage range in this mode is from +1.4 V to +34 V. The maximum output current is 1 A. The input voltage range is +3 V to +36 V and the dropout voltage is 307 mV at 1 A. This component is an ultra-low noise LDO, thus the output voltage noise is 4 μ V (10 Hz, 100 KHz) and the power-supply ripple rejection is ≤ 55 dB (10 Hz, 10 MHz). A typical schematic taken from the data sheet is shown below.

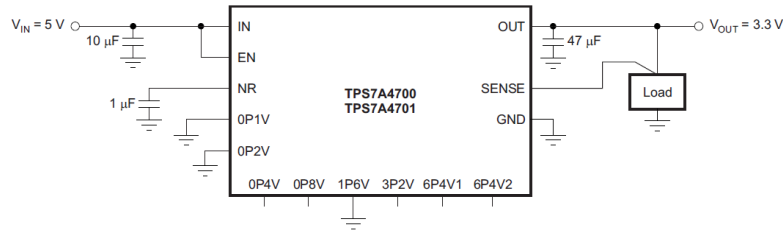


Figure 3.19: LDO schematic to get +5 V [14].

Most of the components or signals that must be connected to the pins have specific values given in the data sheet. However, the calculations written in the data sheet were followed in order to finish the configuration of the values of the components/pins that do not have a recommended value, but depend on the specific application.

ANY-OUT Programmable Output Voltage:

Using the device pins 4, 5, 6, 8, 9, 10, 11, and 12 the output voltage can be configured, each pin connected to ground means active, and each pins left opened means floating. Each active pin adds its value corresponding to the reference voltage ($V_{REF} = 1.4$ V). This is shown in the formula below.

$$V_{OUT} = V_{REF} + \left(\sum ANY - OUT_PINS_TO_GROUND \right) \quad (3.39)$$

In the following table can be seen the corresponding value of each pin:

Tabla 3.7: ANY-OUT Programmable Output Voltage. LaTeX.

ANY-OUT PROGRAM PINS (Active Low)	ADDITIVE OUTPUT VOLTAGE LEVEL
Pin 4 (6P4V2)	6.4 V
Pin 5 (6P4V1)	6.4 V
Pin 6 (3P2)	3.2 V
Pin 8 (1P6)	1.6 V
Pin 9 (0P8)	800 mV
Pin 10 (0P4)	400 mV
Pin 11 (0P2)	200 mV
Pin 12 (0P1)	100 mV

To get +5 V the data sheet recommends the following pin settings:

Tabla 3.8: Corresponding pin settings to get +5 V. LaTeX.

Pin	State
0P1V (100 mV)	GND
0P2V (200 mV)	GND
0P4V (400 mV)	Open
0P8V (800 mV)	Open
1P6V (1.6 V)	GND
3P2V (3.2 V)	Open
6P4V1 (6.4 V)	Open
6P4V2 (6.4 V)	Open

So,

$$V_{OUT} = 1.4V + (0.1V + 0.2V + 1.6V) \quad (3.40)$$

$$V_{OUT} = 3.3V \quad (3.41)$$

Startup time:

$$t_{ss} = 100000 \times C_{NR} \times \ln \left(\frac{V_R + 5}{5} \right) \quad (3.42)$$

Where C_{NR} is the noise reduction capacitor and V_R is the output voltage. Using $C_{NR} = 1\mu F$ (according with the data sheet) and $V_R = 3.3V$, it is obtained:

$$t_{ss} = 100000 \times 1\mu F \times \ln \left(\frac{3.3V + 5}{5} \right) \quad (3.43)$$

$$t_{ss} = 50.7ms \quad (3.44)$$

Power dissipation:

In order to know is the LDO can dissipate a certain amount of power, it is necessary to calculate the maximum junction temperature rise and it must be lower than the maximum operating junction temperature which according to the data sheet is $T_J = 125^\circ C$. So,

$$T_{RT_MAX} = T_A + (R_{\theta JA} \times P_D) \quad (3.45)$$

Where T_{RT_MAX} is the maximum junction temperature rise, T_A is the maximum operating ambient temperature, $R_{\theta JA}$ is the junction to ambient thermal resistance and P_D is the power dissipation. Using $T_A = 85^\circ C$, $R_{\theta JA} = 32.5^\circ C/W$ (according with the data sheet) and P_D can be calculated as follows:

$$P_D = (V_{IN} - V_{OUT}) \times I_{OUT} \quad (3.46)$$

Where V_I is the input voltage, V_{OUT} is the output voltage and I_{OUT} is the output current. Using $V_I = +5V$, $V_{OUT} = +3.3V$ and $I_{OUT} = 400mA$, it is obtained:

$$P_D = (5V - 3.3V) \times 400mA \quad (3.47)$$

$$P_D = 0.68W \quad (3.48)$$

So,

$$T_{RT_MAX} = 85^\circ C + (32.5^\circ C/W \times 0.4W) \quad (3.49)$$

$$T_{RT_MAX} = 107.1^\circ C \quad (3.50)$$

The maximum operating junction temperature is $T_J = 125^\circ\text{C}$. Then $T_{RT_MAX} < T_J$, the requirement is met. Working with less ambient temperature allows greater power dissipation. Working with lower output current decreases the value of T_{RT_MAX} .

3.5.5 LDO: Analog positive output voltage (+3.3V)

The selected LDO was the same used section 3.5.4. Most of the components or signals that must be connected to the pins have specific values given in the data sheet. However, the calculations written in the data sheet were followed in order to finish the configuration of the values of the components/pins that do not have a recommended value, but depend on the specific application.

ANY-OUT Programmable Output Voltage:

Using the device pins 4, 5, 6, 8, 9, 10, 11, and 12 the output voltage can be configured, each pin connected to ground means active, and each pins left opened means floating. Each active pin adds its value corresponding to the reference voltage ($V_{REF} = 1.4\text{ V}$). The formula 3.39 and the table 3.7 are applied to get +5 V with the following pin configuration recommended by the data sheet:

Tabla 3.9: Corresponding pin settings to get +5 V. LaTeX.

Pin	State
0P1V (100 mV)	Open
0P2V (200 mV)	Open
0P4V (400 mV)	GND
0P8V (800 mV)	Open
1P6V (1.6 V)	Open
3P2V (3.2 V)	GND
6P4V1 (6.4 V)	Open
6P4V2 (6.4 V)	Open

So,

$$V_{OUT} = 1.4V + (0.4V + 3.2V) \quad (3.51)$$

$$V_{OUT} = 5V \quad (3.52)$$

Startup time:

$$t_{ss} = 100000 \times C_{NR} \times \ln \left(\frac{V_R + 5}{5} \right) \quad (3.53)$$

Where C_{NR} is the noise reduction capacitor and V_R is the output voltage. Using $C_{NR} = 1\mu F$ (according with the data sheet) and $V_R = 5V$, it is obtained:

$$t_{ss} = 100000 \times 1\mu F \times \ln \left(\frac{5V + 5}{5} \right) \quad (3.54)$$

$$t_{ss} = 69.3ms \quad (3.55)$$

Power dissipation:

In order to know is the LDO can dissipate a certain amount of power, it is necessary to calculate the maximum junction temperature rise and it must be lower than the maximum operating junction temperature which according to the data sheet is $T_J = 125^\circ C$. So,

$$T_{RT_MAX} = T_A + (R_{\theta JA} \times P_D) \quad (3.56)$$

Where T_{RT_MAX} is the maximum junction temperature rise, T_A is the maximum operating ambient temperature, $R_{\theta JA}$ is the junction to ambient thermal resistance and P_D is the power dissipation. Using $T_A = 85^\circ C$, $R_{\theta JA} = 32.5^\circ C/W$ (according with the data sheet) and P_D can be calculated as follows:

$$P_D = (V_{IN} - V_{OUT}) \times I_{OUT} \quad (3.57)$$

Where V_I is the input voltage, V_{OUT} is the output voltage and I_{OUT} is the output current. Using $V_I = +6V$, $V_{OUT} = +5V$ and $I_{OUT} = 400mA$, it is obtained:

$$P_D = (6V - 5V) \times 400mA \quad (3.58)$$

$$P_D = 0.4W \quad (3.59)$$

So,

$$T_{RT_MAX} = 85^\circ C + (32.5^\circ C/W \times 0.4W) \quad (3.60)$$

$$T_{RT_MAX} = 98^\circ C \quad (3.61)$$

The maximum operating junction temperature is $T_J = 125^\circ C$. Then $T_{RT_MAX} < T_J$, the requirement is met. Working with less ambient temperature allows greater power dissipation. Working with lower output current decreases the value of T_{RT_MAX} .

3.5.6 Inverter: Negative voltage to feed the LDO TPS7A33

The inverting converter was design to get -6V and use that output as the input of the positive LDO to establish -5V. The selected inverting converter was the same component described in section 3.5.3. Most of the components or signals that must be connected to the pins have specific values given in the data sheet. However, the calculations written in the data sheet were followed in order to confirm the values and to finish the configuration of the values of the components that do not have a recommended value, but depend on the specific application.

Feedback resistor:

$$R_3 = -R_4 \times \left(\frac{V_{NEG}}{V_{REF}} \right) \quad (3.62)$$

Where V_{REF} is the reference voltage, R_4 is the resistor tied to ground in the voltage divider and V_{NEG} is the negative output voltage. Using $V_{REF} = 1.213V$, $R_4 = 121.2K\Omega$ (according to the data sheet) and $V_{NEG} = -6V$, it is obtained:

$$R_3 = -121.2K\Omega \times \left(\frac{-6V}{1.213V} \right) \quad (3.63)$$

$$R_3 = 599.5K\Omega \quad (3.64)$$

Inductor:

In order to know the value for the inductor it is necessary to compute the peak inductor current I_{L-N} , it must be lower than switch current limit (2A):

$$I_{L-N} = \frac{V_{I_MIN} - V_{NEG}}{V_{I_MIN} \times 0.64} \times I_{NEG} \quad (3.65)$$

Where V_{I_MIN} is the minimum input voltage, V_{NEG} is the negative output voltage and I_{NEG} is the negative output current. Using $V_{I_MIN} = 3.5V$, $V_{NEG} = -6V$ and $I_{NEG} = 400mA$, it is obtained:

$$I_{L-N} = \frac{3.5V - (-6)}{3.5V \times 0.64} \times 400mA \quad (3.66)$$

$$I_{L-P} = 1.7A \quad (3.67)$$

It is now possible to compute the inductor value:

$$L_2 = \frac{V_{I_MIN} \times V_{NEG}}{\Delta I_{L-N} \times f \times (V_{NEG} - V_{I_MIN})} \quad (3.68)$$

Where ΔI_{L-N} is the 20% of I_{L-N} and f is the oscillator frequency given in the data sheet. Using $\Delta I_{L-N} = 0.34A$ and $f = 1380KHz$, it is obtained:

$$L_2 = \frac{3.5V \times -6V}{0.34A \times 1380KHz \times (-6V - 3.5V)} \quad (3.69)$$

$$L_2 = 4.7\mu H \quad (3.70)$$

Output capacitor:

$$C_{5_MIN} = \frac{I_{NEG} \times V_{NEG}}{f \times \Delta V_{NEG} \times (V_{NEG} - V_{I_MIN})} \quad (3.71)$$

Where V_{I_MIN} is the minimum input voltage, V_{NEG} is the negative output voltage, I_{NEG} is the negative output current, f is the oscillator frequency and ΔV_{NEG} is the maximum allowed ripple voltages. Using $V_{I_MIN} = 3.5V$, $V_{NEG} = -6V$, $I_{NEG} = 400mA$, $f = 1380KHz$ and $\Delta V_{NEG} = 10 \text{ mV}$, it is obtained:

$$C_{5_MIN} = \frac{400mA \times -6V}{1380K\Omega \times 0.01V \times (-6V - 3.5V)} \quad (3.72)$$

$$C_{4_MIN} = 18\mu F \quad (3.73)$$

Texas Instruments recommends using a value greater than the calculated one.

Feed forward capacitor:

$$C_{10} = \frac{7.5\mu s}{R_3} \quad (3.74)$$

Where R_3 is the resistor in the voltage divider that was calculated before ($599.5K\Omega$).

$$C_{10} = 12.5pF \quad (3.75)$$

Power dissipation:

The calculations were done in section 3.5.3.

3.5.7 LDO: Analog negative output voltage (-5V)

The selected LDO was the TPS7A33 -36-V, 1-A, Ultralow-Noise Negative Voltage Regulator from Texas Instruments [15], [51]. This component can supply negative output voltage between -1.18 V to -33 V with the help of feedback resistors. The maximum output current is 1 A. The input voltage range is -3 V to -36 V and the dropout voltage is 600 mV at 1 A. This component is an ultra-low noise LDO, thus the output voltage noise is $16\mu V$ (10 Hz to 100 KHz) and the power-supply ripple rejection is 72 dB (10 KHz). A typical schematic taken from the data sheet is shown below.

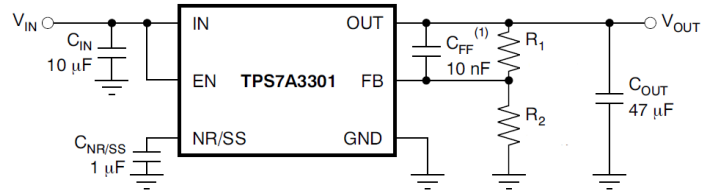


Figure 3.20: LDO schematic to get -5 V [15].

Most of the components or signals that must be connected to the pins have specific values given in the data sheet. However, the calculations written in the data sheet were followed in order to finish the configuration of the values of the components/pins that do not have a recommended value, but depend on the specific application.

Feedback resistor:

$$R_1 = R_2 \times \left(\frac{V_{OUT}}{V_{REF}} - 1 \right) \quad (3.76)$$

Where V_{REF} is the reference voltage, R_2 is the resistor tied to ground in the voltage divider and V_{OUT} is the negative output voltage. Using $V_{REF} = -1.175V$, $R_2 = 102K\Omega$ (according to the data sheet) and $V_{OUT} = -5V$, it get:

$$R_1 = 102K\Omega \times \left(\frac{-5V}{-1.175V} - 1 \right) \quad (3.77)$$

$$R_1 = 332K\Omega \quad (3.78)$$

Power dissipation:

In order to know is the LDO can dissipate a certain amount of power, it is necessary to calculate the maximum junction temperature rise and it must be lower than the maximum operating junction temperature which according to the data sheet is $T_J = 125^\circ C$. So,

$$T_{RT_MAX} = T_A + (R_{\theta JA} \times P_D) \quad (3.79)$$

Where T_{RT_MAX} is the maximum junction temperature rise, T_A is the maximum operating ambient temperature, $R_{\theta JA}$ is the junction to ambient thermal resistance and P_D is the power dissipation. Using $T_A = 85^\circ C$, $R_{\theta JA} = 33.7^\circ C/W$ (according with the data sheet) and P_D can be calculated as follows:

$$P_D = (V_{OUT} - V_{IN}) \times I_{OUT} \quad (3.80)$$

Where V_I is the input voltage, V_{OUT} is the output voltage and I_{OUT} is the output current. Using $V_I = -6V$, $V_{OUT} = -5V$ and $I_{OUT} = 400mA$, it is obtained:

$$P_D = (-5V - (-6V)) \times 400mA \quad (3.81)$$

$$P_D = 0.4W \quad (3.82)$$

So,

$$T_{RT_MAX} = 85^{\circ}C + (33.7^{\circ}C/W \times 0.4W) \quad (3.83)$$

$$T_{RT_MAX} = 98.5^{\circ}C \quad (3.84)$$

The maximum operating junction temperature is $T_J = 125^{\circ}C$. Then $T_{RT_MAX} < T_J$, the requirement is met. Working with less ambient temperature allows greater power dissipation. Working with lower output current decreases the value of T_{RT_MAX} .

3.5.8 Layout considerations

The layout of the PCB was made following the recommendations of Texas Instruments given in the data sheets. This information is specific to each component. However, it is possible to extract some general guidelines.

- Place all components on the same side of the PCB.
- Use a ground reference plane. This plane will be useful for power dissipation.
- Keep short traces between each connection to avoid instability and improve circuit performance.
- Use wide polygons in the connections that must handle the main currents (input / output capacitors, inductors and diodes).
- Connect all the grounds through the power ground of the integrated circuit.
- Place vias in the power ground of the integrated circuit.
- Place the voltage dividers as close as possible to the feedback pin.
- Place all components as close as possible to the integrated circuit.

To design the layout, the possibility of using two or four layers was considered, however, since all the components must be in the same plane, and only some signals require connections in another layer, it was decided to use only two layers. The first layer is the top layer where the components and most connections and polygons are. The second layer is the bottom layer which is the ground plane only interrupted by small traces that could not be connected in the top layer due to the arrangement of the pins in the integrated circuits. In addition, the use of two layers instead of four layers reduces manufacturing costs.

Chapter 4

Results and Discussion

In this chapter, the results of this work are presented and discussed. Section 4.1 is the only one that shows all the figures corresponding to the RMS, peak-to-peak and PSD of each experiment described in table 3.1 of section 3.2.3. This is an illustration of how the results are seen. However,, for later sections only in some cases figures are shown to guide the reader. The relevant information is synthesized in tables to discuss the results.

For all the images corresponding to the RMS and peak-to-peak values, three figures are shown:

1. **a:** Original signal obtained from oscilloscope.
2. **b:** Resulting signal when applying the running average filter with a windows size of 5.
3. **c:** Resulting signal after extracting the signal from figure b to figure a.

4.1 Noise experiments: Without aluminium enclosure

4.1.1 Printed sensor is not coupled to the circuit input

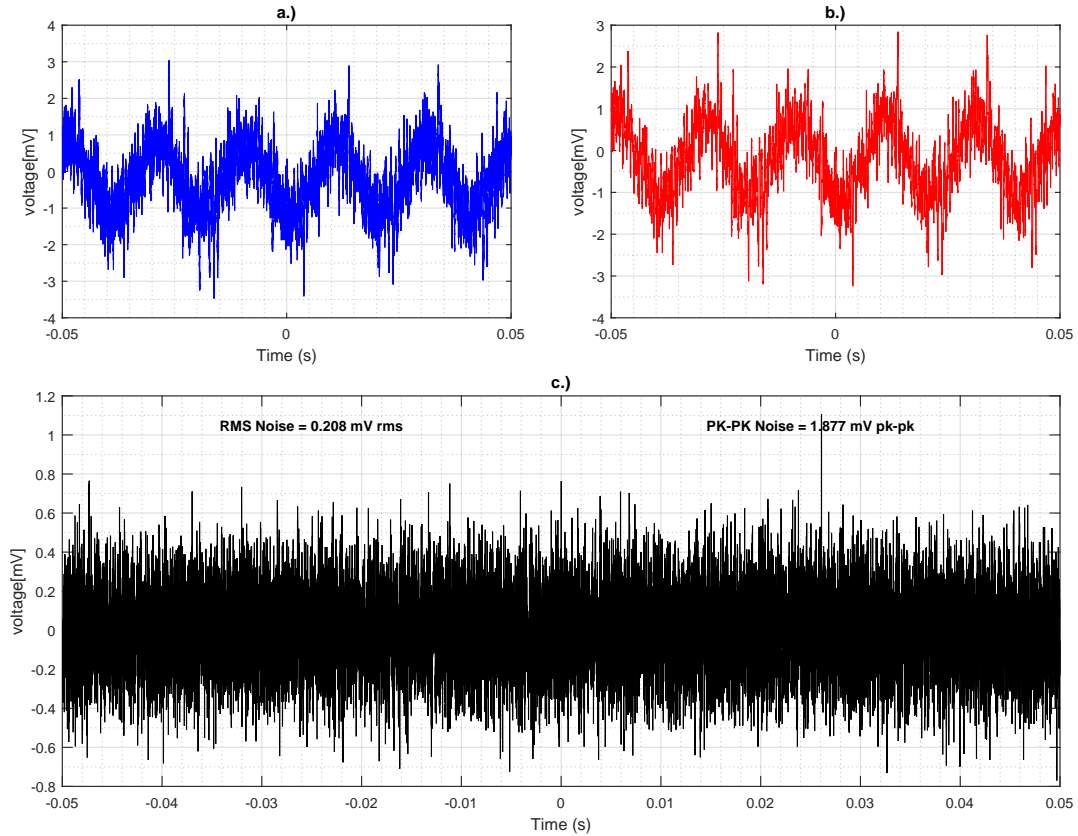


Figure 4.1: Root mean square and peak to peak noise channel 1 when printed sensor is not coupled to the circuit input. MatLab.

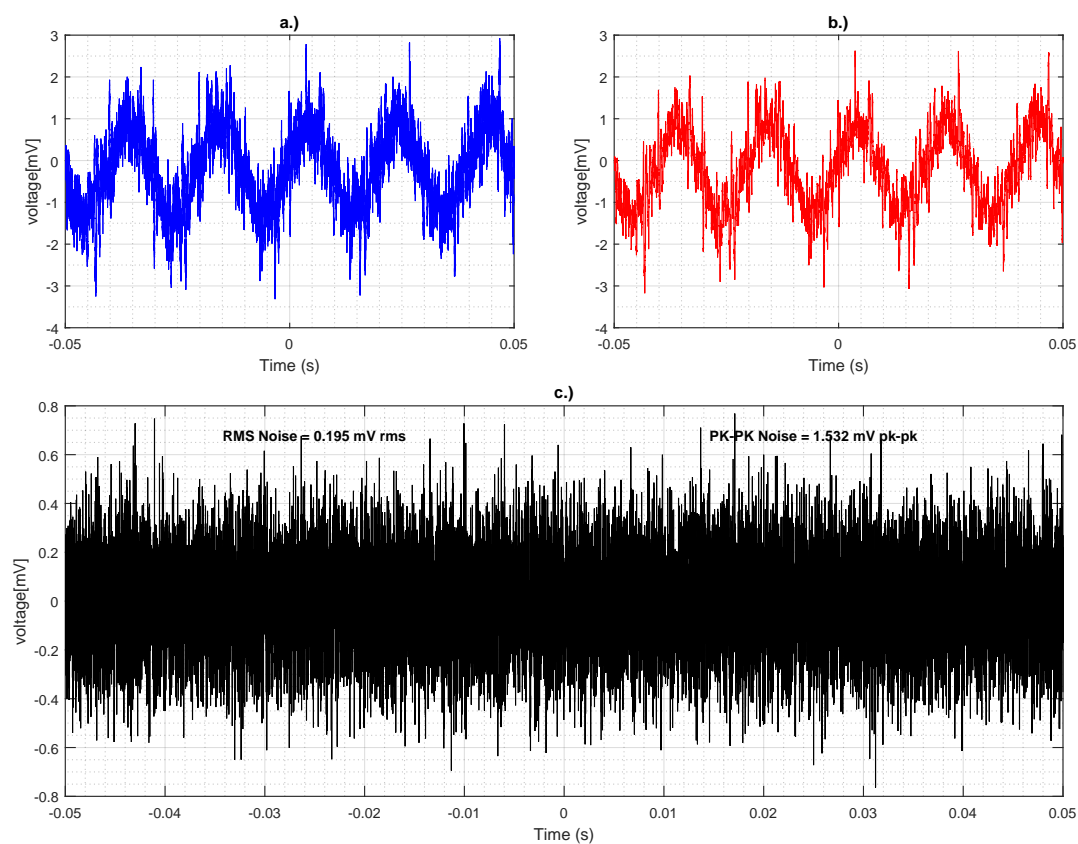


Figure 4.2: Root mean square and peak to peak noise channel 2 when printed sensor is not coupled to the circuit input. MatLab.

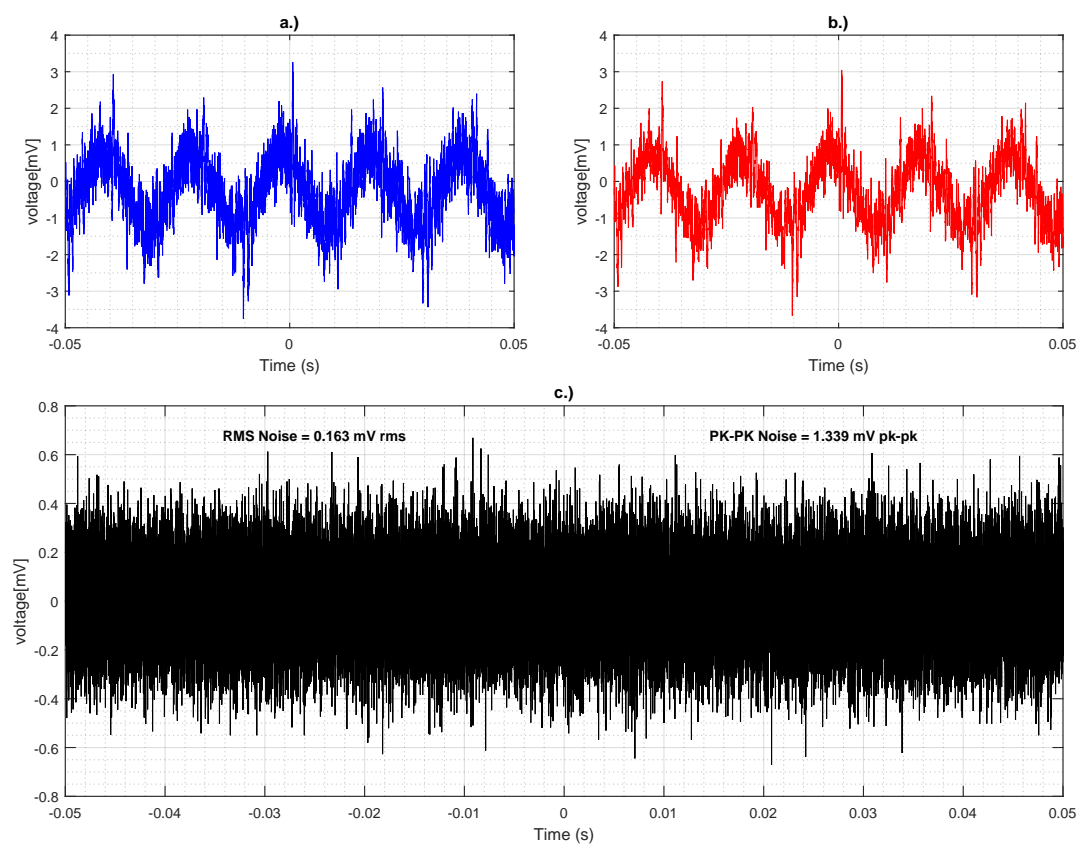


Figure 4.3: Root mean square and peak to peak noise channel 4 when printed sensor is not coupled to the circuit input. MatLab.

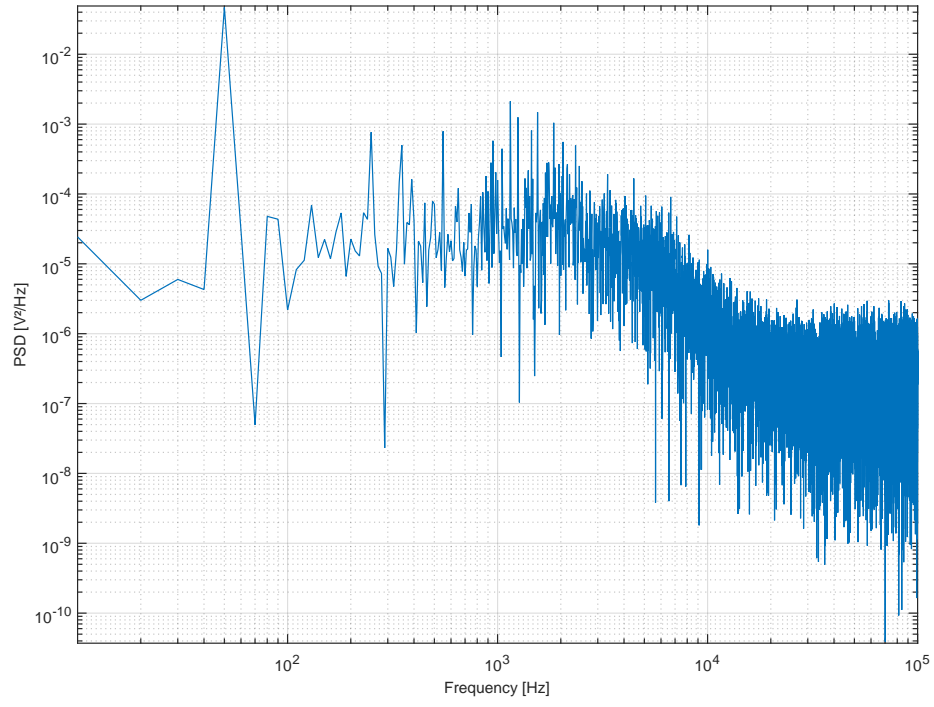


Figure 4.4: Power spectral density channel 1 when printed sensor is not coupled to the circuit input. MatLab.

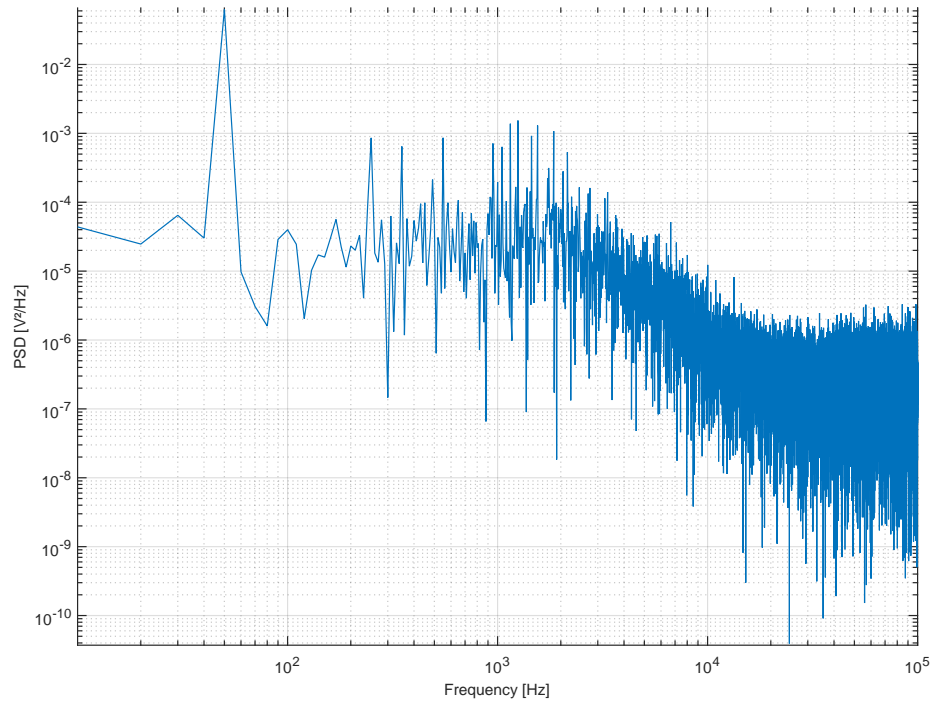


Figure 4.5: Power spectral density channel 2 when printed sensor is not coupled to the circuit input. MatLab.

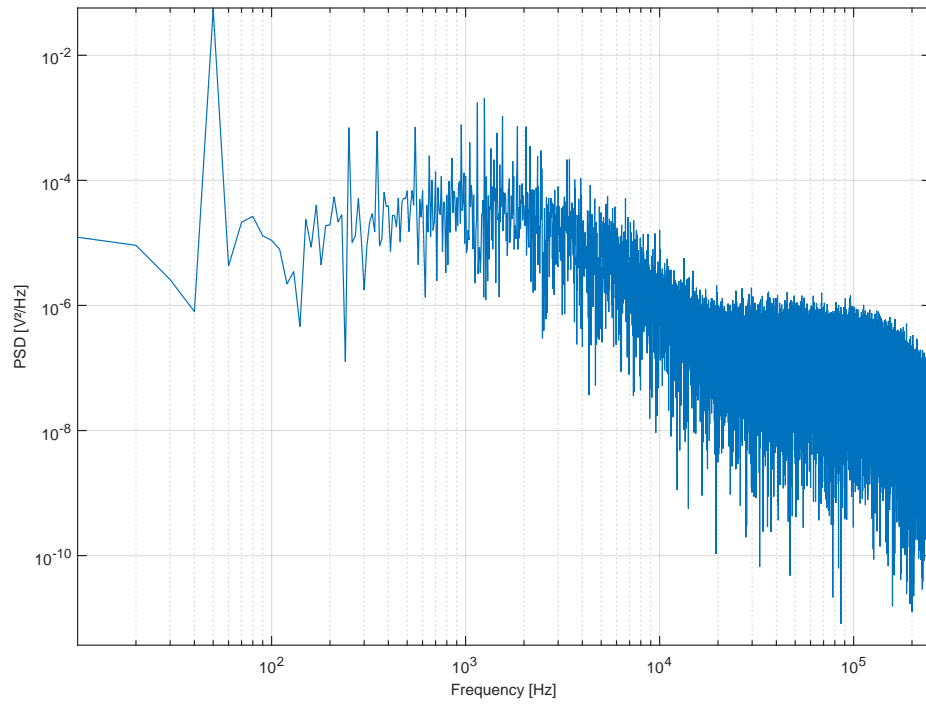


Figure 4.6: Power spectral density channel 4 when printed sensor is not coupled to the circuit input. MatLab.

4.1.2 Printed sensor is not coupled to the circuit input. The circuit input is covered by a Faraday cage

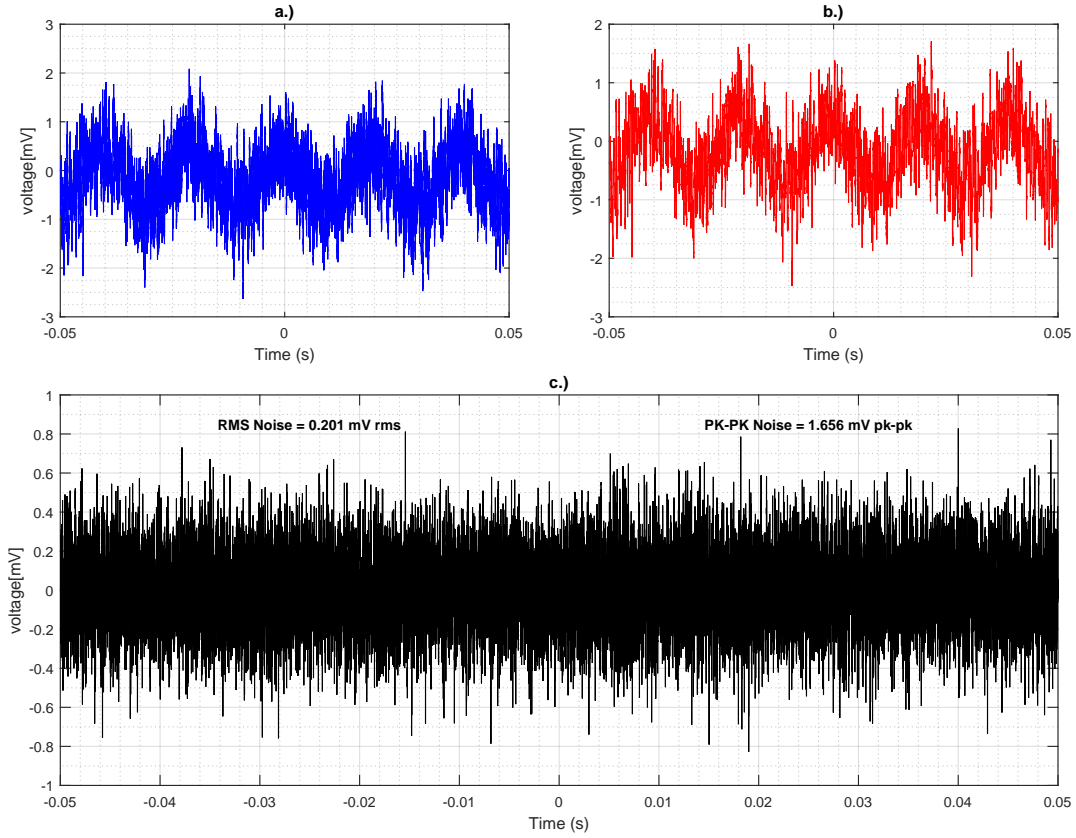


Figure 4.7: Root mean square and peak to peak noise channel 1 when printed sensor is not coupled to the circuit input but a Faraday cage of 30x30 mm is placed on the circuit input. MatLab.

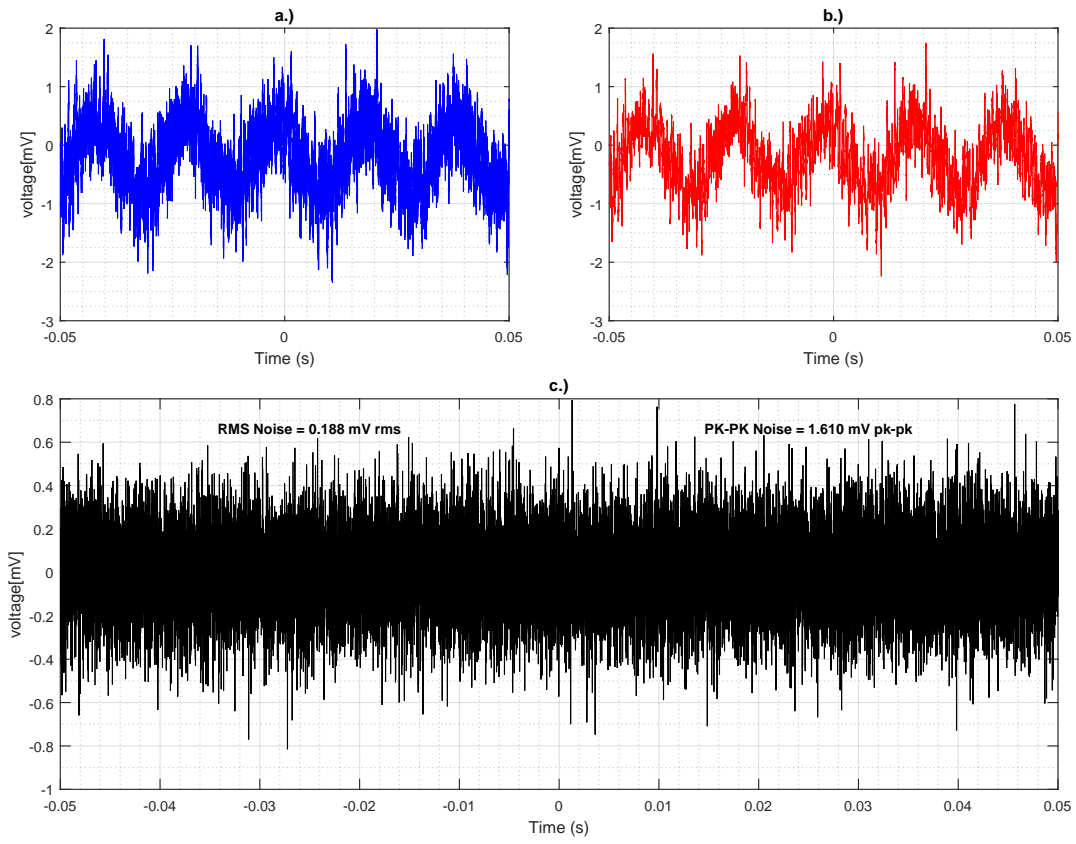


Figure 4.8: Root mean square and peak to peak noise channel 2 when printed sensor is not coupled to the circuit input but a Faraday cage of 30x30 mm is placed on the circuit input. MatLab.

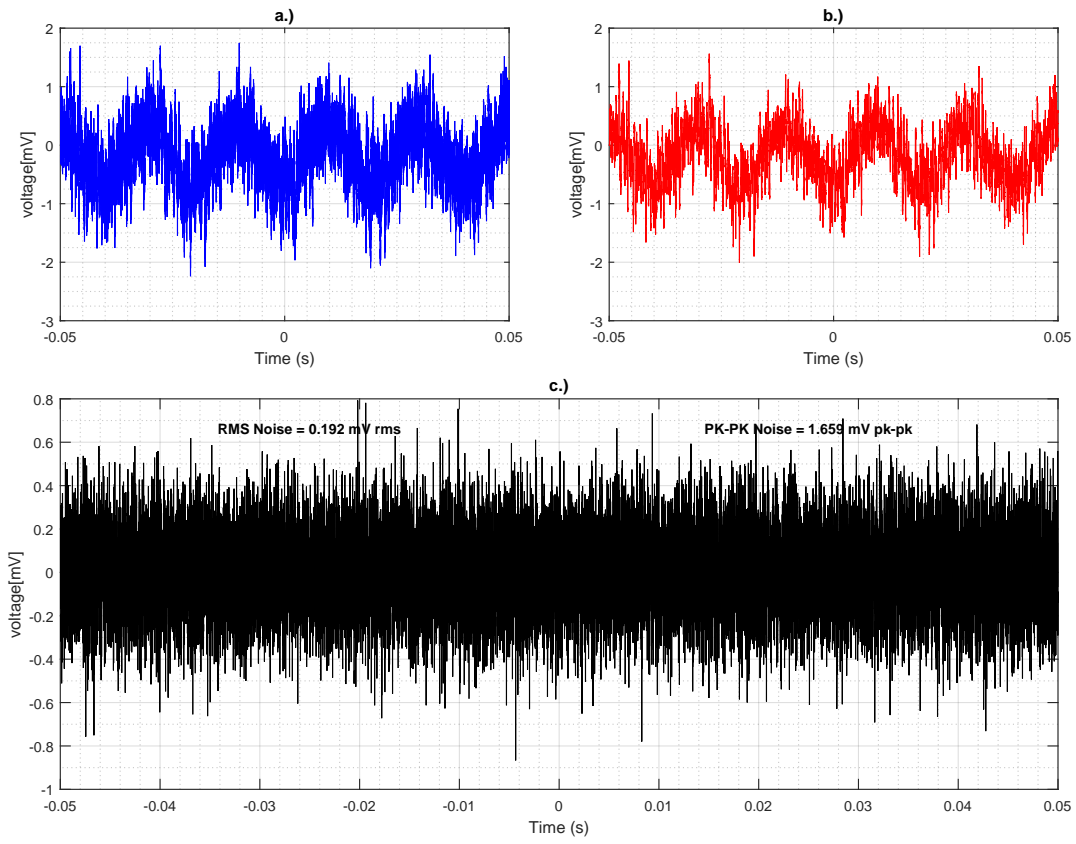


Figure 4.9: Root mean square and peak to peak noise channel 4 when printed sensor is not coupled to the circuit input but a Faraday cage of 30x30 mm is placed on the circuit input. MatLab.

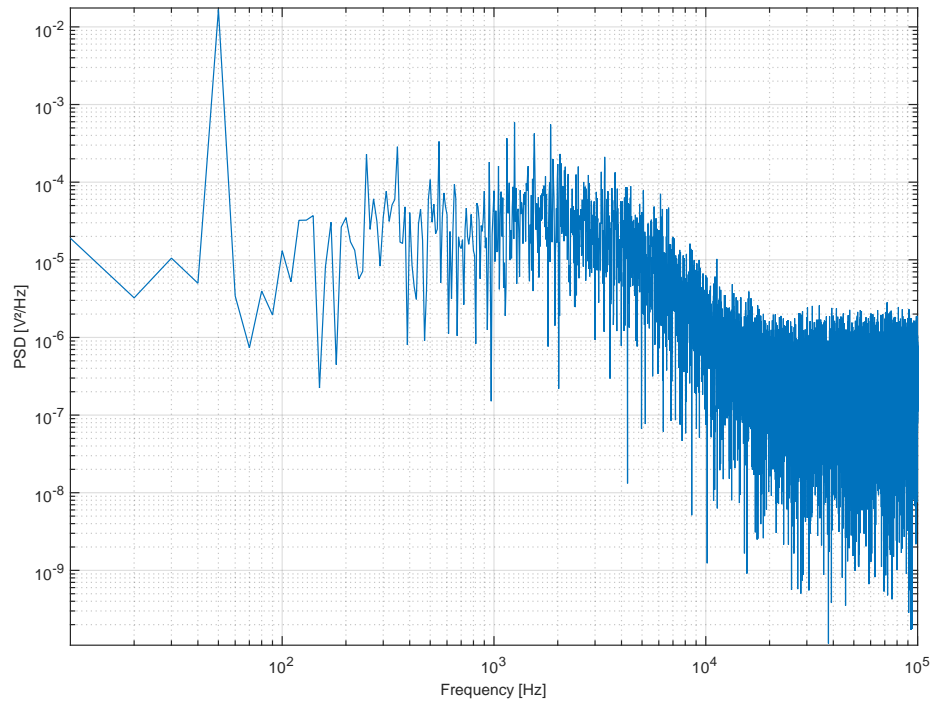


Figure 4.10: Power spectral density channel 1 when printed sensor is not coupled to the circuit input but a Faraday cage of 30x30 mm is placed on the circuit input. MatLab.

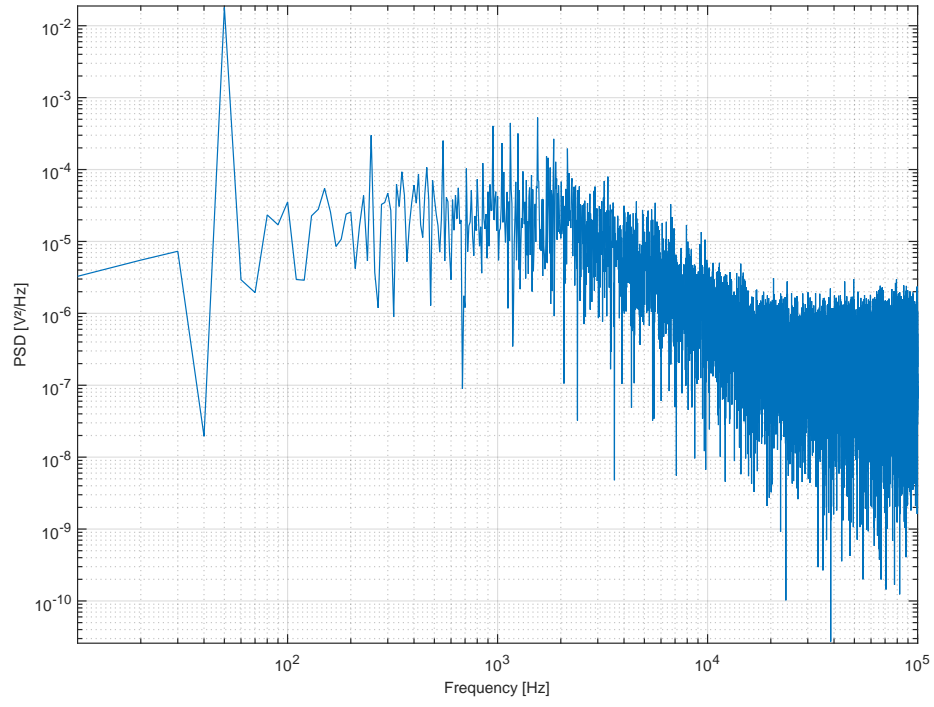


Figure 4.11: Power spectral density channel 2 when printed sensor is not coupled to the circuit input but a Faraday cage of 30x30 mm is placed on the circuit input. MatLab.

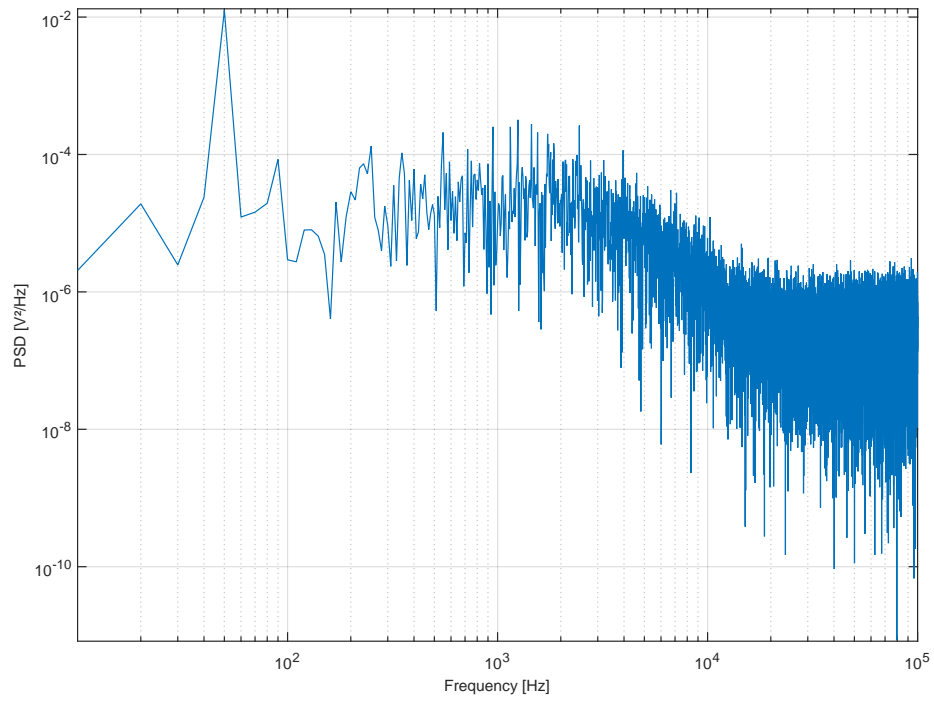


Figure 4.12: Power spectral density channel 4 when printed sensor is not coupled to the circuit input but a Faraday cage of 30x30 mm is placed on the circuit input. MatLab.

4.1.3 Printed sensor is coupled to the circuit input and it is not covered by a Faraday cage

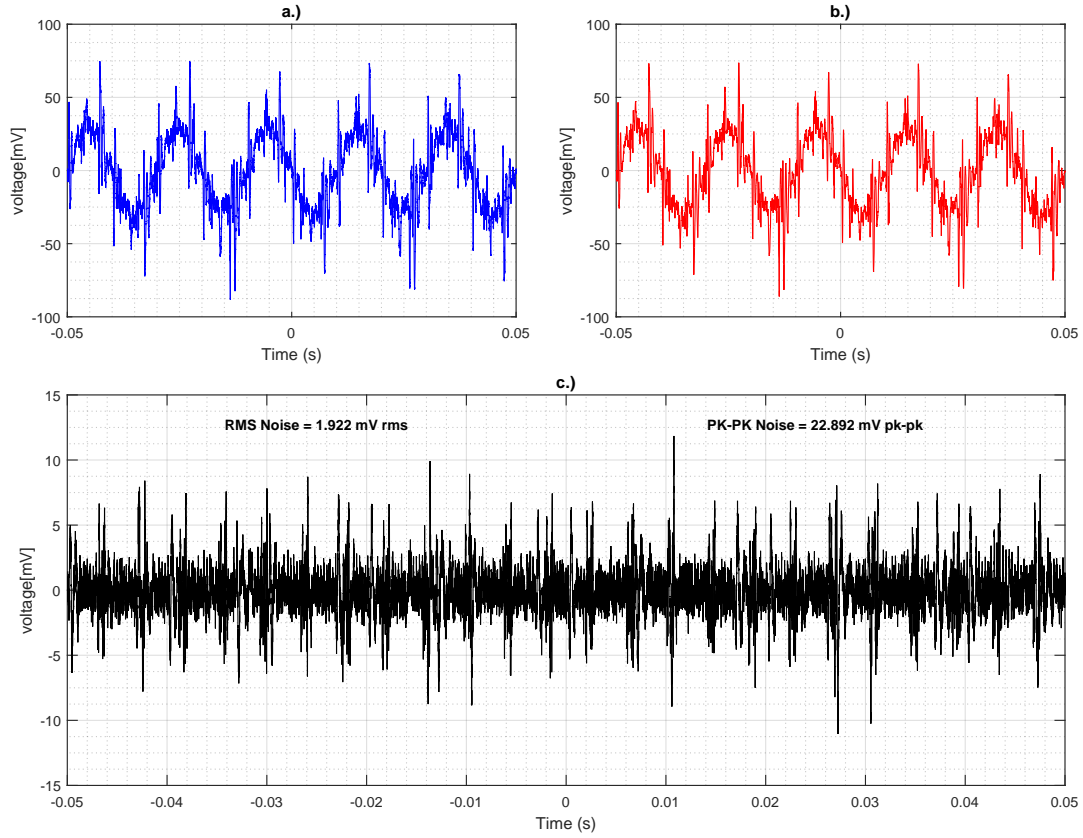


Figure 4.13: Root mean square and peak to peak noise channel 1 when printed sensor is coupled to the circuit input without a Faraday cage. MatLab.

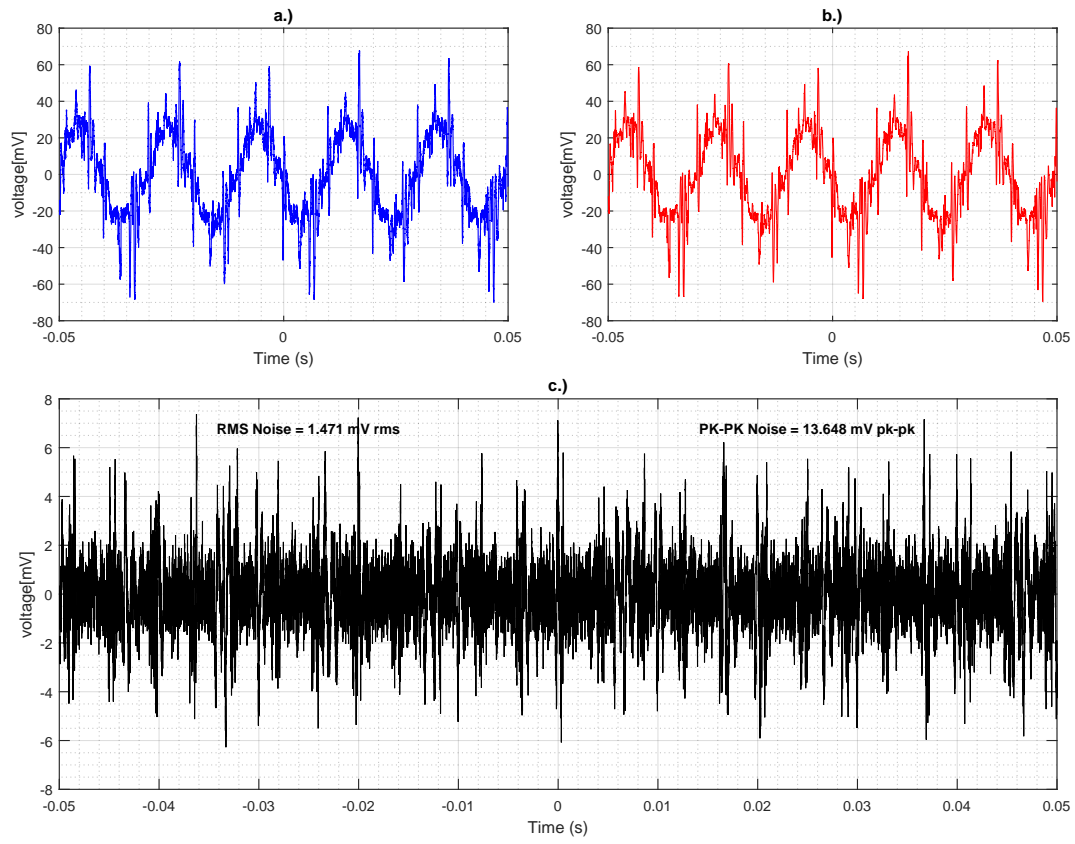


Figure 4.14: Root mean square and peak to peak noise channel 2 when printed sensor is coupled to the circuit input without a Faraday cage. MatLab.

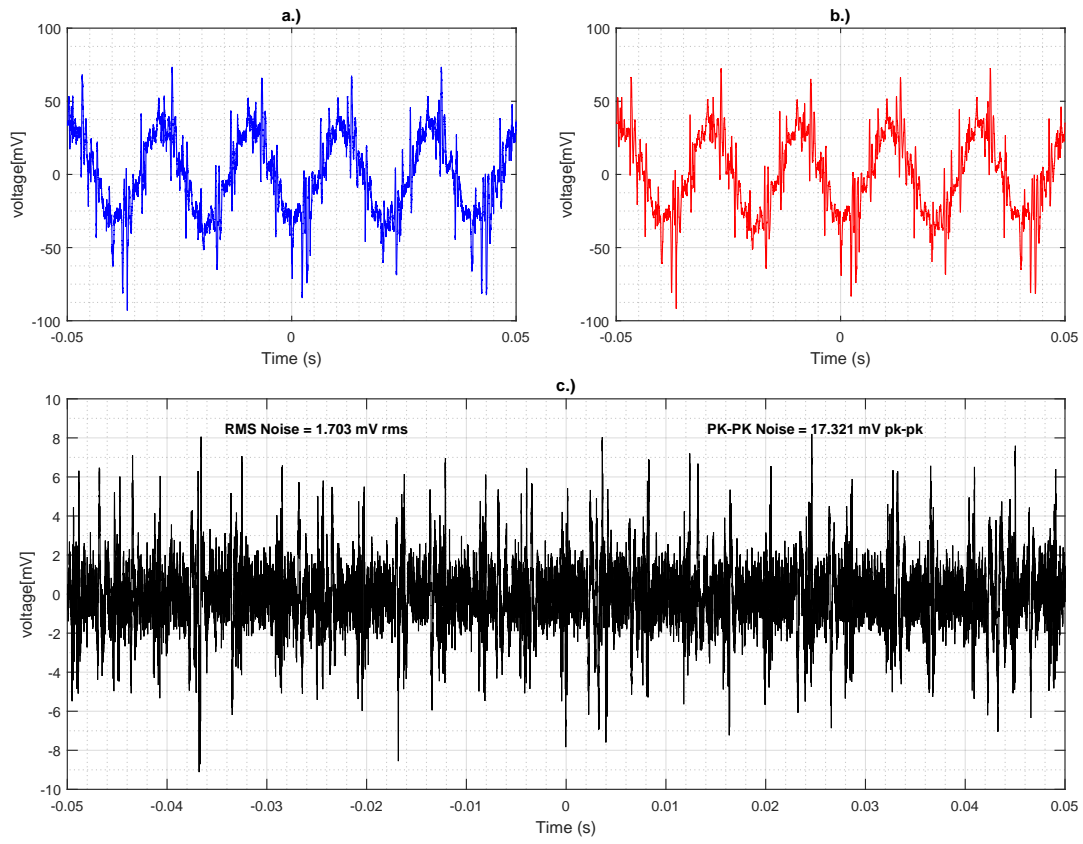


Figure 4.15: Root mean square and peak to peak noise channel 4 when printed sensor is coupled to the circuit input without a Faraday cage. MatLab.

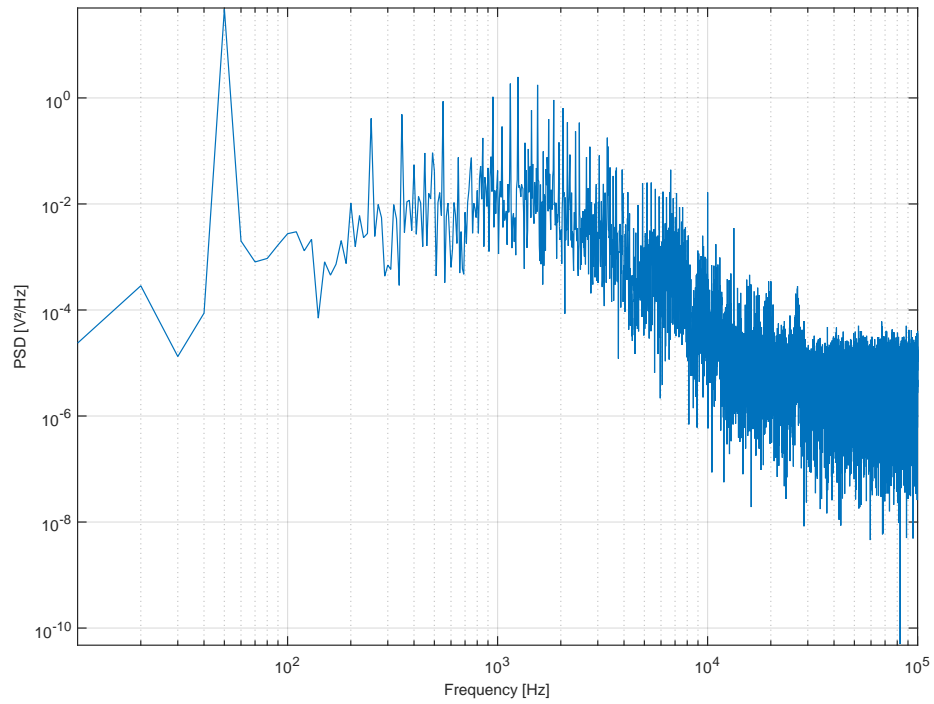


Figure 4.16: Power spectral density channel 1 when printed sensor is coupled to the circuit input without a Faraday cage. MatLab.

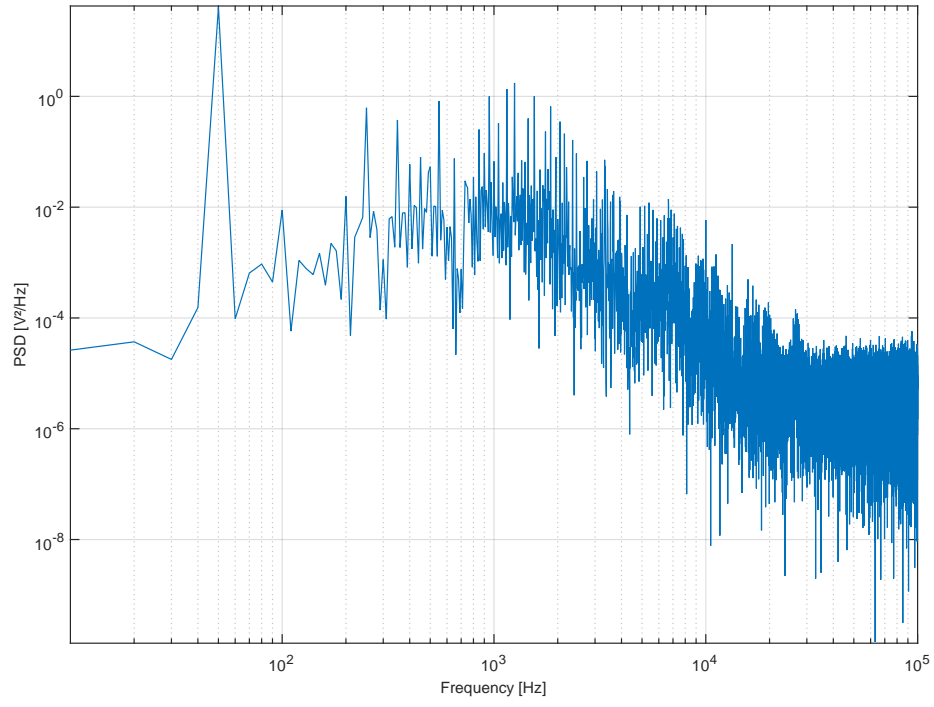


Figure 4.17: Power spectral density channel 2 when printed sensor is coupled to the circuit input without a Faraday cage. MatLab.

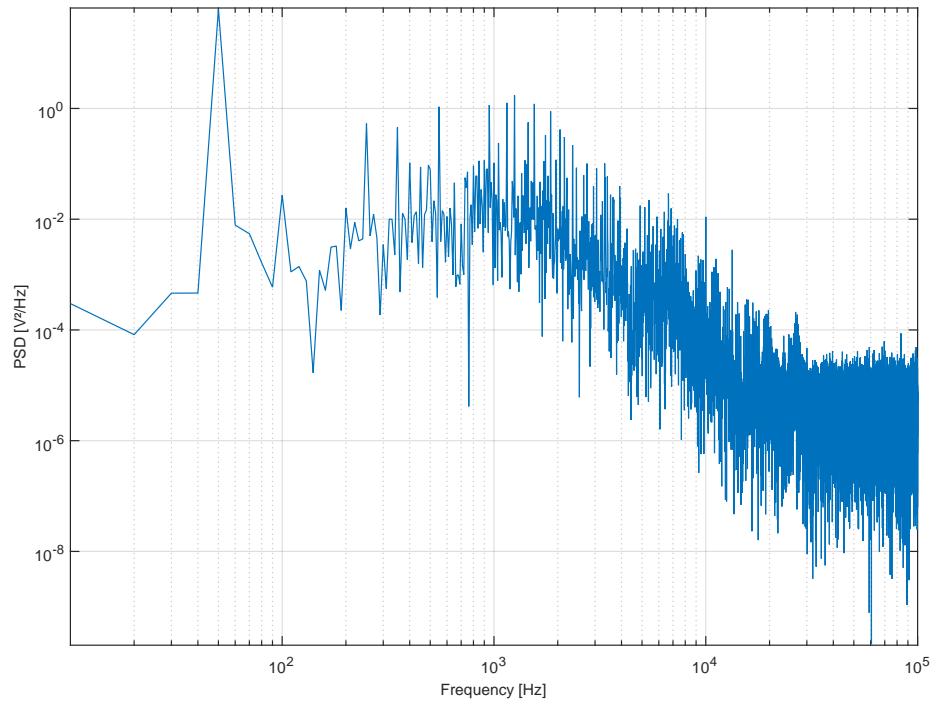


Figure 4.18: Power spectral density channel 4 when printed sensor is coupled to the circuit input without a Faraday cage. MatLab.

4.1.4 Printed sensor is coupled to the circuit input. The printed sensor/circuit input is covered by a Faraday cage

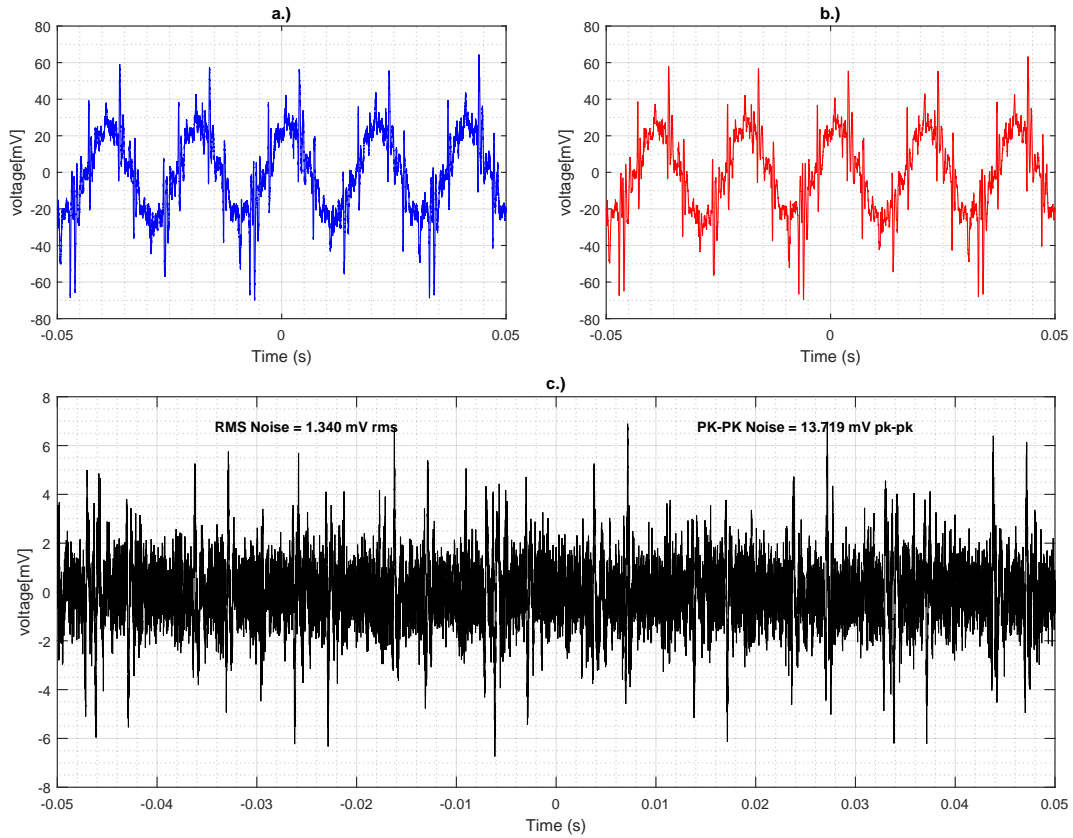


Figure 4.19: Root mean square and peak to peak noise channel 1 when printed sensor is coupled to the circuit input with a Faraday cage of 30x30 mm. MatLab.

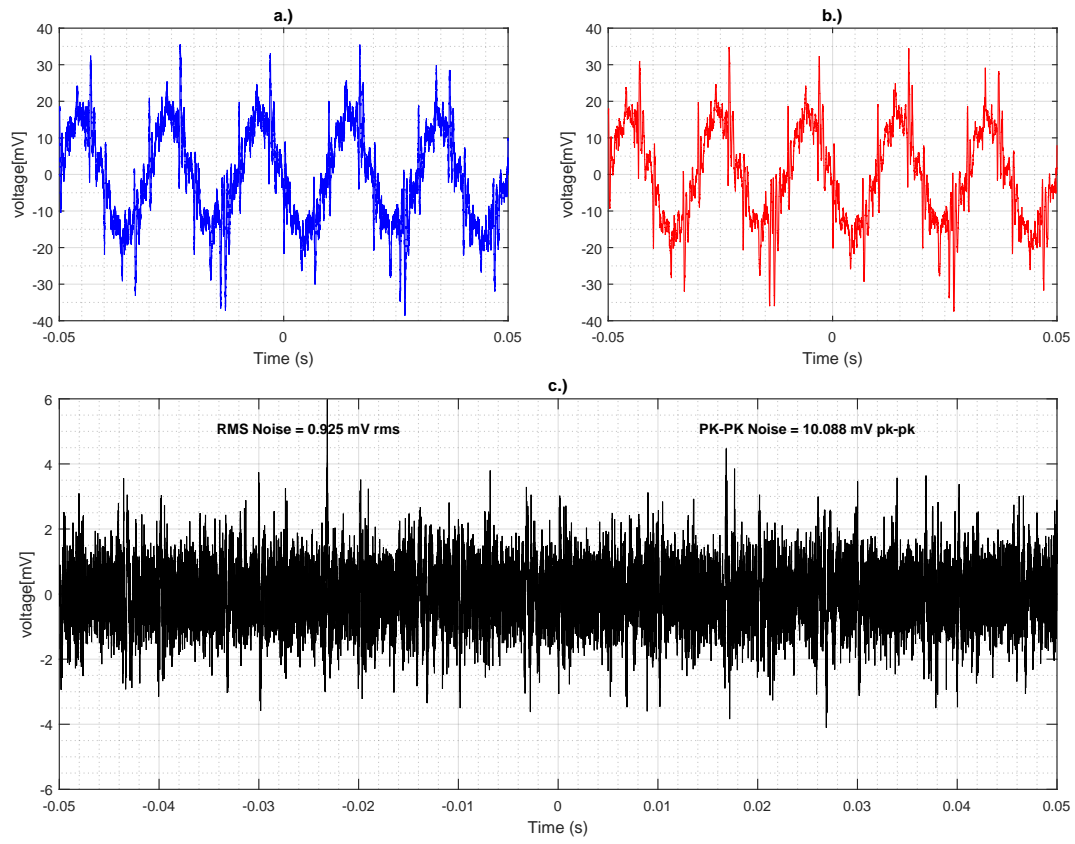


Figure 4.20: Root mean square and peak to peak noise channel 2 when printed sensor is coupled to the circuit input with a Faraday cage of 30x30 mm. MatLab.

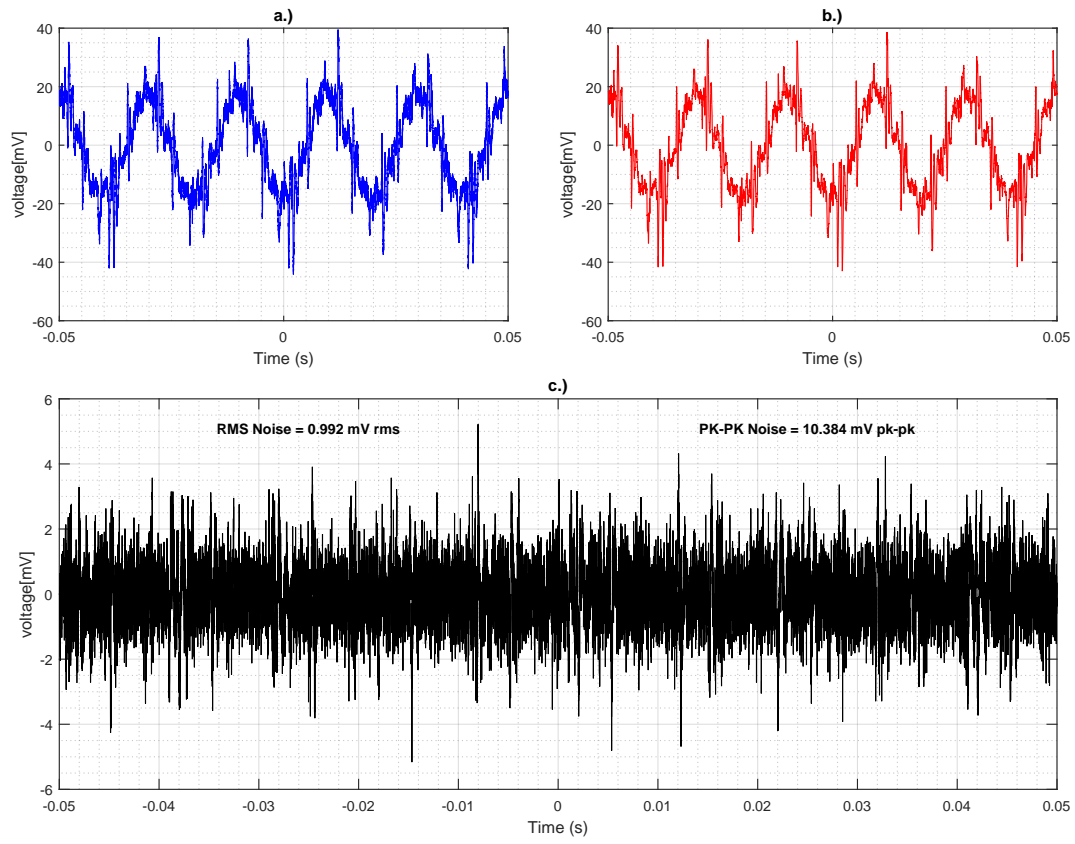


Figure 4.21: Root mean square and peak to peak noise channel 4 when printed sensor is coupled to the circuit input with a Faraday cage of 30x30 mm. MatLab.

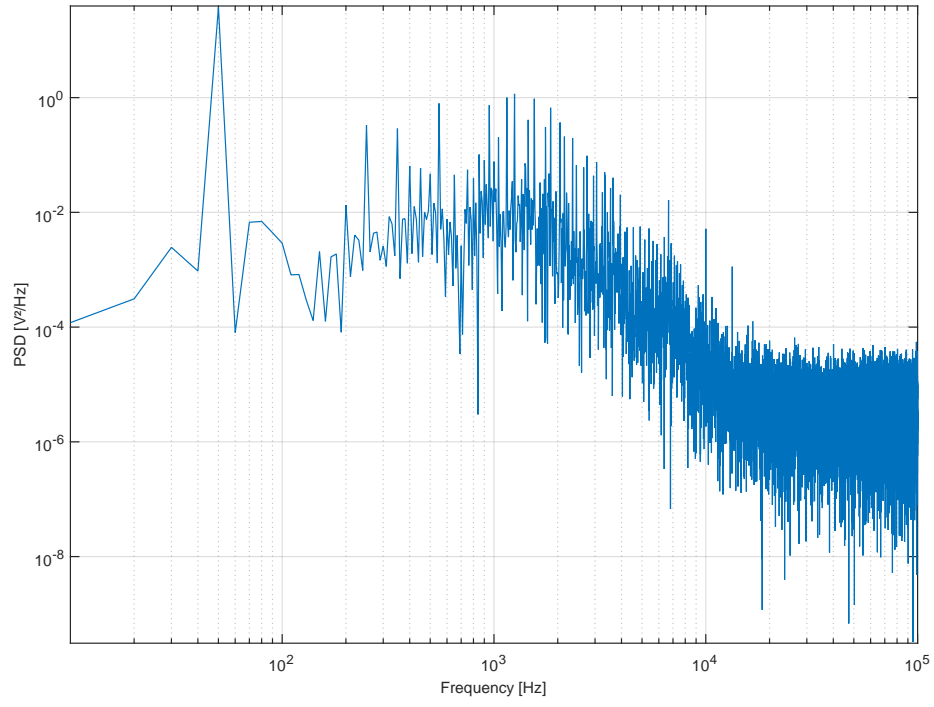


Figure 4.22: Power spectral density channel 1 when printed sensor is coupled to the circuit input with a Faraday cage of 30x30 mm. MatLab.

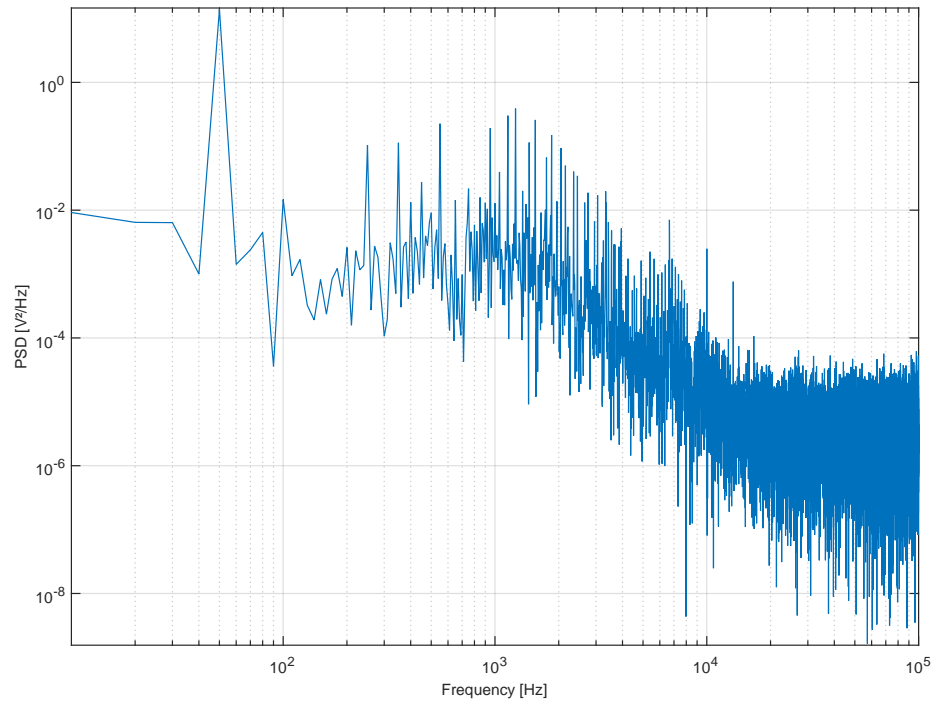


Figure 4.23: Power spectral density channel 2 when printed sensor is coupled to the circuit input with a Faraday cage of 30x30 mm. MatLab.

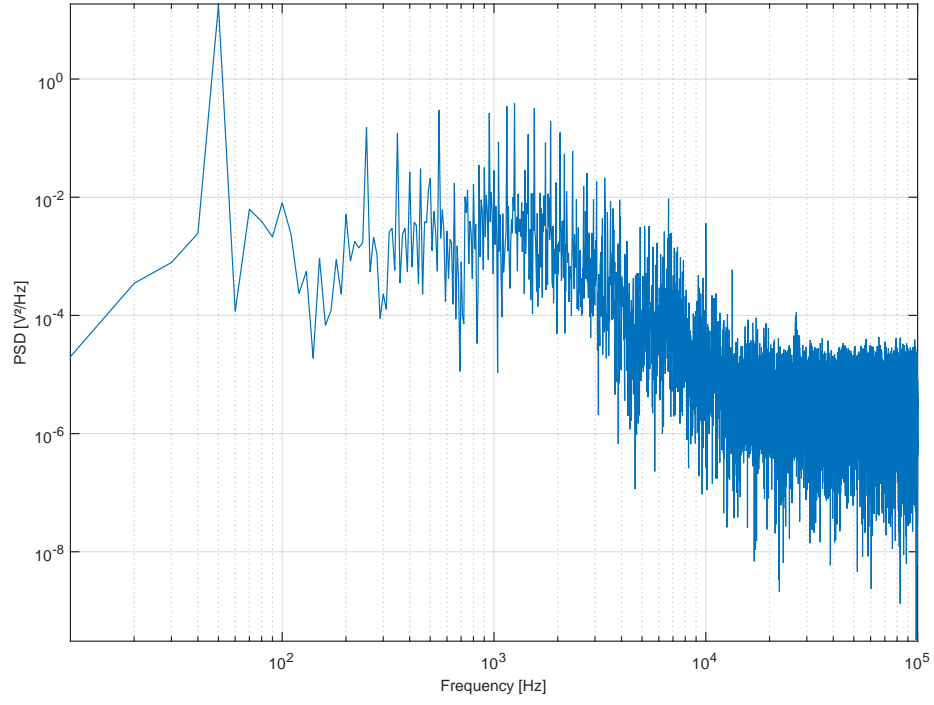


Figure 4.24: Power spectral density channel 4 when printed sensor is coupled to the circuit input with a Faraday cage of 30x30 mm. MatLab.

The next tables summarizes the results.

Tabla 4.1: Noise experiment results for channel 1. LaTeX.

Experiment	RMS (mV)	Pk-Pk Noise (mV)	V^2/Hz at 50Hz
1	0.208	1.877	5×10^{-2}
2	0.201	1.656	2×10^{-2}
3	1.922	22.892	4×10^1
4	1.340	13.719	1×10^1

Tabla 4.2: Noise experiment results for channel 2. LaTeX.

Experiment	RMS (mV)	Pk-Pk Noise (mV)	V^2/Hz at 50Hz
2	0.195	1.532	7×10^{-2}
2	0.188	1.610	2×10^{-2}
3	1.471	13.648	4×10^1
4	0.925	10.088	1×10^1

Tabla 4.3: Noise experiment results for channel 4. LaTeX.

Experiment	RMS (mV)	Pk-Pk Noise (mV)	V^2/Hz at 50Hz
1	0.163	1.399	2×10^{-2}
2	0.192	1.659	1×10^{-2}
3	1.703	17.321	4×10^1
4	0.922	10.384	1×10^1

As could see in tables 4.1, 4.2 and 4.3, channel 4 (table 4.3) present the best performance for the first experiment (when printed sensor is not coupled to the circuit input). It is important to realized that when a printed sensor is coupled at the circuit input (third experiment) the noise is increased because an antenna behavior in the sensor. This effect can be reduced by a Faraday cage (fourth experiment), and the improvement is about 40% in comparison with the third experiment. The worse performance is presented by Channel 1. Channel 3 is not working, all the connections were checked for a fault; however,, no error was found. It is presumed that some of the integrated circuit is not working, perhaps due to the use for tests in the analog circuit prior to the realization of this project. However,, the configuration of the feedback resistors is the same in Channel 1 as in Channel 3, so the placement of the resistance can still be evaluated.

4.2 Noise experiments: With aluminium enclosure

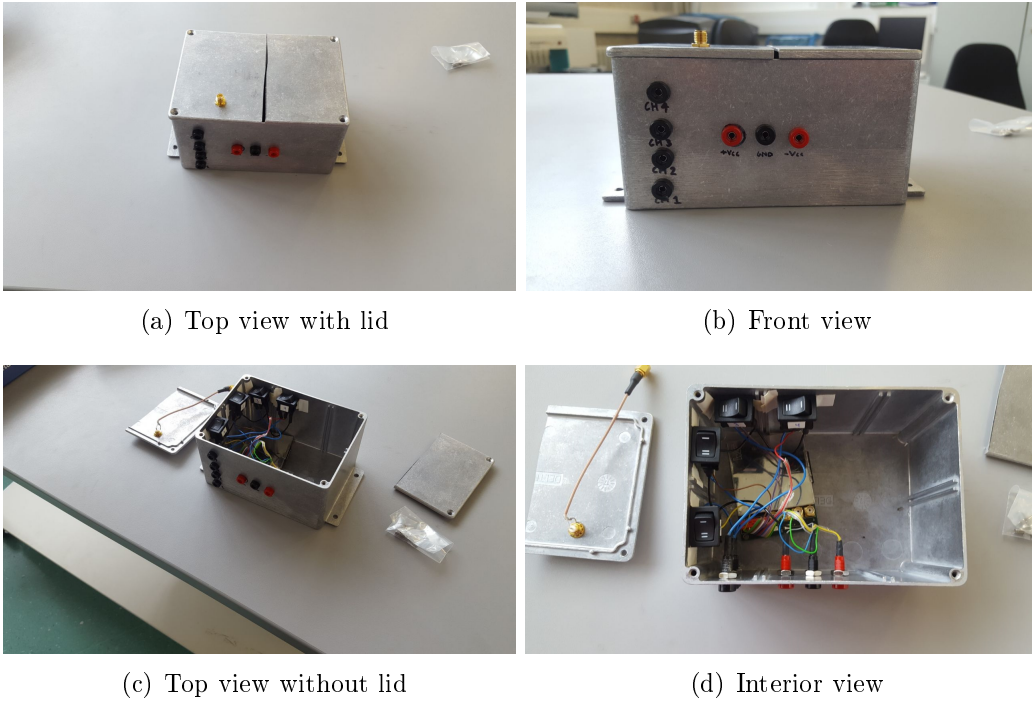


Figure 4.25: Modified aluminium enclosure.

4.2.1 Printed sensor is not coupled to the circuit input

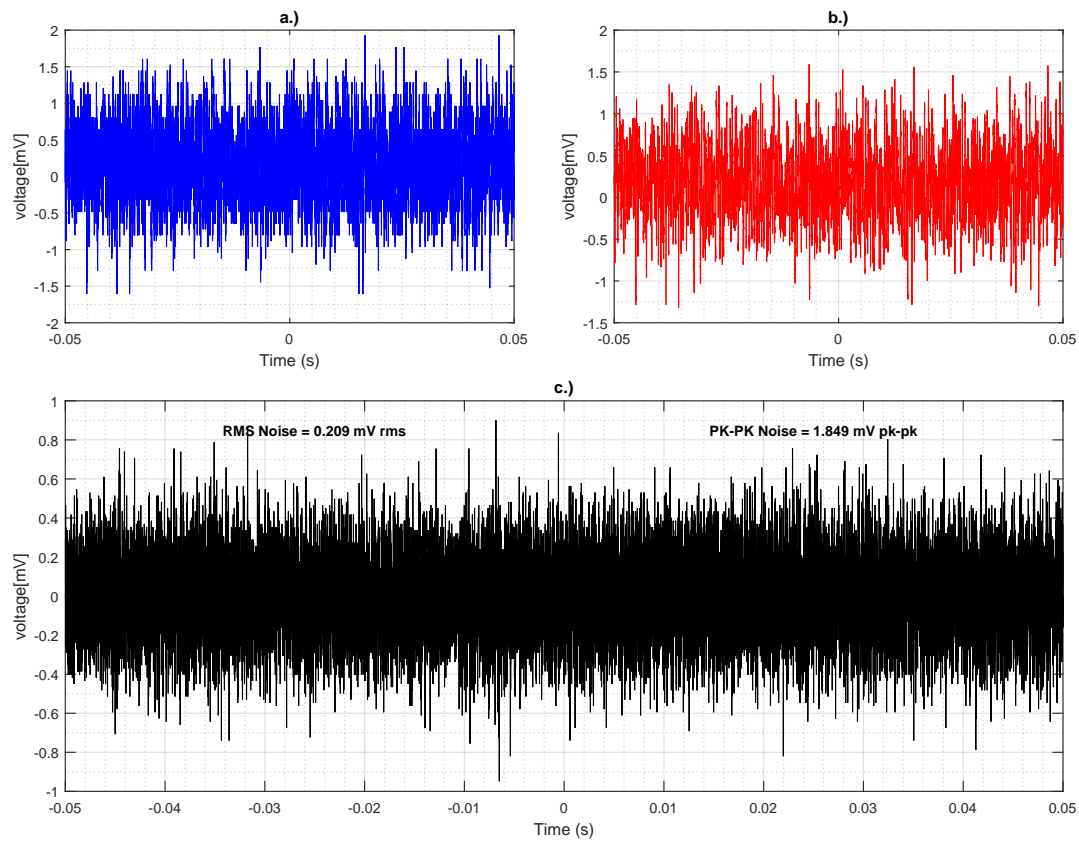


Figure 4.26: Root mean square and peak to peak noise channel 1 when printed sensor is not coupled to the circuit input. MatLab.

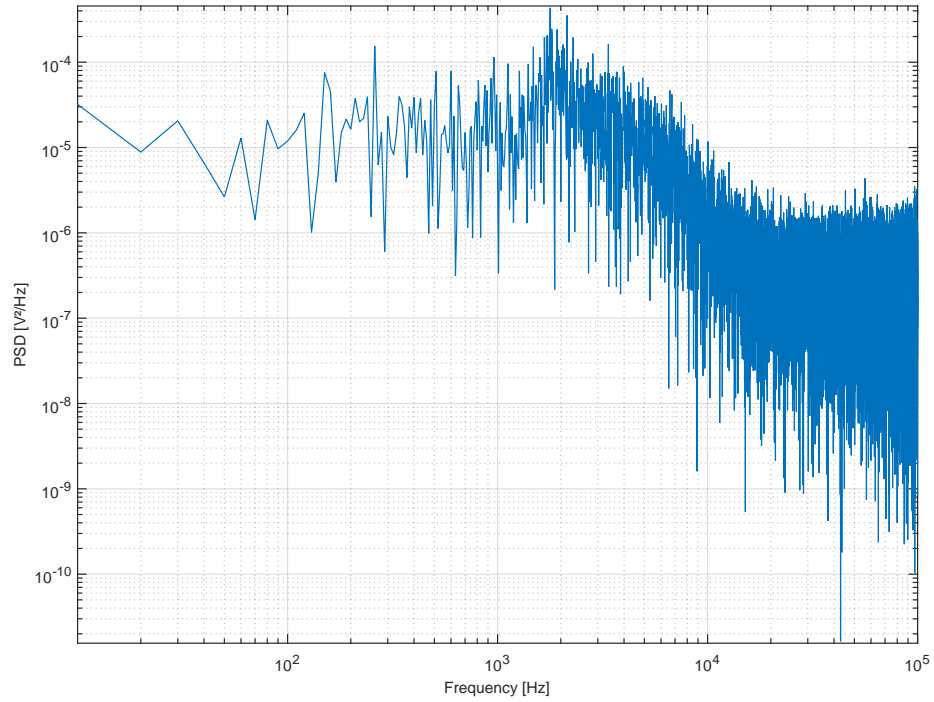


Figure 4.27: Power spectral density channel 1 when printed sensor is not coupled to the circuit input. MatLab.

The next tables summarizes the results.

Tabla 4.4: Noise experiment results for channel 1. LaTeX.

Experiment	RMS (mV)	Pk-Pk Noise (mV)	V^2/Hz at 50Hz
1	0.209	1.849	1×10^{-5}
2	0.208	1.897	2×10^{-5}
3	0.210	1.705	7×10^{-5}
4	0.204	1.737	1×10^{-5}

Tabla 4.5: Noise experiment results for channel 2. LaTeX.

Experiment	RMS (mV)	Pk-Pk Noise (mV)	V^2/Hz at 50Hz
1	0.196	1.817	1×10^{-5}
2	0.196	1.817	3×10^{-5}
3	0.196	1.962	7×10^{-5}
4	0.195	1.576	1×10^{-6}

Tabla 4.6: Noise experiment results for channel 4. LaTeX.

Experiment	RMS (mV)	Pk-Pk Noise (mV)	V^2/Hz at 50Hz
1	0.199	1.640	3×10^{-6}
2	0.199	1.801	1×10^{-5}
3	0.198	1.624	3×10^{-5}
4	0.197	1.576	2×10^{-5}

With the results shown in the tables above can be seen that the use of an aluminium enclosure improves the performance of the analog circuit in such a way that it does not matter if the input circuit has a printed sensor coupled or not, neither the use of a Faraday cage over the input, because the RMS and peak to peak noise as well as the power spectral density present a very little variation between all these situations. The noise due to power line has been eliminated successfully. This allows the frequency response analysis, as well as the characterization of noise added to the circuit when the electrolyte is placed on the printed circuit to emulate nanoparticle impacts. Even more important is the fact that this improvement brings us closer to the detection of silver nanoparticles since external sources of noise that could affect the sensor have been eliminated.

4.3 Frequency response

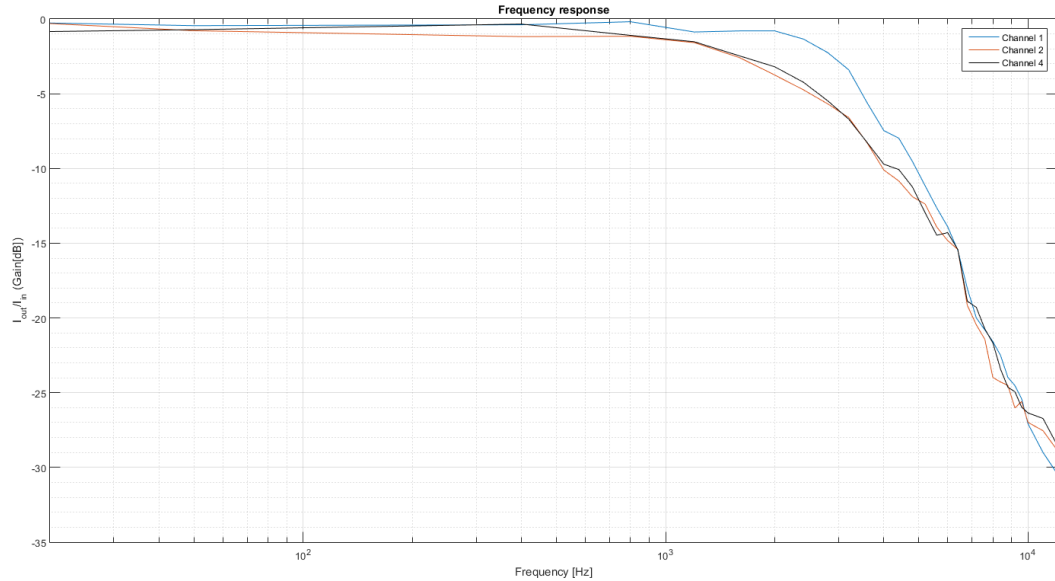


Figure 4.28: Frequency response of channel 1. MatLab.

The following table summarizes the results of the cutoff frequency of the 3 available channels.

Tabla 4.7: Frequency response. LaTeX.

Channel	Cutoff frequency (KHz)
1	3.2
2	2.0
4	2.4

The cutoff frequency of Channel 1 is close to the expected value; however,, that is not the case for Channel 2 and 4, this may be because the circuit has been used extensively in tests and some components may be worn. However,, all the cutoff

frequencies are in the KHz order and that will work for silver nanoparticles detection. On the other hand, an analog circuit update is being planned to increase the number of channels to 8. This brings the possibility of having a new circuit in better conditions.

The phase response of channel 1, 2 and 4 are shown in annex A.3.

4.4 Power board

4.4.1 PCB

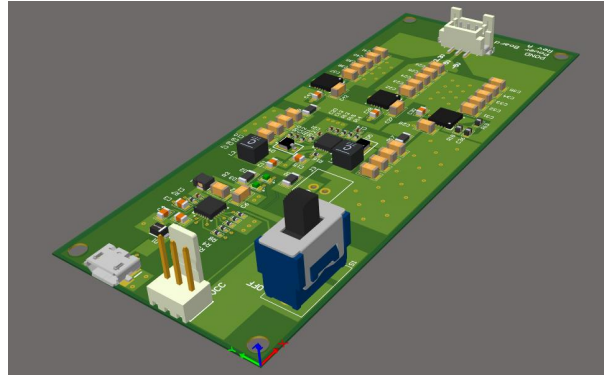
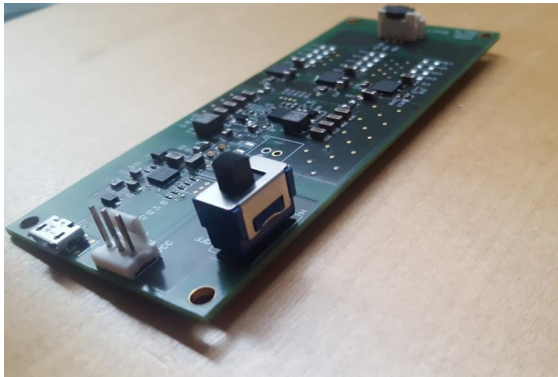


Figure 4.29: PCB Power board: Implementation vs 3D Model.

4.4.2 Noise analysis: TENMA 72-10495 power supply vs power board

Tabla 4.8: RMS and peak-to-peak noise for TENMA 72-10495. LaTeX.

Output voltage (V)	RMS (mV)	Pk-Pk Noise (mV)
3.3	1.747	28.744
5	1.648	29.146
-5	2.581	44.221

Tabla 4.9: RMS and peak-to-peak noise for power board. LaTeX.

Output voltage (V)	RMS (mV)	Pk-Pk Noise (mV)
3.3	0.353	2.894
5	0.367	3.698
-5	0.186	2.332

The power board has a much lower noise level than that of the TENMA 72-10495 power supply. First, the use of a LI-ION battery to feed the system is less noisy than the AC line used by desktop sources. On the other hand, the use of ultra-low noise LDO attenuates the frequency switching signals produced by the switching sources (Boost and Inverter). The design of the PCB was made using the most of recommendations given by the manufacturer, also using the application notes as a guide to avoid as much as possible the adherence of noise due to a poor layout.

4.4.3 Battery charge/discharge curve

The VSP-300 Bio-Logic Science Instruments equipment was used to measure the charging/discharging characteristic curve of the battery. This allows to establish a constant load at the battery output and measure the voltage and current of the input, as well as the voltage and current of the output. It is possible to program a

maximum and minimum voltage, as well as the time of the experiment.

Taking advantage of the ability to establish a constant load connected to the battery, it was possible to test the time of charge and discharge under different conditions. The first test was to establish a current of 166 mA, this is the current needed to supply the 4 channels. The second test was to measure the operating time of the battery if the system is updated to 8 channels, this was tested using a current of 200 mA. Finally, it was tested to extract from the battery the maximum possible current that can be used by the power board, this would be equivalent to feeding 60 channels, this was established by a current of 636 mA. The charge and discharge curve for the case of 4 channels is shown below.

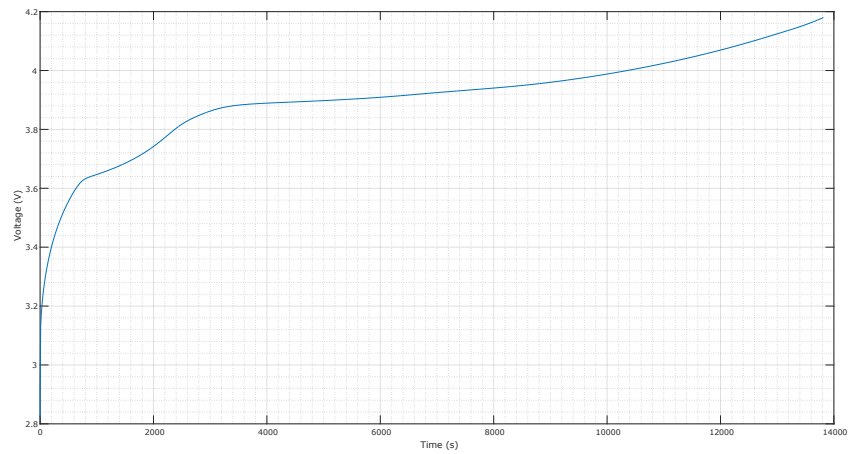


Figure 4.30: Battery charge curve. MatLab.

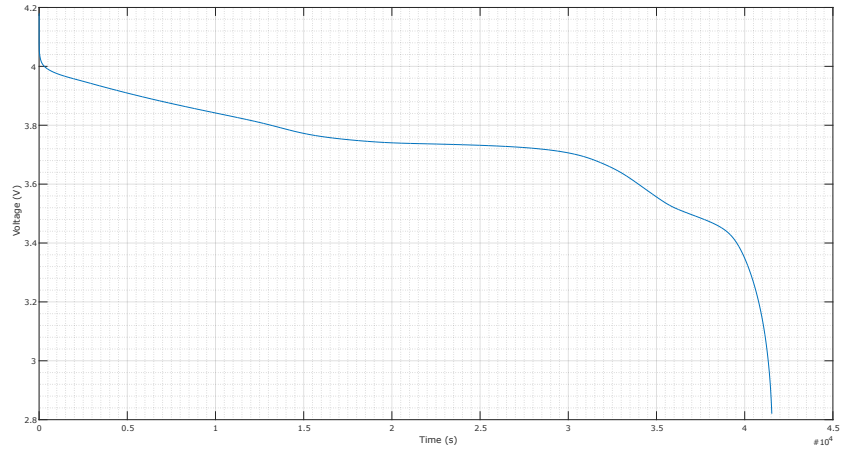


Figure 4.31: Battery discharge curve. MatLab.

From the measurements described above, the following is extracted. The battery is able to supply power for 3 hours and 45 minutes to a system with 60 channels, 9 hours and 45 minutes to a system with 8 channels and 11 hours and 30 minutes to a system with 4 channels. It is important to note that the objective related to the lifetime of the circuit depends on the battery, and a maximum of one hour for the current circuit (4 channels) was the main objective to this part of the project and it has been satisfactorily overcome. The charge time of the battery is similar in all cases, with 3 hours and 50 minutes.

In the charge/discharge curve of the battery can be observed that the battery voltage is not constant in time, and also depends on the load connected to it. This justifies the design of the power board because the boost and the inverter converter were chosen as a previous stage to ensure the stability of the input voltage to the LDO.

4.4.4 Efficiency

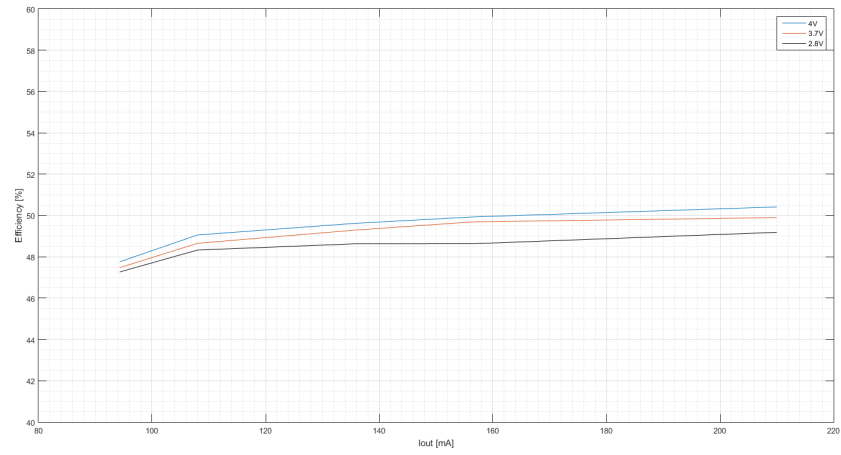


Figure 4.32: Efficiency for 3.3V output voltage. MatLab.

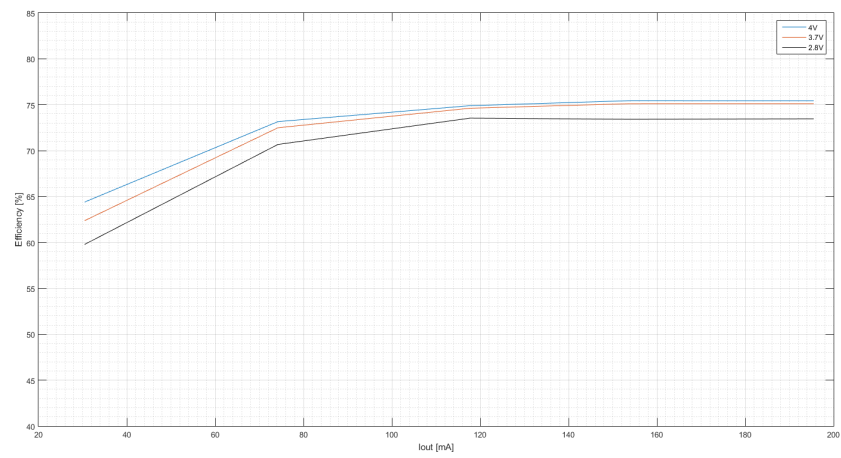


Figure 4.33: Efficiency for 5V output voltage. MatLab.

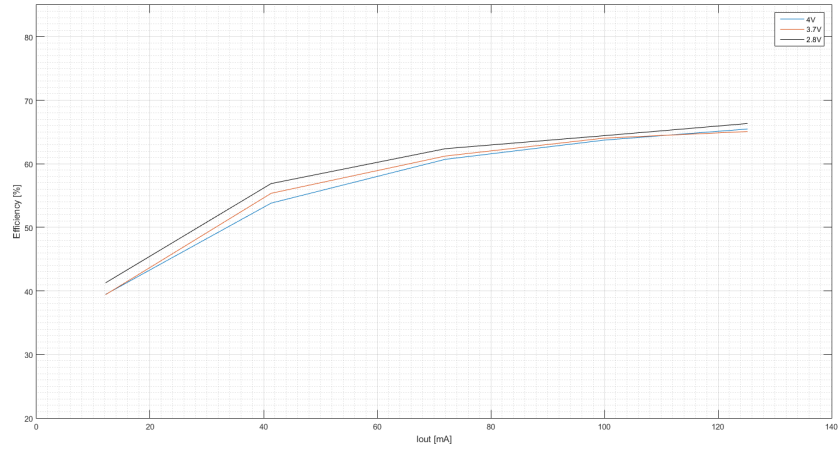


Figure 4.34: Efficiency for -5V output voltage. MatLab.

The efficiency was calculated by measuring the ratio between the output power and the input power. This test was carried out for three different input voltages: maximum charge value of the battery, 4.2V. Nominal value of the battery, 3.7V. Finally, the minimum value allowed by the battery charger before turn off the system to protect the battery from overdischarge, 2.8V.

The output currents were established using a constant load. The maximum value of each output current (corresponding to each output voltage) is that needed to feed 40 channels in the analog circuit, and entire digital circuit. The highest efficiency is presented by the output of 5V, close to 75%. Then there is the voltage output of -5V close to 65%. Finally the output voltage of 3.3V presents the worst efficiency with 50%. This is because the boost converter voltage that is 6V must pass to 3.3V, that is, almost half of its value and this generates power losses. The previous percentages of efficiency take into account the necessary current to operate at least 40 channels.

4.5 Noise experiment: Offset analysis

4.5.1 Without printed sensor

Tabla 4.10: Results of the analysis when applying the offset potential of channel 1 without printed sensor. LaTeX.

Offset (V)	RMS (mV)	Pk-Pk Noise (mV)	V^2/Hz at 50Hz
-0.8	0.511	3.698	9×10^{-6}
-0.4	0.522	3.377	2×10^{-5}
-0.2	0.533	3.779	2×10^{-5}
0	0.525	4.824	1×10^{-5}
0.2	0.512	3.538	2×10^{-6}
0.4	0.512	3.859	1×10^{-5}
0.8	0.522	3.538	4×10^{-5}

Tabla 4.11: Results of the analysis when applying the offset potential of channel 2 without printed sensor. LaTeX.

Offset (V)	RMS (mV)	Pk-Pk Noise (mV)	V^2/Hz at 50Hz
-0.8	0.461	3.055	2×10^{-5}
-0.4	0.452	2.894	7×10^{-5}
-0.2	0.436	3.055	6×10^{-6}
0	0.439	3.055	2×10^{-5}
0.2	0.425	2.894	1×10^{-7}
0.4	0.436	2.573	2×10^{-5}
0.8	0.448	2.814	2×10^{-5}

Tabla 4.12: Results of the analysis when applying the offset potential of channel 4 without printed sensor. LaTeX.

Offset (V)	RMS (mV)	Pk-Pk Noise (mV)	V^2/Hz at 50Hz
-0.8	0.454	3.055	4×10^{-5}
-0.4	0.449	3.055	3×10^{-6}
-0.2	0.432	3.055	8×10^{-6}
0	0.432	3.055	7×10^{-5}
0.2	0.437	2.894	7×10^{-6}
0.4	0.436	2.734	7×10^{-6}
0.8	0.451	3.136	8×10^{-6}

4.5.2 With printed sensor

Tabla 4.13: Results of the analysis when applying the offset potential of channel 1 with printed sensor. LaTeX.

Offset (V)	RMS (mV)	Pk-Pk Noise (mV)	V^2/Hz at 50Hz
-0.8	0.628	4.824	9×10^{-4}
-0.4	0.567	3.940	3×10^{-4}
-0.2	0.585	4.342	9×10^{-5}
0	0.599	4.985	3×10^{-5}
0.2	0.579	4.181	7×10^{-5}
0.4	0.579	4.181	7×10^{-5}
0.8	0.597	4.663	2×10^{-6}

Tabla 4.14: Results of the analysis when applying the offset potential of channel 2 with printed sensor. LaTeX.

Offset (V)	RMS (mV)	Pk-Pk Noise (mV)	V^2/Hz at 50Hz
-0.8	0.465	3.377	1×10^{-5}
-0.4	0.440	3.136	6×10^{-6}
-0.2	0.430	3.296	7×10^{-6}
0	0.436	3.216	2×10^{-5}
0.2	0.432	3.457	1×10^{-4}
0.4	0.434	3.457	7×10^{-5}
0.8	0.440	3.698	2×10^{-5}

Tabla 4.15: Results of the analysis when applying the offset potential of channel 4 with printed sensor. LaTeX.

Offset (V)	RMS (mV)	Pk-Pk Noise (mV)	V^2/Hz at 50Hz
-0.8	0.486	3.377	2×10^{-5}
-0.4	0.504	3.859	9×10^{-6}
-0.2	0.489	3.377	4×10^{-5}
0	0.492	4.342	3×10^{-5}
0.2	0.497	4.261	1×10^{-7}
0.4	0.499	4.503	9×10^{-5}
0.8	0.486	3.698	3×10^{-5}

As stated in section 1.2.1 of chapter 1, adding a offset potential should not add noise to the system because this offset is eliminated before the output of the circuit is obtained. The above is demonstrated in the previous tables, since different offset potentials are applied to the circuit to study if there is any alteration in the noise. However,, there is no significant difference between the results obtained.

The experiments done in this section follow the same procedure described in 3.2.4

with the difference that in this case the running average filter is not used. The reason for not using the running average filter is because the external noise has been eliminated satisfactorily by the aluminium enclosure and therefore the signal obtained corresponds to the internal noise of the circuit. The signal obtained directly from the oscilloscope is used for the analysis made in this section. Therefore, the tables above correspond to the characterization of the internal noise of the analog circuit in two cases. The first case corresponds to when the printed sensor coupled to the input is not used, that is, only the noise due to the analog circuit is analyzed, this is shown in tables 4.10, 4.11 and 4.12. The second case studies the noise when the printed sensor is coupled to the analog circuit, the results are shown in tables 4.13, 4.14 and 4.15.

4.6 Noise experiment: Noise added by the electrolyte

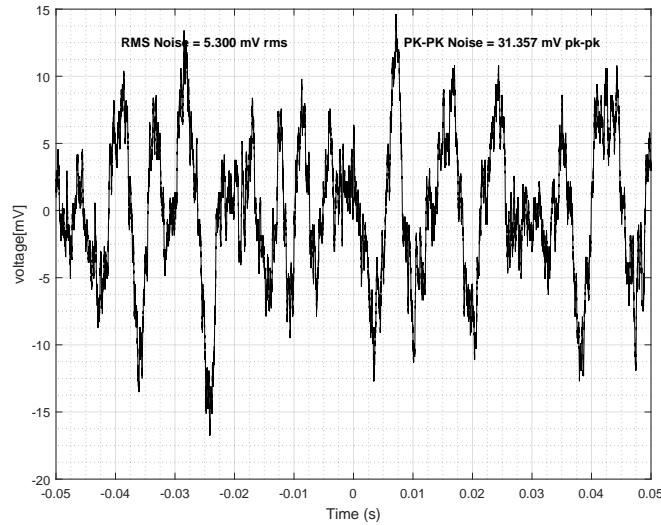


Figure 4.35: Noise added by the electrolyte: Channel 1. MatLab.

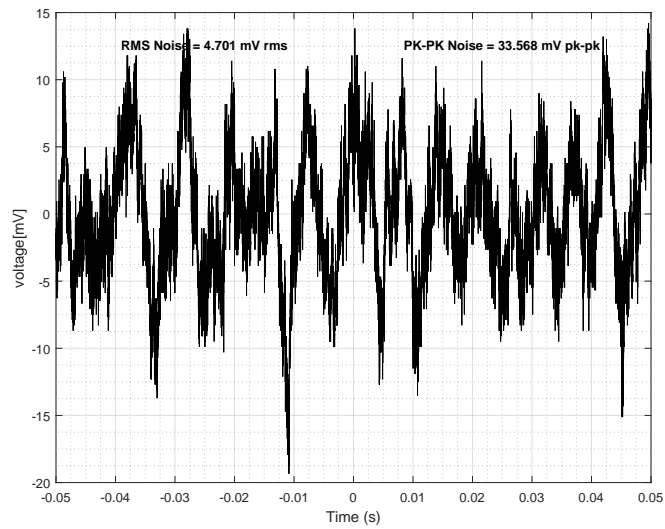


Figure 4.36: Noise added by the electrolyte: Channel 2. MatLab.

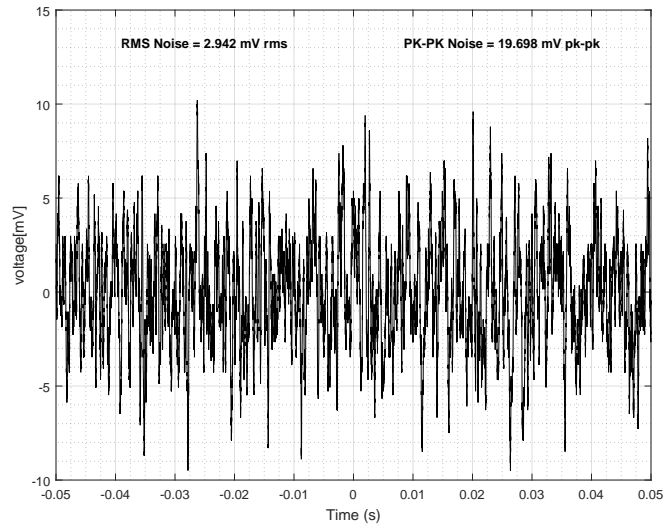


Figure 4.37: Noise added by the electrolyte: Channel 4. MatLab.

Tabla 4.16: Evaluation of noise when the electrolyte is placed on the printed sensor and the power board is used. LaTeX.

Channel	RMS (mV)	Pk-Pk Noise (mV)
1	5.300	31.357
2	4.701	33.568
4	2.942	19.698

Finally, table 4.16 shows the noise in the analogue circuit when coupled to varying input signals emulating nanoparticle impacts at the microelectrode. This experiment could not have been carried out at the beginning since the signal due to the power line hid any other signal. The implementation of the aluminium enclosure was necessary to study this case.

Channel 4 has the least noise. Likewise in other experiments where the printed sensor is used, it is channel 4 that has shown the best performance. While it is true that the cutoff frequency could be related to this effect, it is important to consider the placement of the feedback resistor. This could be an improvement in a future design and again evaluate the noise characteristics to confirm this fact.

Chapter 5

Conclusions

Using the appropriate measurement procedures and the use of frequency signal analysis, it was possible to identify external sources of noise. In addition, a shield against external noise was implemented for the analog circuit. This is made up by the aluminium enclosure. The use of this shielding not only eliminates external sources of noise, but is one of the fundamental steps for the measurement and characterization of internal noise in a circuit. This means that it is now possible to know the internal noise of the system, and study it under different conditions.

It was shown that the use of the printed sensor adds noise to the system by acting as an antenna. However, with the possibility of studying the internal noise of the analog circuit, it was shown that when it is adequately shielded, the addition of a printed sensor does not significantly increase the noise of the circuit. On the other hand, varying the offset potential in the analog circuit does not add any noise to the system either, as it is eliminated within the internal operations of the Pico Amp circuit. Finally, the noise in the analogue circuit when coupled to varying input signals emulating nanoparticle impacts at the microelectrode (using the electrolyte) was determined. This achieved the objective of characterizing the internal noise of the analog circuit, under different conditions. Sections 4.1 and 4.2 are of special interest since they show the comparison between the original state of the circuit and the state with the modifications made, that is, the aluminium enclosure, thus demonstrating an improvement with respect to the original state of the analog circuit in the noise analysis.

It was possible to characterize the frequency response, confirming that for Channel 1 the cutoff frequency is 3.3KHz. For the other two available channels, the cutoff frequency is in the order of KHz. All of them are sufficient for the detection of silver nanoparticles, at least to work as proof of principle.

A power board was designed and implemented to specifically meet the power requirements of the silver nanoparticle sensor. This was designed to power the current circuit for more than an hour. It allows the addition of up to 60 extra channels and operate for at least one hour. The use of LDO benefits the reduction of noise in the system, substantially improving with respect to the desktop power supply previously used to power the circuit. The system is also portable due a LI-ION battery. The circuit integrates a battery charger.

Finally, all previous measurements and improvements made, meet the specific objectives. The above achieves the general objective of this project which is the optimization of the silver nanoparticle sensor, thus ending this project.

Chapter 6

Recommendations

It is suggested an update of the PCB of the analog circuit and perform the frequency response analysis again, to verify that the correct cut-off frequency values in all channels. In addition, it is recommended to perform a noise analysis for the case of place the electrolyte on the printed sensor, in order to determine which placement of feedback resistors provides an improvement in the noise level in the circuit.

A possible improvement in the design of the PCB of the power board is to use headers to configure the positive outputs of the LDO. To configure a specific value, it is only necessary to ground those pins that produce the desired value according to formula 3.40. This would give flexibility to configure different positive output voltages.

Tests performed with different printed sensor lengths did not show an increase in the internal noise of the circuit. However, long sensors become much more sensitive to holes in the aluminum enclosure and the presence of vibrations. The sensitivity to vibrations happens because the printed sensor is not properly coupled with the circuit input, so when there is vibration, the electrical contact produces oscillations in the signal. The longer the sensor is, the greater this effect. It is recommended to use short sensors. On the other hand, in a future update of the analog circuit it is recommended to look for a better mechanical coupling with the printed sensor.

The power board PCB was designed to reduce the noise of the switching power supplies using the LDOs. However, it is of interest to analyze how the analog circuit behaves in the noise analysis if the outputs of the boost and the inverter are used directly to establish the output voltages of +5V and -5V. This would also help improve the efficiency of the 3.3V LDO. This implementation corresponds to the solution 2 described in section 3.4.2. In addition, the economic cost would be reduced if it is demonstrated that this solution is enough.

Bibliography

- [1] Rapp, J. *Compact sensitive Amplifier Circuit for the Detection of Nanoparticles Design und Evaluation einer Verstärkerschaltung für die Kon- zentrationsmes- sung von Nanopartikel*. Bachelor thesis (2017).
- [2] Kumsa, D. W. *et al.* Electron transfer processes occurring on platinum neural stimulating electrodes: a tutorial on the $i(V_e)$ profile. *Journal of Neural Engi- neering* **13**, 052001 (2016). URL <http://stacks.iop.org/1741-2552/13/i=5/a=052001>.
- [3] Sokolov, S. V., Eloul, S., Kätelhön, E., Batchelor-McAuley, C. & Compton, R. G. Electrode-particle impacts: a users guide. *Phys. Chem. Chem. Phys.* **19**, 28–43 (2017). URL <http://dx.doi.org/10.1039/C6CP07788A>.
- [4] Texas Instruments. Noise Analysis in Operational Amplifier Circuits Application Report (2007).
- [5] Mancini, R. Op Amps For Everyone Design Reference (2001).
- [6] Keysight Technologies. Spectrum Analysis Basics 1–89.
- [7] Texas Instruments. Understanding Buck Power Stages in Switchmode Power Supplies: Application Report (1999).
- [8] Texas Instruments. Understanding Boost Power Stages in Switchmode Power Supplies: Application Report (1999).
- [9] Day, M. Understanding Low Drop Out (LDO) Regulators (2002).
- [10] Lee, B. S. Application Report: Understanding the Terms and Definitions of LDO Voltage Regulators. *Texas Instruments* 1–13 (1999).

- [11] Texas Instruments. LM2576,LM3420,LP2951,LP2952: Battery Charging .
- [12] Figueiredo, P. G., Grob, L., Rinklin, P., Krause, K. J. & Wolfrum, B. On-chip stochastic detection of silver nanoparticles without a reference electrode. *ACS Sensors* **3**, 93–98 (2018). URL <https://doi.org/10.1021/acssensors.7b00559>. PMID: 29276833, <https://doi.org/10.1021/acssensors.7b00559>.
- [13] Texas Instruments. TPS6513x Positive and Negative Output Dc-Dc Converter (2016). URL <http://www.tij.co.jp/jp/lit/ds/symlink/tps65131.pdf>.
- [14] Texas Instruments. TPS7A470x RF LDO Voltage Regulator (2014). URL <http://www.ti.com/lit/ds/symlink/tps7a47.pdf>.
- [15] Texas Instruments. TPS7A33 - 36-V , 1-A , Ultralow-Noise Negative Voltage Regulator (2015). URL <http://www.ti.com/lit/ds/symlink/tps7a33.pdf>.
- [16] BAK. Specification of Li-ion Rechargeable Battery, Model No.: 103456A-1S-3M (2013). URL http://www.farnell.com/datasheets/1806915.pdf?{_}ga=2.47852967.1611366094.1533932846-651301841.1531047920.
- [17] Chitra, K. & Annadurai, G. Antibacterial activity of pH-dependent biosynthesized silver nanoparticles against clinical pathogen. *BioMed Research International* **2014**, 6 (2014). URL <https://doi.org/10.1155/2014/725165>.
- [18] Sambale, F. *et al.* Investigations of the toxic effect of silver nanoparticles on mammalian cell lines. *J. Nanomaterials* **16**, 6:6–6:6 (2015). URL <https://doi.org/10.1155/2015/136765>.
- [19] Krause, K. J., Yakushenko, A. & Wolfrum, B. Stochastic on-chip detection of subpicomolar concentrations of silver nanoparticles. *Analytical Chemistry* **87**, 7321–7325 (2015). URL <https://doi.org/10.1021/acs.analchem.5b01478>. PMID: 26079741.
- [20] Mohammadi Bardbori, A., Korani, M., Ghazizadeh, E., Korani, S. & Hami, Z. Effects of silver nanoparticles on human health **7**, 51–62 (2015). URL <https://doi.org/10.1515/ejnm-2014-0032>.
- [21] Caliskan, H. Digital circuit design for a nanoparticle detection device (POND) using printed sensors. Tech. Rep. June (2017).

- [22] Shuang, T. H. & G., C. R. “Nano-impacts”: An electrochemical technique for nanoparticle sizing in optically opaque solutions. *ChemistryOpen* **4**, 261–263. URL <https://onlinelibrary.wiley.com/doi/abs/10.1002/open.201402161>.
- [23] Grob, L. *Design and Implementation of a Miniaturised Bipotentiostat*. Master thesis (2015).
- [24] Wilamowski, B. M. & Irwin, J. D. Noise in Semiconductor Devices. chap. 11, 737 (CRC Press, 2010), second edn.
- [25] Leach, W. M. & Senior Member. Fundamentals of Low-Noise Analog Circuit Design. *IEEE Proc* 1515–1538 (1994). URL <http://dx.doi.org/10.1109/5.326411>.
- [26] Kish, L. B. Thermal noise engines 1–15 (2010).
- [27] Kiely, R. Understanding and Eliminating 1 / f Noise 3–6 (2017).
- [28] Armstrong, K. Testing Conducted Emissions 1–20 (2002).
- [29] A.H. Systems, Inc. Radiated Emissions Measurement How To 4–5.
- [30] Valavan, S. Understanding electromagnetic compliance tests in digital isolators .
- [31] Pini, A. Analyze noise with time, frequency and statistics (2017).
- [32] Smith, S. W. Statistics, Probability and Noise. In technical Publishin, California (ed.) *The Scientist and Engineer’s Guide to Digital Signal Processing Statistics, Probability and Noise*, chap. 2, 664 (San Diego, California, 1999), second edn.
- [33] Kay, A. *Operational Amplifier Noise: Techniques and Tips for Analyzing and Reducing Noise*. January (2012), first edn.
- [34] Moulin, E. RMS Calculation for Energy Meter Applications Using the ADE7756 1–8.
- [35] Deakin, R. E. & Kildea, D. G. A NOTE ON STANDARD DEVIATION AND RMS **44**, 74–79 (1999).
- [36] Teel, J. C. Understanding noise in linear regulators 5–8 (2005).

- [37] Renterghem, K. V. How to measure LDO noise (2015).
- [38] Maxim Integrated. Regulator Topologies for Battery-Powered Systems 1–8 (2001).
- [39] Hussien, F. & Eckmann, B. Guide to Choosing the Best DCDC Converter for Your Application (2016).
- [40] Roy, R. V. Power Management Introduction 1–11 (2014).
- [41] Torres, J. *et al.* Low Drop-Out Voltage Regulators : Capacitor-less Architecture Comparison. *IEEE Circuits and Systems Magazine* **14**, 6–26 (2014). URL <http://dx.doi.org/10.1109/MCAS.2014.2314263>.
- [42] Texas Instruments. AN-1148 Linear Regulators : Theory of Operation and Compensation 1–15 (2013).
- [43] Gamry Instruments. The Faraday Cage : What Is It ? How Does It Work ? 1–3 (2010).
- [44] Sadiku, M. N. O. *Elements of Electromagnetics* (Oxford, United Kingdom, 2000), 3 edn.
- [45] Kumar, A. & Madaan, P. Top 10 EMC Design Considerations. *Cypress Semiconductor* 4 (2011).
- [46] Texas Instruments. bq25606 Standalone 3 . 0-A Single Cell Battery Charger (2017). URL <http://www.ti.com/lit/ds/symlink/bq25606.pdf>.
- [47] Texas Instruments. bq25606 PWR772 Evaluation Module (2017). URL <http://www.ti.com/lit/ug/sluubl3a/sluubl3a.pdf>.
- [48] Texas Instruments. TPS65131EVM User’s Guide (2010). URL <http://www.ti.com/lit/ug/slvu119c/slvu119c.pdf>.
- [49] Texas Instruments. TPS65131EVM-839 User’s Guide (2017). URL <http://www.ti.com/lit/ug/slvuaw7/slvuaw7.pdf>.
- [50] Texas Instruments. TPS7A47xxEVM-094 Evaluation Module (2013). URL <http://www.ti.com/lit/ug/slvu741a/slvu741a.pdf>.
- [51] Texas Instruments. TPS7A3301EVM-061 (2011). URL <http://www.ti.com/lit/ug/slvu602/slvu602.pdf>.

Appendix A

Appendix

A.1 Abbreviations

TEM: Transmission electron microscopy.

SEM: Scanning electron microscope.

DLS: Dynamic Light Scattering.

RMS: Root mean square.

Pk-to-Pk: Peak to peak voltage.

PSD: Power spectral density.

A.2 DCDC converter parameters

Difference between input and output voltage: Depends of the relation between input and output voltage there is specific topologies to use:

1. **$V_{in} > V_{out}$:** Linear dropout regulators (LDO), step-down (Buck converter) [39], [40].
2. **$V_{in} < V_{out}$:** Step-up (Boost converter) [39].
3. **$V_{in} < V_{out}$ or $V_{in} > V_{out}$:** Buck-Boost converter [39].
4. **V_{in} have opposite polarity than V_{out} :** Inverting converter [39].

DC line regulation: It is a measure of how much the output voltage change when the input voltage change [39].

DC load regulation: It describes how much the output voltage change when the load current change [39].

Efficiency: It is a measure of how well the input power is transferred to the output, due to the internal power losses the output power is lower than the input power and is defined by the following formula [39]:

$$\text{Converter efficiency (\%)} = \frac{100 \times (I_{out_{av}} \times V_{out_{av}})}{(I_{in_{av}} \times V_{in_{av}})} \quad (\text{A.1})$$

Input voltage range: It is the maximum and minimum input voltage with which the converter can work. Increase the input voltage more than the maximum limit can damage the converter [39].

Output voltage range: It is the maximum and minimum output voltage that the converter can supply [39].

Maximum output current: It is the maximum output current that the converter can supply [39].

Output voltage noise: Switching converters have a power transistor that is used to control the output voltage, this transistor commutes in a specific frequency that produces harmonics. Output voltage noise is the RMS voltage of the noise produced by the converter in a specific frequency range when is given a fix output current and specific input voltage [39].

Output voltage accuracy: It describes how much the output voltage change respect the nominal output voltage [39].

Over-current protection: If the output current increase more than a specific limit this feature protects not only the converter but also the system connected to it [39].

Over-temperature protection: This feature provides protection to the converter against temperatures that exceeds a specific limit [39].

Power supply rejection ratio (PSRR): It is a measure of how the output voltage is affected by the noise at the input voltage, ideally the output voltage should be stable as possible face this input noise [39].

Quiescent current (I_q): It is the current consumed by the converter where is not load at the output [39].

Soft start operation: When a power supply is turn on it can produce some current spikes that can damage the converter and the system, soft start is a way to avoid that, the output voltage increases slowly from zero to the established output voltage [39].

Soft-stop operation: Similar to the last concept, the output voltage drops slowly from the established voltage to zero when the converter is turn-off [39].

Shutdown current (I_{sd}): It is the leakage current present in the converter when this is turn-off [39].

Interface protocol: It is the interface communication protocol to control the converter in case that it has digital components [39].

A.3 Phase response

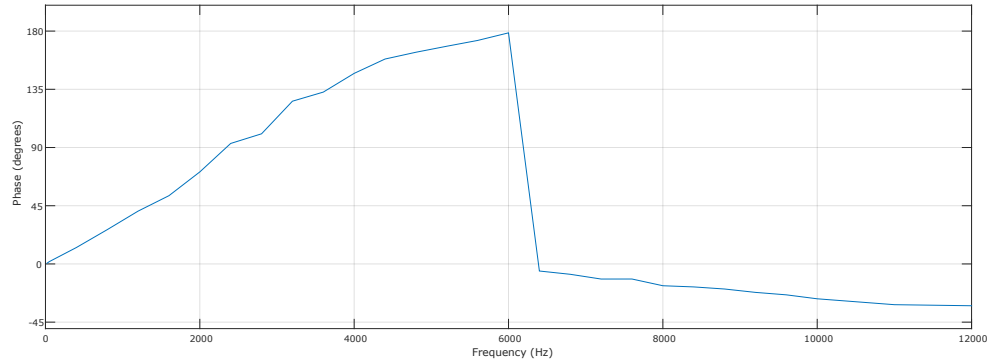


Figure A.1: Phase response channel 1. MatLab.

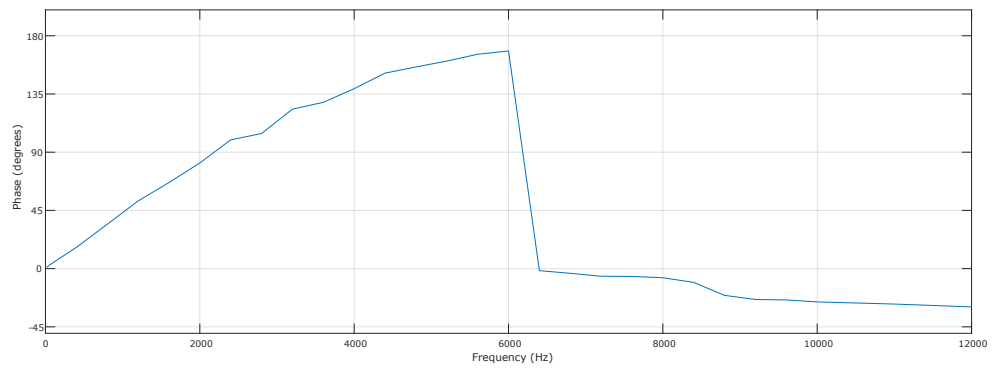


Figure A.2: Phase response channel 2. MatLab.

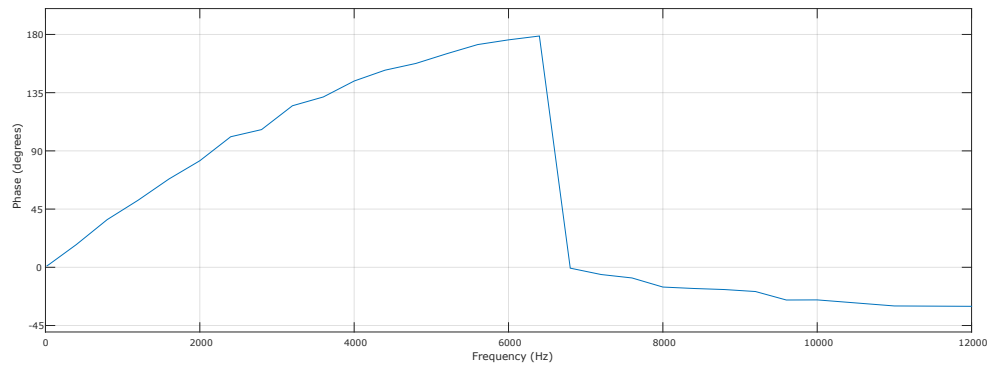


Figure A.3: Phase response channel 4. MatLab.

A.4 Schematics

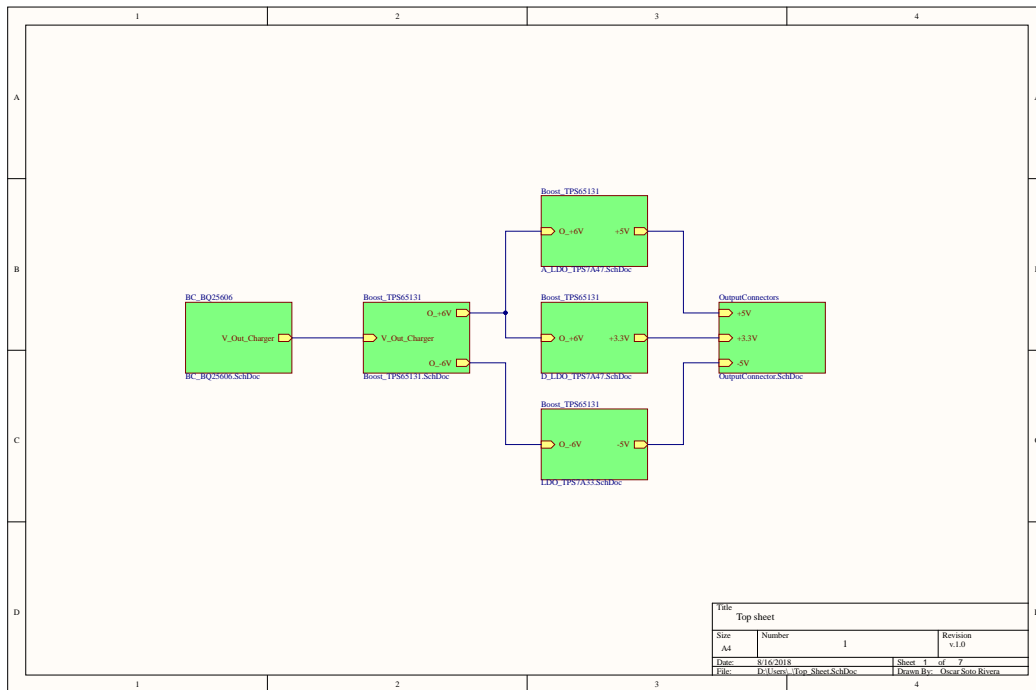


Figure A.4: Schematic top sheet. Altium designer 18.

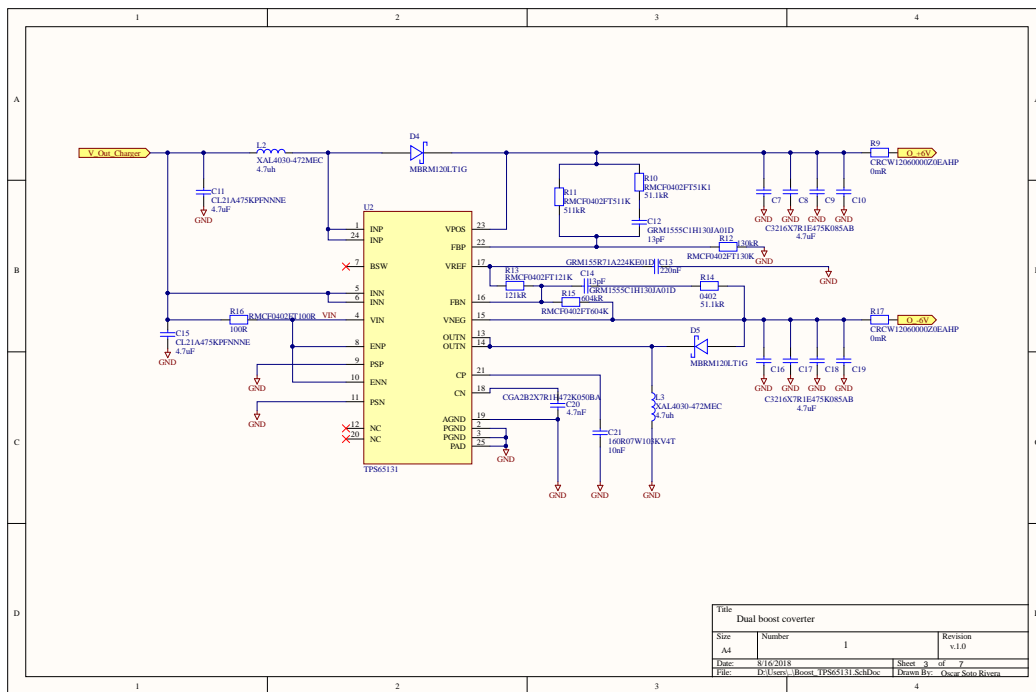


Figure A.6: Schematic boost/inverter TPS65131. Altium designer 18.

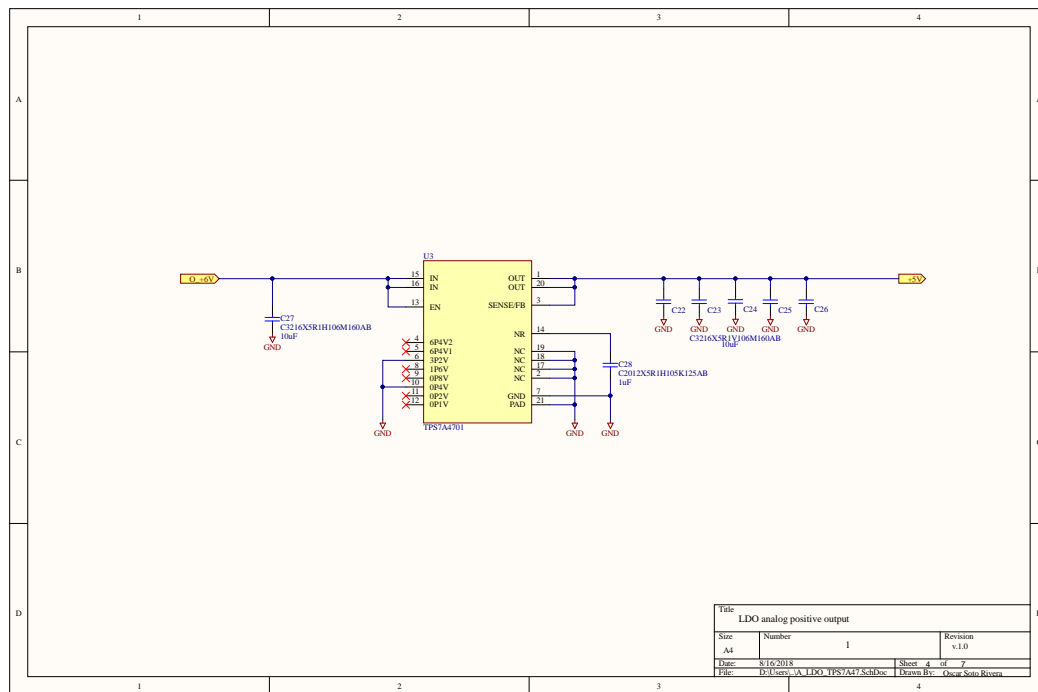


Figure A.7: Schematic LDO TPS7A47 to obtain 5V. Altium designer 18.

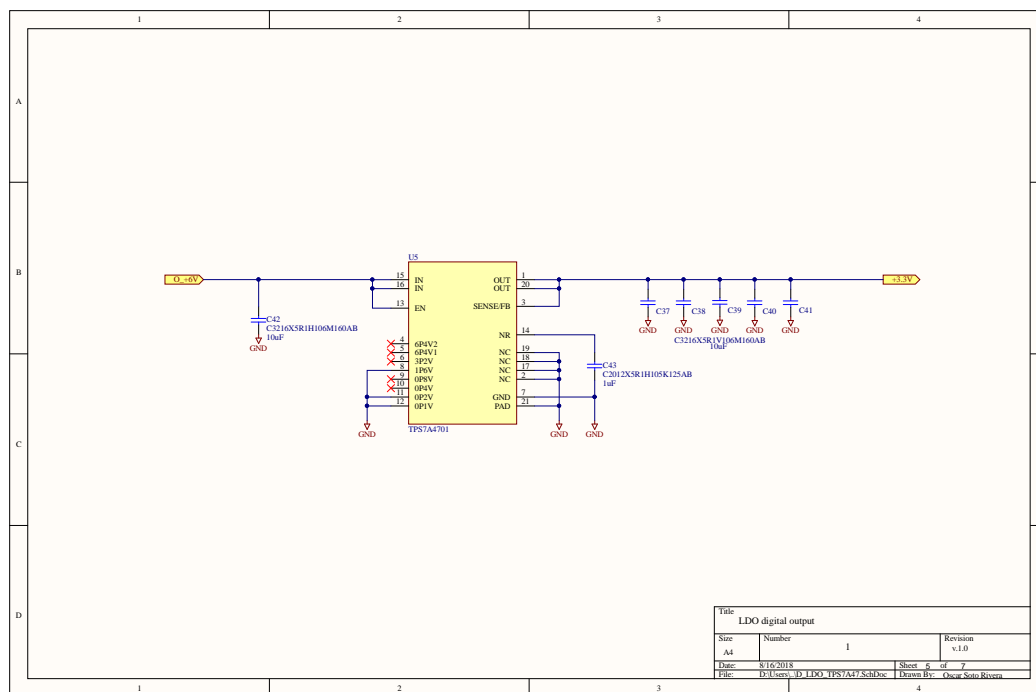


Figure A.8: Schematic LDO TPS7A47 to obtain 3.3V. Altium designer 18.

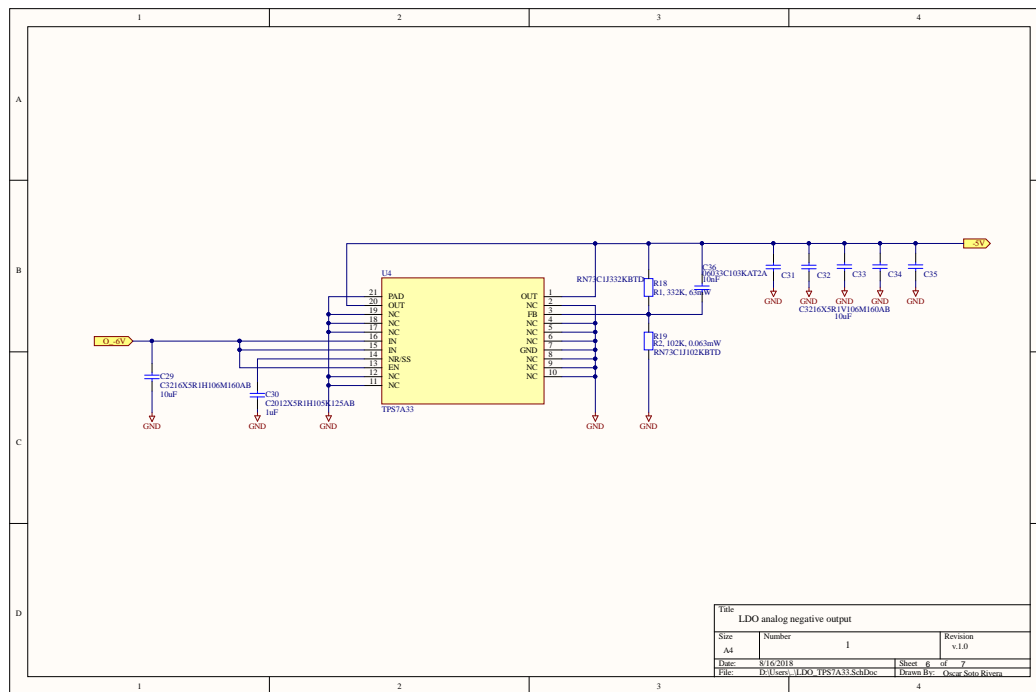


Figure A.9: Schematic LDO TPS7A33 to obtain -5V. Altium designer 18.

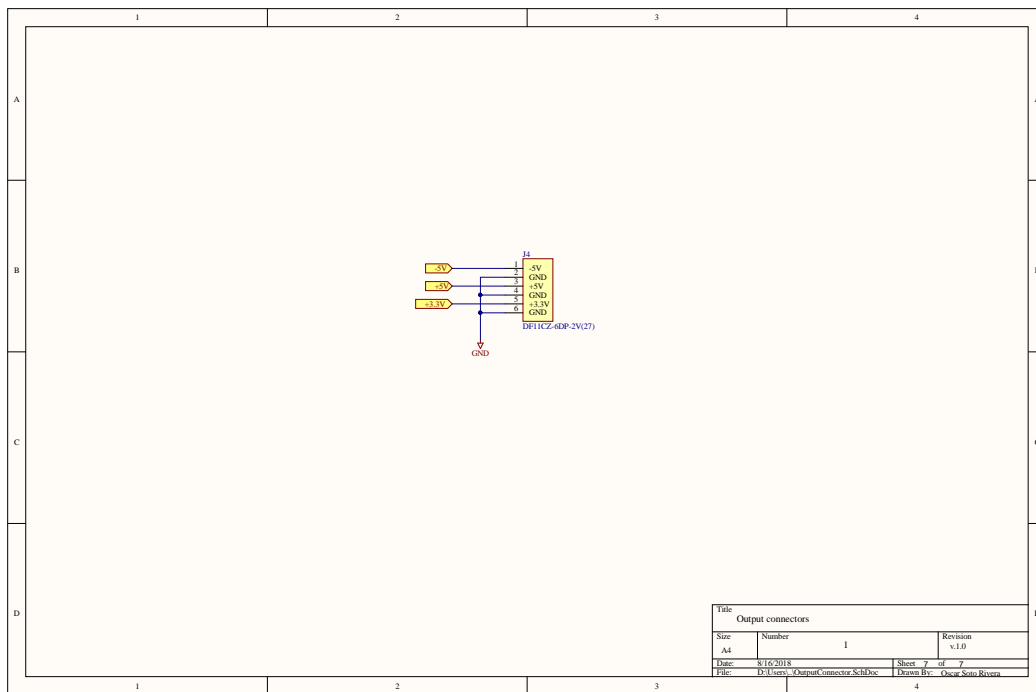


Figure A.10: Schematic output connector. Altium designer 18.

A.5 Layout

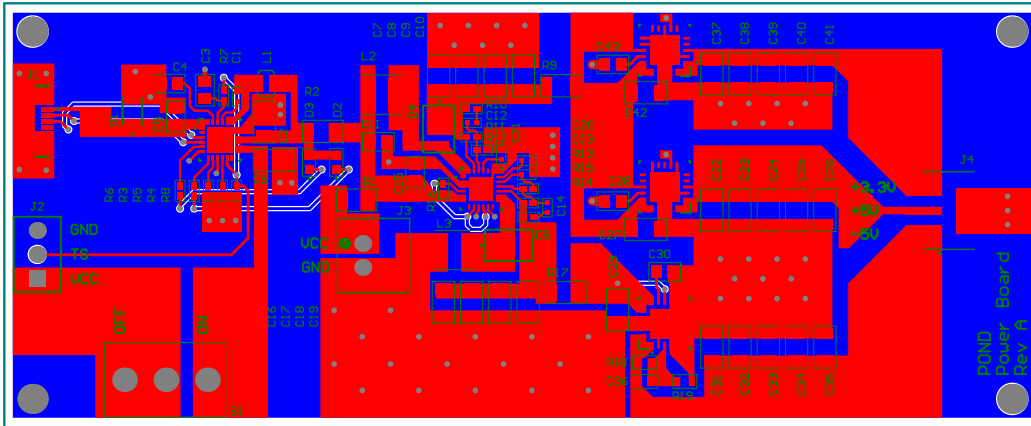


Figure A.11: Layout power board. Altium designer 18.